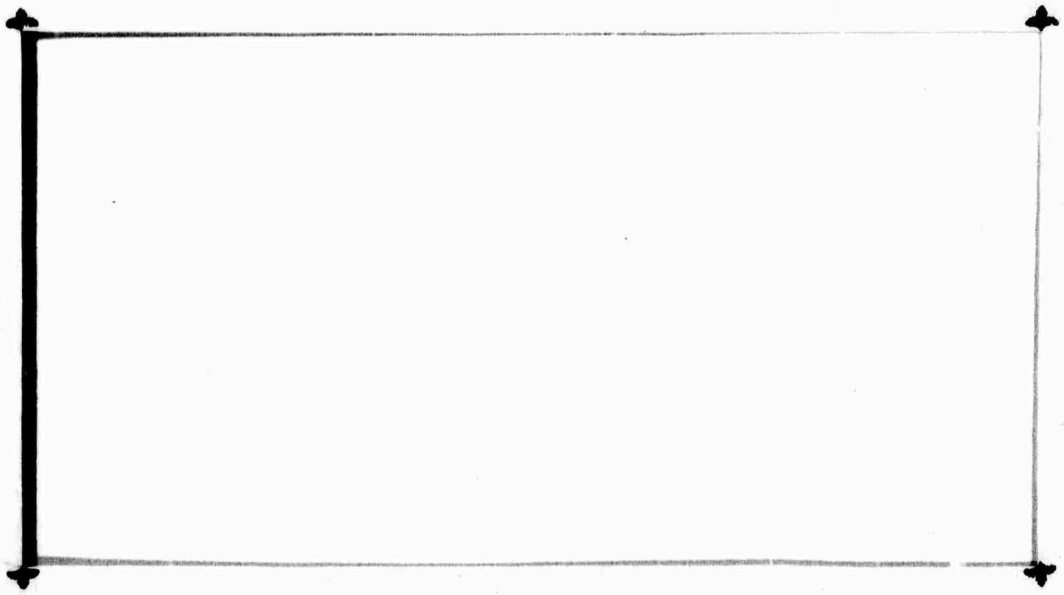

ENGINEERING AND INDUSTRIAL EXPERIMENT STATION

College of Engineering

University of Florida

Gainesville

STRUCTURE, PROPERTIES AND RADIATION SENSITIVITY OF ELECTRICALLY BISTABLE MATERIALS

Technical Report No. 3
6 September 1971

Second Semiannual Report
(ARPA DAHC04-70-C-0024)

ARPA Order Number:	1562
Program Code Number:	OD10
Name of Contractor:	University of Florida
Effective Date of Contract:	6 February 1970
Contract Expiration Date:	6 February 1972
Amount of Contract:	$102,816
Contract Number:	DAHC04-70-C-0024
Principal Investigator:	Dr. Derek B. Dove, Telephone 904-392-1497
Project Scientist: (Technical Coordinator)	Dr. Charles Boghosian, AROD, Telephone 919-286-2285

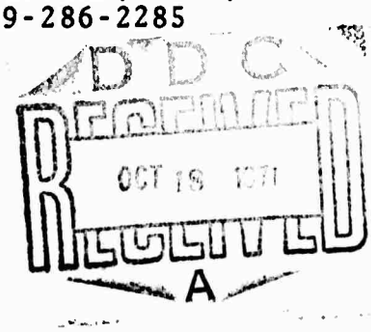

Submitted by

D. B. Dove, L. L. Hench,
R. W. Gould and R. E. Loehman
Department of Metallurgical and
Materials Engineering
University of Florida
Gainesville, Florida 32601

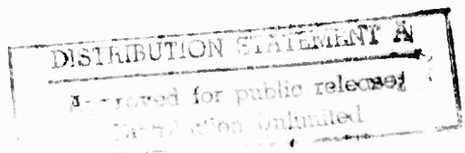

Security Classification

DOCUMENT CONTROL DATA - R & D

(Security classification of title, body of abstract and indexing annotation must be entered when the overall report is classified)

1. ORIGINATING ACTIVITY (Corporate author) University of Florida, Engineering and Industrial Experiment Station, Gainesville, Florida 32601	2a. REPORT SECURITY CLASSIFICATION Unclassified 2b. GROUP

3. REPORT TITLE

STRUCTURE, PROPERTIES AND RADIATION SENSITIVITY OF ELECTRICALLY BISTABLE MATERIALS

4. DESCRIPTIVE NOTES (Type of report and inclusive dates)

Technical Report, 2nd Semiannual, 6 February 1971 to 6 September 1971

5. AUTHOR(S) (First name, middle initial, last name)

Derek B. Dove, Larry L. Hench, Robert W. Gould and Ronald E. Loehman

6. REPORT DATE 6 September 1971	7a. TOTAL NO. OF PAGES 122	7b. NO. OF REFS 68
8a. CONTRACT OR GRANT NO. DAHC04-70-C-0024 b. PROJECT NO. P-8993-P c. d.	9a. ORIGINATOR'S REPORT NUMBER(S) Technical Report No. 3 9b. OTHER REPORT NO(S) (Any other numbers that may be assigned this report)	

10. DISTRIBUTION STATEMENT

11. SUPPLEMENTARY NOTES This research was supported by Advanced Research Projects Agency	12. SPONSORING MILITARY ACTIVITY Army Research Office, Durham

13. ABSTRACT

This semiannual report contains copies of papers to be published in the proceedings of the Fourth International Conference on Amorphous and Liquid Semiconductors. The first reports measurements on the thermal properties of germanium selenides using differential thermal analysis; the second describes changes in local atomic order in thin films of composition $GeTe_2$ produced by deposition conditions and heat treatment; the third paper summarizes work on the effect of microstructure on the radiation sensitivity of semiconducting glasses. Also included is a discussion of the structure of amorphous Ge_xSe_{1-x} films and their response to heat treatment. This work has been accepted by the University of Florida as partial fulfillment of the requirements of the M.S. degree of Mr. B. Molnar.

DD FORM 1 NOV 68 1473

Security Classification

14. KEY WORDS	LINK A		LINK B		LINK C	
	ROLE	WT	ROLE	WT	ROLE	WT
Amorphous semiconductors						
Vanadate glasses						
Radial Distribution Analysis						
Thin film devices						
Radiation defects						

Abstract

This semiannual report contains copies of papers to be published in the proceedings of the Fourth International Conference on Amorphous and Liquid Semiconductors. The first reports measurements on the thermal properties of germanium selenides using differential thermal analysis; the second describes changes in local atomic order in thin films of composition $GeTe_2$ produced by deposition conditions and heat treatment; the third paper summarizes work on the effect of microstructure on the radiation sensitivity of semiconducting glasses. Also included is a discussion of the structure of amorphous Ge_xSe_{1-x} films and their response to heat treatment. This work has been accepted by the University of Florida as partial fulfillment of the requirements of the M.S. degree of Mr. B. Molnar.

COMPOSITION AND PHYSICAL PROPERTIES OF AMORPHOUS BULK AND THIN FILM MATERIALS IN THE SYSTEM Ge-Se-Te-As*

By

R. E. Loehman, A. J. Armstrong,
D. W. Firestone and R. W. Gould
Department of Metallurgical and Materials Engineering
University of Florida
Gainesville, Florida 32601

*Work supported by AROD under
Contract No. ARPA DAHC04-70-C-0024

Abstract

Bulk samples of Ge-Se, Ge-Se-As, Ge-Te, Ge-Te-As and Se-Te-As have been prepared by quenching from the melt. Densities and degree of crystallinity have been measured. Scanning electron micrographs of glassy $GeSe_x$ ($1.5 \leqslant x \leqslant 6$) and $GeSe_{5.33}As_{0.33}$ show no evidence of gross diphasic structure. Bulk GeSe, $GeSe_2$ and $GeSe_4$ have been flash evaporated to form thin films; x-ray fluorescence analyses give film compositions of $GeSe_{0.7}$, $GeSe_{1.6}$ and $GeSe_{2.4}$, respectively. Crystallization temperatures of glassy $GeSe_{1.5}$, $GeSe_{2.4}$, $GeSe_3$ and $GeSe_4$ as determined by thermal analysis are reported. Crystallization of amorphous $GeSe_{1.5}$ as a function of heat treatment at 450°C has been determined.

The present report describes one aspect of a comprehensive study of the germanium chalcogenides underway in this laboratory. A few relatively simple compositions have been chosen for examination in an attempt to relate physical properties to the method of preparation. Furthermore, it was hoped that information gained on these simpler compositions would lead to a better understanding of the structural changes which occur upon switching in the more complex materials.

Three to seven gram mixtures of the appropriate elements of four nines purity or better were sealed in 11 mm O.D. evacuated silica ampoules, heated with periodic agitation from 24 to 48 hours and then quenched in an ice-salt water mixture.

Table I gives the results of density measurements and powder x-ray diffraction determinations of crystallinity of some compositions in the Ge-Se-Te-As system. As can be seen, in the case of Ge-Se-As all compositions of 60 atomic percent Se or greater are x-ray amorphous for the quenching rates of this study. This compares with the smaller glass formation region of 70 to 100 atomic percent Se for the Ge-Se system as reported by Chun-hua et al.[1] and by Khar'yuzov and Evstropiev.[2] With the exception of $GeSe_{1.5}$ the densities show a consistent trend toward higher values for increasing amounts of Se and As. The value of 4.25 g/cm^3 for glassy $GeSe_2$ compares with the literature value of 4.68 g/cm^3[3] for the crystalline form of the same material.

Also presented in Table I are data on the Ge-Te-As and Se-Te-As systems. With the exception of GeTe, there is a

Table I

Composition, Density and Structure of Bulk Water-Quenched Material in the Ge-Se-Te-As System

Composition	Density (g/cm^3 at 25°C)	Structure*
GeSe	5.39±0.03	X
$GeSe_{1.5}$	4.36	A
$GeSe_2$	4.25	A
$GeSe_{1.95}As_{0.05}$	4.24	A
$GeSe_{2.4}$	4.27	A
$GeSe_3$	4.29	A
$GeSe_{2.9}As_{0.1}$	4.32	A
$GeSe_{3.5}$	4.31	A
$GeSe_4$	4.33	A
$GeSe_{5.33}As_{0.33}$	4.36	A
$GeSe_6$	4.32	A
Ge_4Te	5.65	X
GeTe	6.14	X
$GeTe_2$	5.83	X
$GeTe_{1.95}As_{0.05}$	5.90	-
$GeTe_3$	5.90	X
$GeTe_{2.9}As_{0.01}$	5.75	X
$GeTe_4$	6.13	X
$GeTe_{5.33}As_{0.33}$	--	A
$GeSe_{0.98}Te_{0.98}As_{0.04}$	4.83	A
$AsSe_3$	4.30	A
$AsSeTe_2$	5.27	A
$AsTe_3$	6.16	X

*X - crystalline
A - amorphous

rather consistent trend toward greater density with increasing amounts of tellurium. The bulk quenched samples of Ge-Te were found to be crystalline as has been reported previously in the literature.[4,5]

Table II shows the results of x-ray fluorescence determinations of composition of several thin films of $GeSe_x$ prepared by conventional flash evaporation techniques from bulk glasses. As can be seen, the films (thickness ~1,000 Å) are consistently deficient in selenium as compared with the bulk material from which they were made. Several explanations are possible, among them that selenium re-evaporates preferentially from the glass substrates during the initial stages of evaporation. Although the temperature of the films was not measured during evaporation, it is believed that they did not rise appreciably above room temperature since the glass substrates on which they were deposited were tightly clamped to a water-cooled metal block. An alternative explanation is that the selenium vapor beam is less focussed than that of Ge and thus deposits in smaller concentrations in the substrates. The angular distribution studies required to verify this possibility have not been completed. In all cases the films were x-ray amorphous and showed no signs of gross structure in the transmission electron microscope.

Bulk amorphous samples, with compositions $GeSe_{1.5}$, $GeSe_2$, $GeSe_4$, $GeSe_6$ and $GeSe_{5.33}As_{0.33}$ were examined in a Cambridge Stereoscan Electron Microscope for evidence of structure; at magnifications of up to 5,000X all these materials appeared

Table II

Comparison of Compositions of Bulk $GeSe_x$ and Thin Films Prepared from Them

Composition of Bulk	Composition of Film	Structure*
GeSe	GeSe	A
$GeSe_2$	$GeSe_{1.6}$	A
$GeSe_4$	$GeSe_{2.4}$	A

*A - amorphous

homogeneous. Figure 1 shows a typical electron micrograph at 1,400X, in this case for $GeSe_4$.

The thermal behavior of the Ge-Se system in the glass formation region was investigated by Direct Calorimetric Analysis (DCA)[6] using an Orton Thermal Analyzer. Two to three gram samples of amorphous bulk material of compositions $GeSe_{1.5}$, $GeSe_{2.4}$, $GeSe_3$ and $GeSe_4$ were powdered and placed in small silica crucibles in the apparatus. Heating rates of one to two degrees per minute were employed to raise the temperature of the sample from room temperature to about 700°C. The system was maintained at all times under an atmosphere of purified argon. Thermal analysis of bulk noncrystalline material with compositions $GeSe_{1.5}$, $GeSe_{2.4}$ and $GeSe_3$ gave traces showing slow exothermic transitions which were interpreted to be due to crystallization of the amorphous samples. $GeSe_4$ showed no transitions whatsoever in the DCA curves. X-ray analysis of a portion of the $GeSe_4$ at the conclusion of a run showed it still to be amorphous. Figure 2 shows the data obtained in these experiments superimposed on part of the Ge-Se phase diagram. This particular diagram is a composite of those published by several workers.[1,7-9] Dembovskii and coworkers[10] have reported that the ability of the Ge-Se glasses to crystallize falls as Se content increases and reaches a minimum at 92 atomic percent Se. The present results are consistent with this finding.

X-ray powder diffraction traces of $GeSe_{1.5}$ heat treated at 450°C for varying lengths of time in sealed evacuated ampoules showed sharp peaks for heat treatments in excess of 10

minutes. The patterns were indexed and Se was found to be the predominant crystallizing species. Se was also observed to be the crystallizing species in Ge-Se glasses of higher selenium concentration as reported by Dembovskii et al.;[10] Takemori, Roy and McCarthy[4] find that Te is the species which crystallizes from the analogous Ge-Te glass system. Thin film crystallization studies of Ge-Se by Dove, Chang and Molnar[11] also show selenium to be the crystallizing species. Figure 3 shows the relative area under the selenium 101 peak as a function of heat treatment time, giving a curve proportional to V_v, the volume of crystallites. It is seen that $GeSe_{1.5}$ essentially is fully crystallized after 60 minutes at 450°C. These results corroborate nicely the slow transitions observed in the DCA traces.

Application of a simple Scherrer treatment[12] to the previous data gives the size of the crystallites that form as a function of heat treatment. These results also are shown in Figure 3. The close similarity in the two curves of Figure 3 shows that at this level crystallization is largely controlled by crystal growth and not by simultaneous nucleation and crystallization. A more rigorous Line Profile Analysis is presently underway as is the extension of the crystallization experiments to other temperatures and to other compositions in the Ge-Se system.

The results presented here pose an interesting contrast to the data of Takemori, Roy and McCarthy[4] on the Ge-Te system. They found that the glass formation region in Ge-Te is much

narrower than that for Ge-Se reported here; furthermore, crystallization in the Ge-Te system occurs at much lower temperatures than for Ge-Se. In both cases the chalcogenide constituent crystallizes preferentially. Ge-Se does not show the gross diphasic structure as has been reported for germanium-tellurium. In the Ge-Se system the crystallization temperature increases with increasing Se concentration, while in Ge-Te it is reported to peak and then decrease with increasing Te.[4]

It has been found that films of germanium-selenium and germanium-tellurium show similar structural features.[11] However, this study has shown that the crystallization kinetics of the two systems are markedly different and these differences must be considered in any potential use of materials in the Ge-Se system.

Bibliography

1. Liu Chun-hua, A. S. Pashinkin and A. V. Novoselova, Dok. Akad. Nauk SSSR, 146 [5], 1092 (1962).

2. V. A. Khar'yuzov and K. S. Evstropiev, Optiko-mekhanicheskaya Promyshlennost, 10, 17 (1961).

3. Liu Chun-Hua, A. S. Pashinkin and A. V. Novoselova, Russ. J. Inorg. Chem., 7, 1117 (1962).

4. T. Takemori, R. Roy and G. J. McCarthy, Mat. Res. Bull., 5, 529 (1970).

5. P. Duwez and R. H. Willens, Trans. Met. Soc. AIME, 227, 362 (1963).

6. W. B. Shook, paper presented at the 73rd Annual American Ceramic Society meeting, Chicago, Illinois, April 26-29, 1971.

7. L. Ross and M. Bourgen, Can. J. Chem., 47, 2555 (1969).

8. S. G. Karbanov, V. P. Zlomanov and A. V. Novoselova, Vestn. Mosk. Univ. Khim. 23, 96 (1968).

9. G. Z. Vinogradova, S. A. Dembovskii and N. B. Sivkova, Russ J. Inorg. Chem., 13, 1051 (1968).

10. S. A. Dembovskii, G. Z. Vinogradova and A. S. Pashinkin, Russ. J. Inorg. Chem., 10, 903 (1965).

11. D. B. Dove, J. Chang and B. Molnar, to be published in J. Non-Cryst. Solids (this issue).

12. B. D. Cullity, Elements of X-Ray Diffraction, Addison-Wesley Publishing Co., Reading, Mass., 1956, p. 99.

Figure Captions

Figure 1 - Scanning electron micrograph of $GeSe_4$ at 1,400X.

Figure 2 - Crystallization temperatures of Ge-Se as determined by Direct Calorimetric Analysis.

Figure 3 - Relative area of characteristic x-ray peak for crystallizing $GeSe_{1.5}$ as a function of heat treatment time (triangles, left scale). Size of crystallites of $GeSe_{1.5}$ as a function of heat treatment time (circles, right scale).

Figure 1

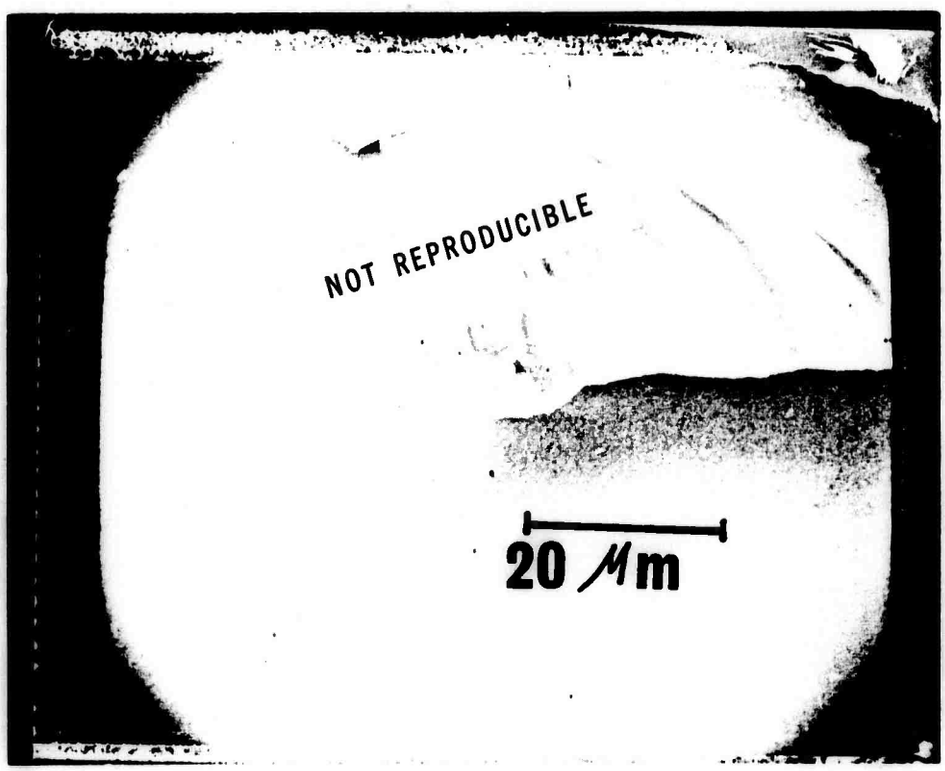

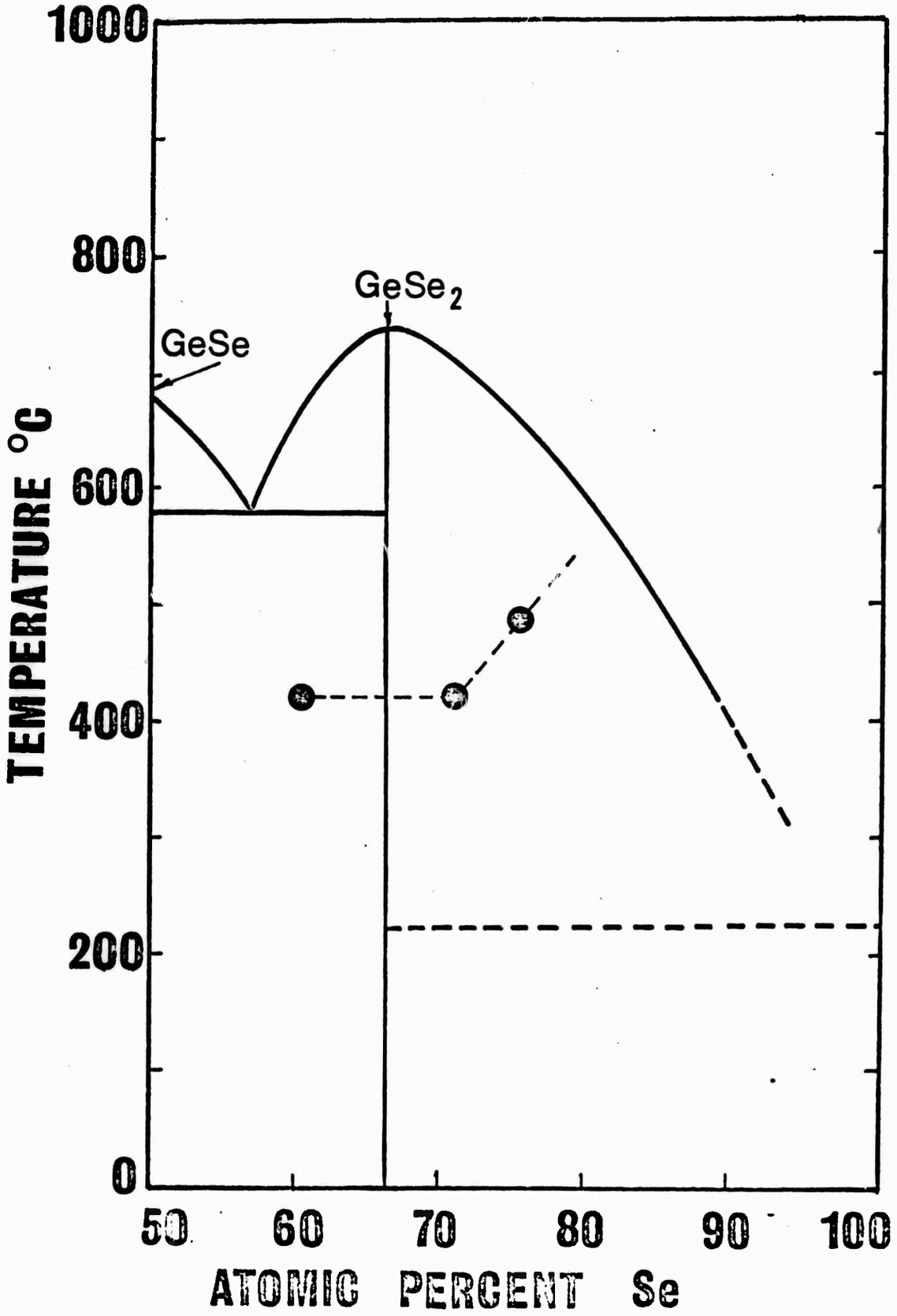
1000
800
600
400
200
0
TEMPERATURE °C
GeSe
GeSe2
50
60
70
80
90
100
ATOMIC PERCENT Se

LOCAL ORDER AND MICROSTRUCTURE OF GERMANIUM CHALCOGENIDE FILMS

by

D. B. Dove, J. Chang and B. Molnar

Department of Metallurgical and Materials Engineering
University of Florida, Gainesville, Florida 32601

Amorphous films of nominal composition $GeTe_2$ have been observed by energy filtered electron diffraction and by electron microscopy. The diffracted intensity curves may vary from region to region within a film and changes may be brought about by electron beam heating, giving rise to observable changes in the radial distribution functions. Gross features are not apparent in the electron micrographs and glassy phase separation if it exists in these films must be restricted to a very fine scale (20 A or less). Similar effects have been observed in a variety of other telluride and also selenide films.

1. INTRODUCTION

The systems Ge_xTe_{1-x} and Ge_xSe_{1-x} are characterized by their ability to form glasses when chalcogen rich compositions are quenched from the melt; films formed by vapor deposition however are amorphous over almost the entire compositional range when formed on substrates at room temperature. Previous work on telluride films by Bienenstock and collaborators,[1,2] and others,[3,4] has shown that structural models in which Ge and Te possess four fold and two fold valencies respectively are consistent with the experimental radial distribution functions (rdfs). Mikolaichuk and Kolgut[5] on the other hand report the local order of amorphous GeTe and GeSe films to correspond to the crystalline compounds in which nearest neighbor distances are expanded and an average coordination as high as 6 applies.

In the present work electron diffraction and electron microscopic observations on films of (nominal) composition $GeTe_2$ are described. This is part of a systematic study of films of a variety of compositions including GeSe, $GeSe_2$, $GeSe_4$, GeTe, $GeTe_2$, and $GeTe_4$ that will be reported more fully at a later date.

2. EXPERIMENTAL PROCEDURES

Thin, 200 A, amorphous films were prepared in a vacuum of 10^{-5} to 10^{-6} torr by flash evaporation of finely powdered bulk $GeTe_2$ onto substrates of mica and rock salt held at room temperature. The films were floated off of the substrates under water and were picked up on 1000 line copper mesh for examination by electron diffraction and electron microscopy. The electron diffraction system employs electronic recording and an electrostatic filter to remove inelastically scattered electrons.[6,7]

3. Results

Radial Distribution Analysis

Figure 1 shows curves of intensity of elastically scattered electrons versus scattering parameter s, where $s = 2 \sin \theta/\lambda$, 2θ is the angular deviation of the electron beam and λ is the effective electron wavelength. Curves a, b and c were obtained from different regions of a $GeTe_2$ film. Curve a is similar to those reported previously for GeTe and for Ge_xTe_{1-x} films generally. It was found that the above films were quite sensitive to exposure to the electron beam in the diffractometer and it was necessary to keep the beam to very low intensity to avoid changes in the films. The effect of the beam was to change the curve from a particular region in the sequence a to b to c. The reverse process was never observed. In the diffractometer the current density at the specimen is several orders of magnitude smaller than in the electron microscope; however, approximately half of the beam energy (45 kv, $\sim$ 1μA) is absorbed in the support mesh and some small heating of the specimens must occur. Experiments with molybdenum mesh are in progress to examine the possibility of systematic effects that may be correlated with mesh material.

The intensity curves were run to beyond s = 2.2 and were numerically analyzed to obtain the rdfs shown in Fig. 2. The curves were smoothed at low r values by a procedure described by Kaplow and collaborators[8] but extrapolation of data to high s values was not carried out. The peaks of the rdfs shown are broadened by the finite data range employed, and the symbol $\rho'(r)$ is employed to indicate that deconvolution to obtain true peak widths for the distributions has not been carried out.

The nearest neighbor distance obtained from $\rho'(r)$ curves was 2.55 Å for curve a increasing to 2.65 Å for curve c. Area under the first peak of the rdf curve $4\pi r^2\rho(r)$ increased from 2.3 to 3.7 and an extra peak overlapping the primary peak appears at approximately 3.0 Å. It is to be emphasized that this represents a very general trend that has been observed in both telluride and selenide films of various compositions, the numerical values varying of course from case to case. In films of $GeSe_{2.4}$ the nearest neighbor distance shifts from 2.37 to 2.47 Å and peak area grew from 2.3 to 3.0 for a similar sequence of curves. An extra peak overlapping the first peak could be found at approximately 2.9 A.

Electron Microscopy

Examination of the films by microscopy has shown them to be devoid of gross features or the evident phase separation noted in bulk glasses by Roy and collaborators.[9] At the highest magnification some fine mottled contrast can typically be seen and inhomogeneities on a 20 A scale cannot be ruled out. Occasionally a few small crystallites could be found in the as deposited films although peaks were not apparent in the diffraction patterns. On a rare occasion a film was obtained in which a glassy microstructure could be discerned, which gave no special contrast in dark field pictures. The diffraction pattern was essentially as obtained for featureless films, i.e. as shown by curve a in Fig. 1

4. Discussion

The diffraction curves show that structural changes may be brought about in the amorphous chalcogenide films by both deposition conditions and exposure to electron beam heating. The effect seems to occur in both selenide and telluride films and is not restricted to

the $GeTe_2$ films described here. Induced changes appear to be irreversible, do not give rise to features easily observable in the electron microscope, and occur prior to the detection of a crystalline phase. The intensity curve labeled a appears to be most characteristic of untreated films and is similar to the results of the previous observations refered to above. The first peak in the rdf is taken to be a superposition of Ge-Te, Ge-Ge and Te-Te interatomic distances estimated at 2.54, 2.44, and 2.64 A respectively from Pauling's tetrahedral covalent radii,[10] in reasonable agreement with the experimental mean distance. The area under the peak consists of the sum of the coordination numbers appropriate to these bonds weighted by factors $f_{Ge}f_{Te}/F^2$, $f_{Ge}{}^2/F^2$ and $f_{Te}{}^2/F^2$ where f_{Ge},f_{Te} are the electron atomic scattering amplitudes at $s = 0$, $F^2 = (xf_{Ge} + (1-x)f_{Te})^2$, and x is the atomic fraction of Ge. The area under the peak is then readily estimated for widely varying models such as complete immixibility, random and ordered mixing. The result is that the expected area varies only slightly from a value of 2.5 providing 4 fold and 2 fold valencies are assumed for Ge and Te respectively. A glassy phase separation in which the 4 and 2 coordination numbers are conserved would therefore produce little change in the area of the first peak of the rdf but could possibly give rise to changes in other peaks. Interpretation of higher order peaks in the rdf is rendered difficult by the variety of interatomic separations that may arise when variations in bond angles may occur.

The changes observed in the rdfs in the present work are suggestive of structural effects involving a change in bond type. The additional peak at 3.0 corresponds to the Ge-Te interatomic distance in the high temperature phase of GeTe, although it has not been established that microcrystallites

of GeTe have formed in the films at this stage, while the change in first peak area may indicate a departure from 4 and 2 fold coordinations. The implications of the present results for the structure of amorphous chalcogenide films will be discussed at a later date.

ACKNOWLEDGMENT

The authors gratefully acknowledge the interest and support of AROD under contract ARPA DAHC09-70-C0024.

REFERENCES

1. A. Bienenstock, F. Betts and S. R. Ovshinsky, J. Non-Crystalline Solids 2, 347 (1970).
2. F. Betts, A. Bienenstock and S. R. Ovshinsky, J. Non-Crystalline Solids 4, 554 (1970).
3. P. Duwez, Trans. ASM 60, 607 (1967); H. L. Luo, Thesis, Cal Tech (1964).
4. D. B. Dove, M. B. Heritage, K. L. Chopra and S. K. Bahl, Appl. Phys. Letters 16, 138 (1970).
5. A. G. Mikolaichuk and A. N. Kolgut, Sov. Phys.-Cryst. 15, 294 (1970).
6. C. W. B. Grigson, Rev. Sci. Instr. 36, 1587 (1965).
7. D. B. Dove and P. N. Denbigh, Rev. Sci. Instr. 37, 1687 (1966).
8. R. Kaplow, S. L. Strong and B. L. Averbach, Phys. Rev. 138A, 1136 (1965).
9. T. Takamori, R. Roy and G. J. McCarthy, Matl. Res. Bull. 5, 529 (1970).
10. L. Pauling, The Nature of the Chemical Bond (Cornell Univ. Press, Ithaca, New York, 1960).

FIGURE CAPTIONS

Fig. 1 — Curves a, b and c are intensity profiles along a radius of the diffuse diffraction patterns from different regions of a flash evaporated $GeTe_2$ film. Inelastic background has been removed experimentally. Intensity zero has been shifted vertically for clarity.

Fig. 2 — Curves a, b and c are atomic radial distributions obtained from the corresponding curves of Fig. 1. The prime $\rho'(r)$ indicates that the peaks are termination broadened and do not reflect the actual widths appropriate to the films.

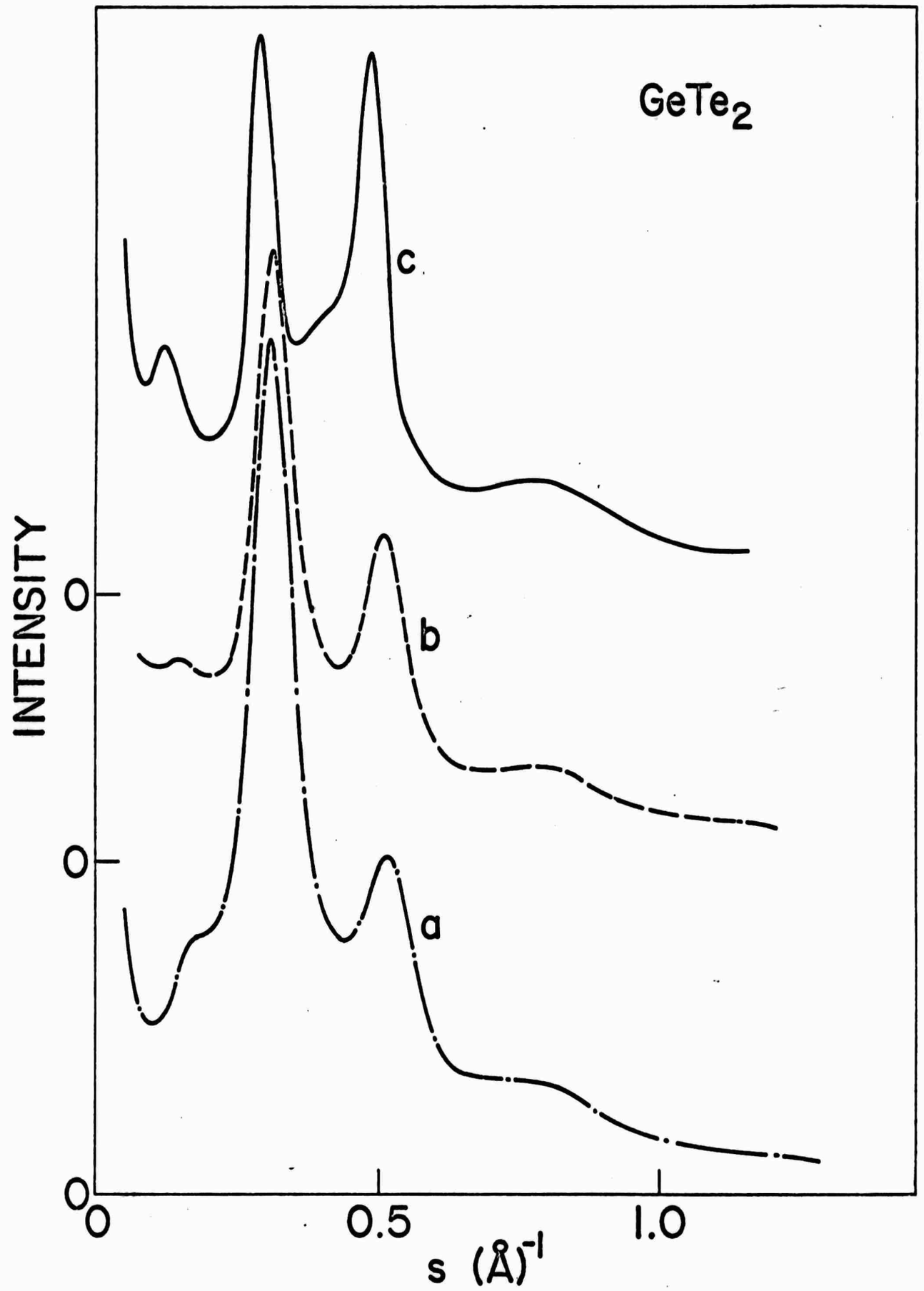
GeTe2
c
b
a
INTENSITY
0
0
0
0.5
1.0
s (Å)-1

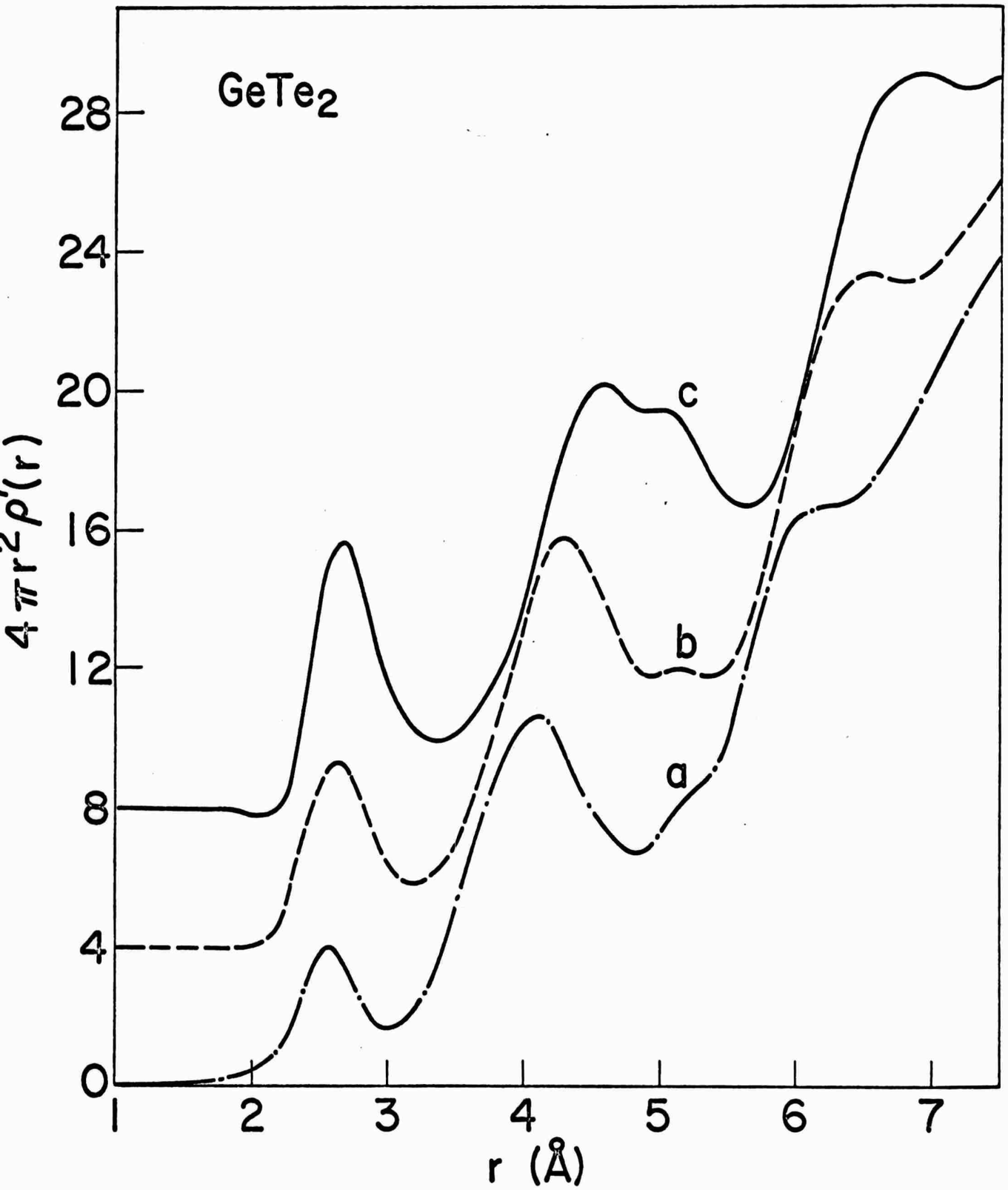
GeTe2
28
24
20
16
12
8
4
0
1
2
3
4
5
6
7
r (Å)
4πr²ρ'(r)
a
b
c

EFFECTS OF MICROSTRUCTURE ON THE RADIATION STABILITY OF AMORPHOUS SEMICONDUCTORS

By

L. L. Hench, A. E. Clark and H. F. Schaake

Introduction

Because of the structural randomness of amorphous semiconductors they offer the promise of radiation insensitive electronic properties. Studies have demonstrated that there is only minor alteration of the electrical properties of non-crystalline V_2O_5-P_2O_5 and K_2O-V_2O_5-P_2O_5 amorphous semiconductors at fast neutron fluences of 4×10^{17} nvt and γ-ray dosages of 1.2×10^8 rads.[1,2]

However, it has been shown for both oxide[2,3] and chalcogenide[4,5] amorphous semiconductors that structural heterogeneities are present in many compositional systems. The data indicate that heterogeneities result from: 1) microcrystallization during quenching of bulk or thin films; 2) glass-glass phase separation; 3) nucleation and growth of crystals from a glassy phase; and 4) compositional fluctuations. Can such structural heterogeneities influence the radiation sensitivity of these materials? Several recent reports[6-9] show chalcogenide thin film switching devices, which contain filamentary heterogeneities, are stable up to fluences of 10^{16} n/cm^2 and 3.3×10^7 R of fission γ-rays. However, heterogeneous vanadia

based amorphous semiconductors in bulk form exhibit marked changes in electronic behavior at fluences of 1 x 10^{17} nvt and above.[2,10]

Consequently, one objective of the present paper is to extend the range of the previous work by reporting the extent of radiation sensitivity of a 33 mole % KPO_3, 67 mole % V_2O_5 glass when crystallized to a large volume fraction, ~0.4. Secondly, a basis for selecting compositions for improved irradiation stability is suggested.

Experimental Procedure

The glasses were melted in air in Pt and melt cast at 900°C into graphite molds. The 1.8 cm diameter discs were heat treated at 288°C for 30.8 hours in air after polishing.[2] Previous studies[2,11,12] of thermal treatment of glasses in the K_2O-P_2O_5-V_2O_5 system have shown that a 90 Å phase separation is enhanced by a thermal treatment for 1/2 hour at 288°C. The matrix appears to order during heating with the D.C. conductivity increasing by 10^4. Longer treatments at 288°C result in the precipitation of P_2O_5-$2(V_2O_5)$ crystallites until at 30.8 hours ~0.4 volume fraction of crystals are present. D.C. conductivity increases during this process to a 25°C value of 5 x 10^{-3} $ohm^{-1}cm^{-1}$. Evaporated double guard ring gold electrodes were annealed at 150°C for 1/2 hour. Measurements were made as described elsewhere.[13]

Irradiation was done in the Wright-Patterson Air Force Base test reactor having a fast neutron flux capability of 1.5 x 10^{13} n/cm^2 (>0.1 meV). Cadmium wrapping protected the gold electrodes. The sample temperature was maintained near 50°C during the run. Samples held at 50°C without radiation showed no property changes.

Results

The conductivity frequency dependence at 25°C of the 288°C/30.8 hour sample is shown in Fig. 1 before and after

cumulative exposures of 1.0×10^{17} nvt and 2.1×10^{17} nvt. The total conductivity first increases with nvt and then decreases. The conductivity increase is similar to that seen in the quenched and heat treated glasses previously studied.[1,2] The decrease in σ_{tot} at higher nvt was also observed in the 288°C/0.5 hour glasses at nvt $>2 \times 10^{17}$.[11]

The A.C. conductivity, $\sigma_{AC}(\omega) = \sigma_{meas}(\omega) - \sigma_a$, before and after irradiation is shown to be a function of ω^2 in Fig. 2. σ_{AC} of the multiphase material is considered to be the average of the A.C. conductivities of the phases and σ_o is defined as shown in Fig. 1. There is no detectable $\omega^{0.8}$ conductivity in any samples. A fluence of 1×10^{17} nvt causes the ω^2 conductivity to increase by a factor of 2. Further radiation to 2.1×10^{17} results in no change in the ω^2 conductivity, but does introduce a new low frequency dependence of $\omega^{1.3}$. The behavior of σ_o is as follows:

Pre-irradiation	$\sigma_o = 5.2 \times 10^{13}$ ohm^{-1}cm^{-1}
1×10^{17} nvt	$\sigma_o = 6.8 \times 10^{-3}$ ohm^{-1}cm^{-1}
2.1×10^{17} nvt	$\sigma_o = 5.9 \times 10^{-3}$ ohm^{-1}cm^{-1}

The loss angle of the material is greatly increased with 1×10^{17} nvt, as shown in Fig. 3. After 2.1×10^{17} a large loss peak appears in the tanδ-frequency plot.

Discussion

The results show that fast neutron irradiation affects: 1) σ_{DC} magnitude, 2) σ_{AC}-ω dependence, and 3) tanδ peaks. The increases in σ_{DC} may be attributed to an increase in mobile carrier concentration due to γ-ray ionization processes. As shown[1] γ-ray dosages of 1.2×10^8 rads produce a 15% increase in σ_{DC} in V_2O_5-P_2O_5 glasses. A disordering of the glass matrix, reversing the thermal treatment effects, is proposed for the conductivity decrease after 2.1×10^{17} nvt. The matrix

disordering would isolate high conductivity crystallites providing barriers suitable for Maxwell-Wagner-Willars (MWS) peaks which appear at 2.1×10^{17} nvt.

Explanations for the variations in ω dependence are more speculative. Localized state pairs may be present in the heterogeneous material which would result in an ω^2 dependence via adiabatic hopping.[14] The irradiation may produce a sufficient redistribution of nearest neighbors, as reported for fused silica[15] that a complex $\omega^{1.3}$ behavior produced. It is also possible that excess carrier generation or other effects could produce an electrode barrier behavior altering the dependence.

The nvt threshold for degradation of electrical properties related to heterogeneities is plotted as a function of softening point* for heterogeneous K_2O-V_2O_5-P_2O_5 and Li_2O-$2SiO_2$ glasses[19,16] in Fig. 4. In both systems the onset of changes in the MWS loss peaks is taken as nvt threshold. The threshold for significant structural change of fused silica and crystalline quartz is used for the SiO_2 data point[17] since partially devitrified SiO_2 has not been studied.

Figure 4 shows that as the softening point increases the threshold for damage to heterogeneities increases. This is reasonable since the softening point is related to the magnitude of bond ene.gies in the material. Thus a larger cumulative number of events is requires to damage the boundaries and crystallites of higher bond energy materials.

Extrapolation of the plot in Fig. 4 indicates that damage to ordered heterogeneities in chalcogenide systems, e.g., on-state filaments, may occur at $>5 \times 10^{16}$ nvt. The higher threshold for glasses with larger crystallites[10] indicates that the damage threshold of devices may be increased as the on-state filament diameter is increased. The correlation

---

*Although other criteria might be used for comparison, e.g., T_x, T_g, T_m, an advantage of the softening point is that it is sensitive to previous thermal history and heterogeneities in the material.

shown in Fig. 4 suggests that another way to improve radiation tolerance is to increase the softening points of amorphous semiconductors by compositional modification.

Acknowledgements

The authors would like to gratefully acknowledge the financial support of the Advanced Research Projects Agency of the Department of Defense monitored by the ARCRL under Contract No. F-19628-68-8-0058 and AROD Contract No. DAHC04-70-C-0024.

The continuing assistance of Lt. B. Wilson, Major F. Buoni, and Mr. A. Bauer of the Wright-Patterson Reactor Facility is also acknowledged.

BIBLIOGRAPHY

1. L. L. Hench and G. A. Daughenbaugh, J. Nuclear Materials, 25, 58-63 (1968).

2. L. L. Hench, J. Non-crystalline Solids, 2, 250-277 (1970).

3. D. L. Kinser, J. Electrochem. Soc., 117 [4] 546 (1970).

4. B. G. Bagley and W. R. Northover, J. Non-crystalline Solids, 2, 161 (1970).

5. This Conference, papers HB1, HB3, BA4, DB4, BA5.

6. S. R. Ovshinsky, E. J. Evans, D. L. Nelson and H. Fritzsche, "Radiation Hardness of Ovonic Devices," IEEE Trans. on Nuclear Science, December 1968.

7. a. R. R. Shanks, J. H. Helbers and D. L. Nelson, "Ovonic Computer Circuits Development," Technical Report AFAL-TR-69-309, June 1970.

   b. R. R. Shanks, D. L. Nelson, R. L. Rowler, H. C. Chambers and D. J. Neihaus, "Radiation Hardening Circuitry Using New Devices," Technical Report AFAL-TR-70-15, March 1970.

8. E. J. Evans, "A Feasibility Study of the Applications of Amorphous Semiconductors to Radiation Hardening of Electronic Devices," Picatinny Arsenal Technical Report 3698.

9. R. B. Nicolaides and W. Doremus, this Conference, paper HB8.

10. L. L. Hench, W. D. Tuohig and A. E. Clark, "Fast Neutron Effects in Glass-Ceramics and Amorphous Semiconductors," Ceramics in Severe Environments Conference, North Carolina State Univ., December 1970, Kreigl and Palmour, eds., Plenum Press.

11. L. L. Hench, D. L. Kinser and S. R. Bates, "Microstructural Effects in a K_2O-V_2O_5-P_2O_5 Amorphous Semiconductor,"to be published.

12. A. Fuwa, "Electrical Properties of Glasses and Crystals in the K_2O-V_2O_5-P_2O_5 System," M.S. Thesis, University of Florida, 1970.

13. L. L. Hench, "Dielectric Relaxation in Materials Analysis," Society of Aerospace Materials and Process Engineers, Proceedings of the 14th Annual Symposium, Cocoa Beach, November 1968; reprinted as Technical Paper 428, Engineering Progress at the University of Florida, Gainesville.

14. H. F. Schaake, "Heterogeneous Semiconducting Glasses," in Physics of Electronic Ceramics, L. L. Hench and D. B. Dove, eds., M. Dekker, Inc. 1971.

15. C. V. Gokularathnam, "X-ray Diffraction Studies of Structural Changes in Vitreous SiO_2," Ph.D. Thesis, University of Florida, 1971.

16. W. D. Tuohig and L. L. Hench, J. Nuclear Materials, 31, 86-92 (1969).

17. H. Bale, R. E. Shepler and G. W. Gibbs, J. Appl. Phys., 41 [1] 241 (1970).

Figure Captions

1 Effect of fast neutron irradiation on the total conductivity of a 33 mole % K_2PO_3 - 67 mole % P_2O_5 glass previously heat treated for 30.8 hours at 288°C.

2 Change in A.C. conductivity of a heat treated vanadia-phosphate glass with fast neutron irradiation.

3 Influence of fast neutron irradiation on the loss tangent of a partially crystallized vanadia-phosphate glass.

4 A correlation between the dilatometric softening point of glasses with the threshold fluence for fast neutron structural changes.

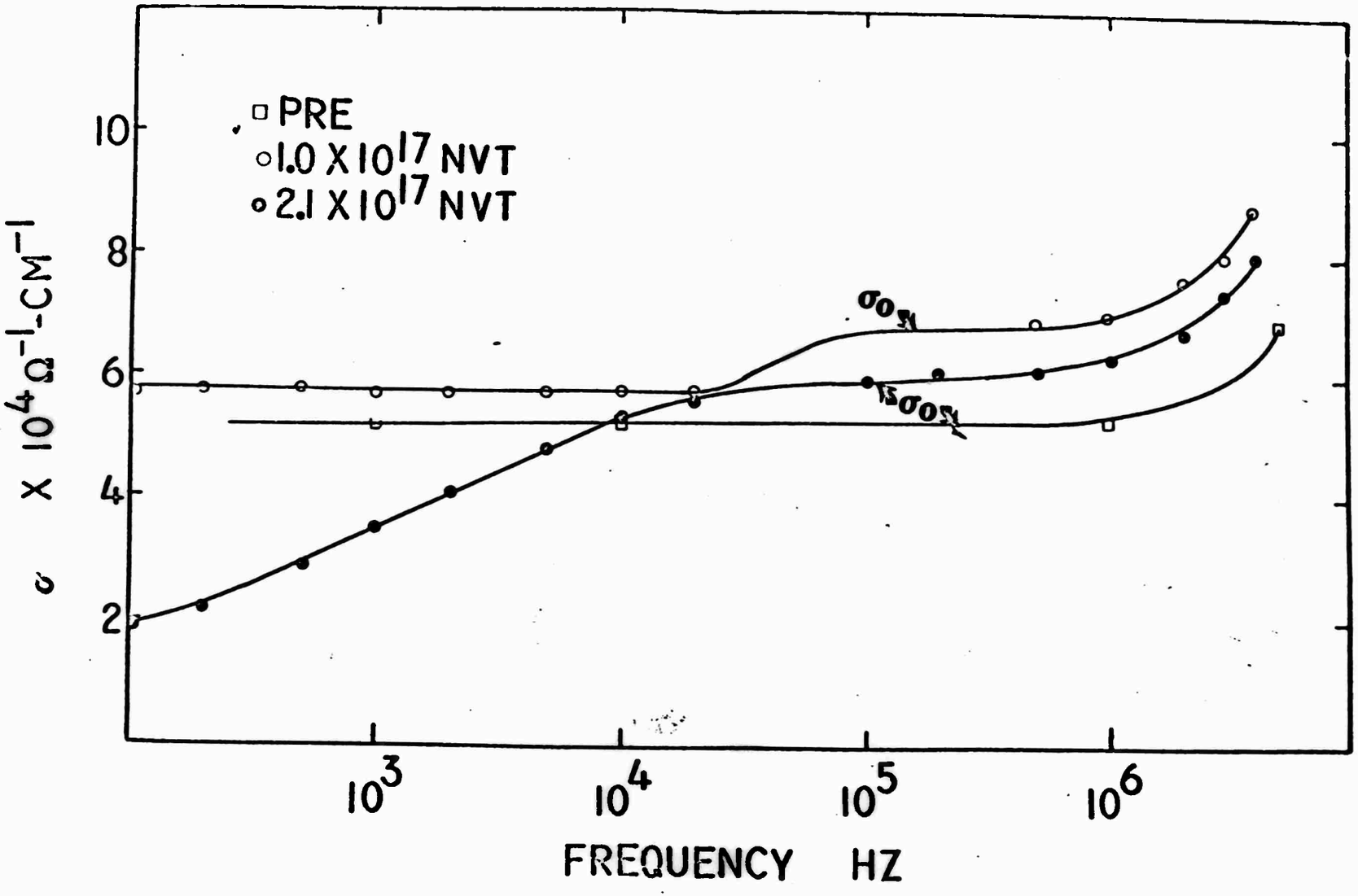
□ PRE
○ 1.0 X 10^17 NVT
○ 2.1 X 10^17 NVT
σ X 10^4 Ω^-1-CM^-1
10
8
6
4
2
10^3
10^4
10^5
10^6
FREQUENCY HZ

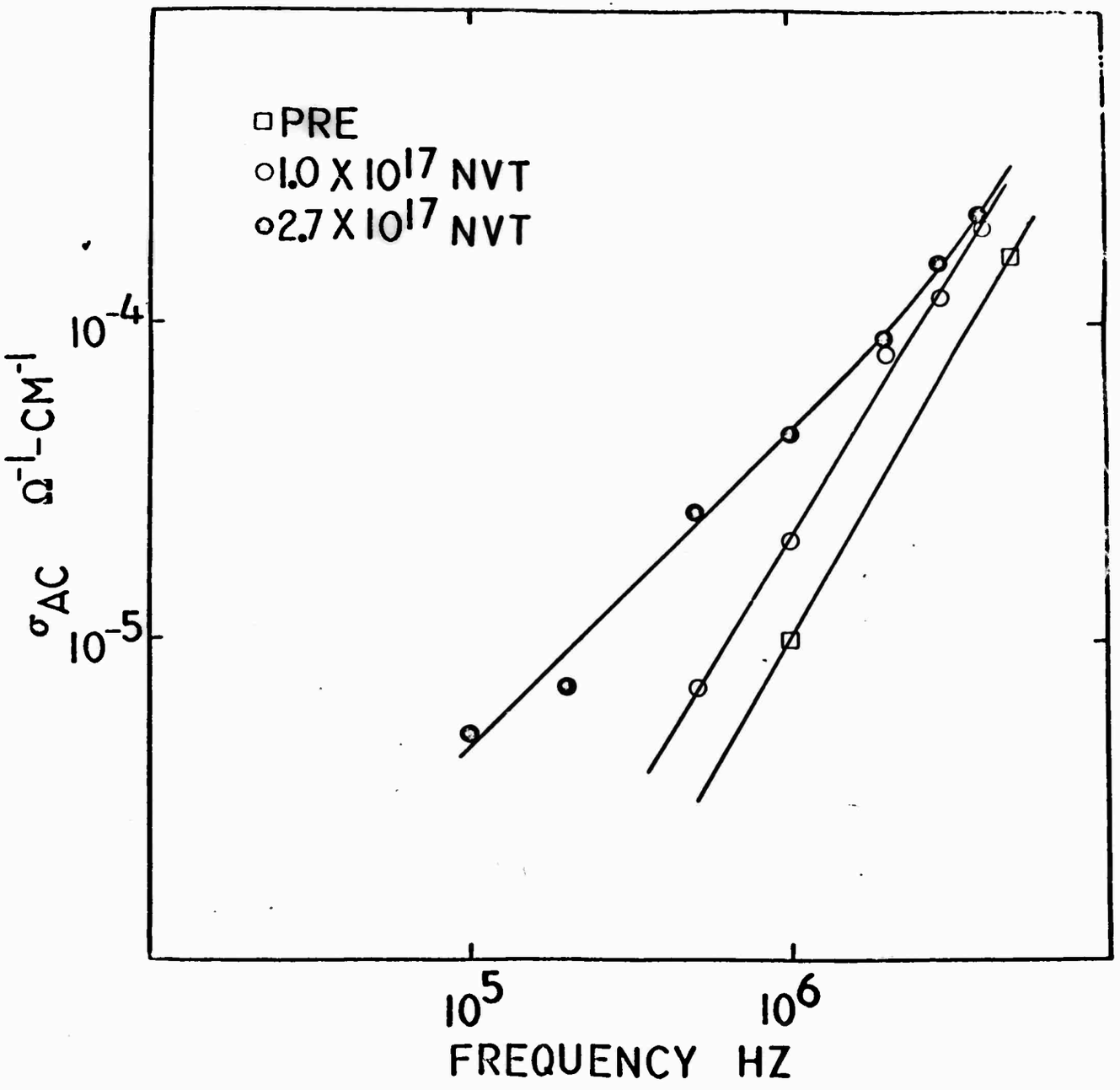
□PRE
○1.0 X 10^17 NVT
○2.7 X 10^17 NVT
σAC Ω^-1-CM^-1
10^-4
10^-5
10^5
10^6
FREQUENCY HZ

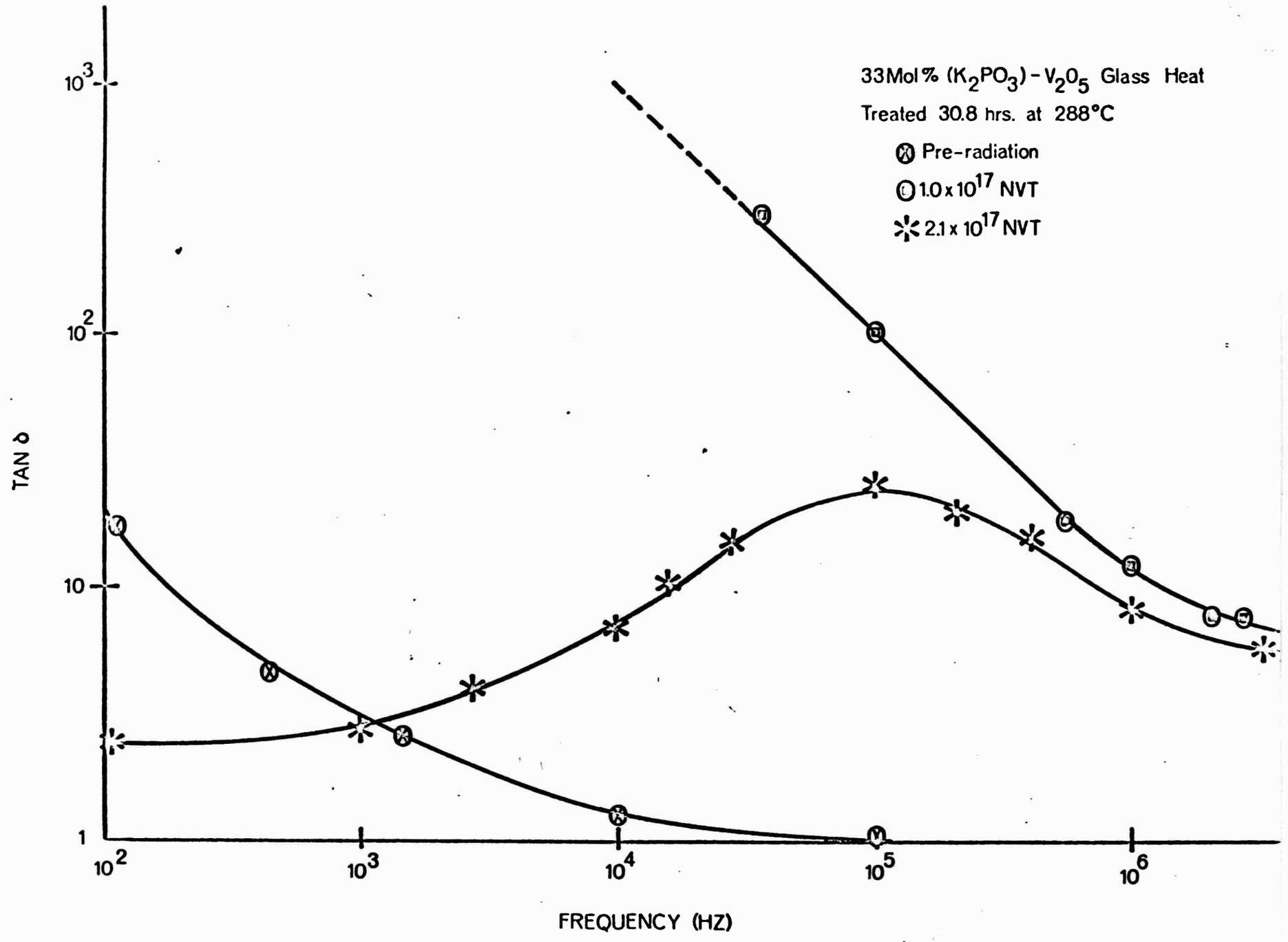
33Mol% (K_2PO_3) - V_2O_5 Glass Heat
Treated 30.8 hrs. at 288°C
Pre-radiation
1.0 x 10^{17} NVT
2.1 x 10^{17} NVT
TAN δ
10^3
10^2
10
1
10^2
10^3
10^4
10^5
10^6
FREQUENCY (HZ)

Glass Softening Point vs Fast Neutron Damage Threshold for Structural Change (nvt)

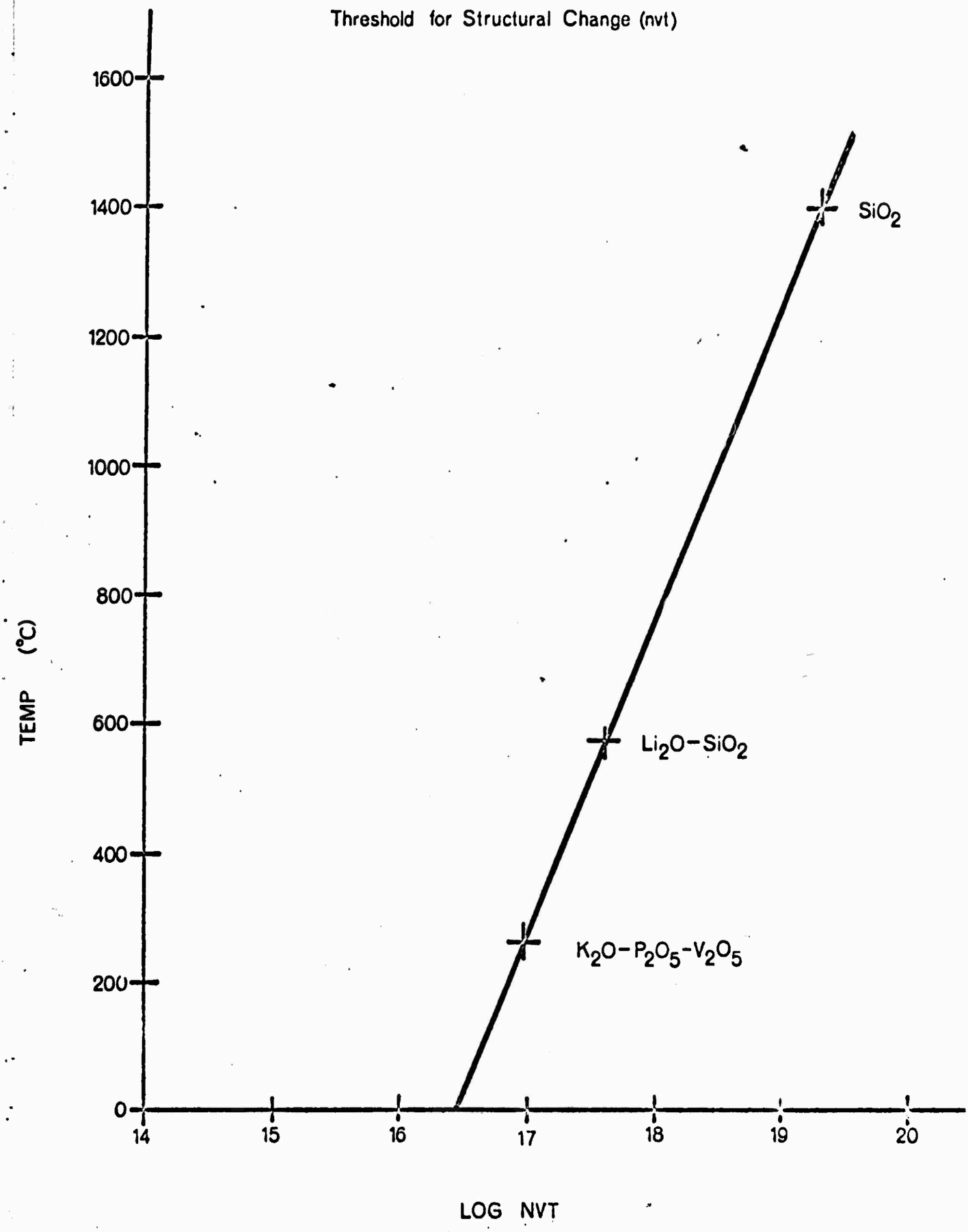

Abstract of Thesis Presented to the Graduate Council of the University of Florida in Partial Fulfillment of the Requirements for the Degree of Master of Science in Engineering

STRUCTURE OF AMORPHOUS Ge-Se THIN FILMS

By

Bernard J. Molnar

August, 1971

Chairman: Dr. D. B. Dove
Major Department: Metallurgical and Materials Engineering

The intensity profiles across the electron diffraction patterns of amorphous thin films of $GeSe_{0.7}$ and $GeSe_{2.4}$ have been directly recorded with electrostatic rejection of inelastically scattered electrons. Radial distribution analysis of the $GeSe_{0.7}$ intensity curves indicates that the local atomic order of these films differs from the distorted rocksalt structure of bulk crystalline GeSe. Radial distribution studies also indicate a change in the structure of $GeSe_{0.7}$ and $GeSe_{2.4}$ films as they are heated with an electron beam. A tentative model is presented in which these structural changes are explained in terms of a separation of the film microstructure into several amorphous phases.

CHAPTER I

INTRODUCTION

During the last few years there has been a greatly increased research effort directed toward the study of both the structure and the optical, electronic, and thermal properties of amorphous solids. The term "amorphous" solid is used to designate any solid which lacks both the long-range atomic order of a crystalline material and the short-time fluidity of a liquid.[1] One general class of amorphous solids consists of those materials which assume a disordered structure when rapidly cooled from their high-temperature liquid or gaseous state. At high enough cooling rates atomic motions are restricted and the ordering required to form a crystalline phase does not take place. The chalcogenide glasses and the amorphous thin films made from these glasses compose one group of amorphous solids of current research interest. The chalcogenide glasses consist of a combination of one or more of the chalcogen elements selenium, tellurium, and sulfur, with one or more of the Group IV or Group V elements such as germanium, bismuth, arsenic, silicon, phosphorous, and antimony. Certain thin-film chalcogenides have already found successful use as infrared photodetectors[2] and solid-state switches.[3]

Although no long-range atomic order exists in amorphous thin films, some degree of short-range (local) order is present. Such films also show at least some microstructural features when observed by high resolution electron microscopy. Many amorphous chalcogenides, e.g., As_2S_3,[4] possess a local order which is the same as that found in their crystalline state. Some materials, however, such as GeTe,[5] possess a local order in the amorphous state which differs from that found in the crystalline. Electron transport theories postulated for amorphous solids often assume perfect short-range order, and then proceed to introduce the perturbation on the band structure caused by the presence of long-range disorder.[6] It is therefore of fundamental interest to determine the specific local order present in chalcogenide thin films and to ascertain whether the disorder in these films is spatially homogeneous or whether density and/or composition fluctuations are present.

One method which can be used to obtain information regarding the local order in amorphous films is the analysis of the diffuse electron or x-ray diffraction patterns of these films. Transmission electron diffraction patterns of amorphous films consist of very diffuse concentric rings (or halos), as opposed to the very sharp rings found in the diffraction patterns of crystalline films. By measuring the intensity profile along a radius of the diffuse ring pattern, an interference function may be obtained. In the

case of thin films of a single element, a numerical Fourier transform of this interference function yields a measure of the radial distribution function (RDF), which provides a spectrum of prominent interatomic distances in the specimen in addition to an estimate of the atomic coordination number. In the case of thin films of materials composed of more than one element, the transform of the interference function yields a sum of convolution products, each of which consists of a component of the RDF convoluted with a component of a quantity which is a function of the scattering factors of the elements composing the film. This convoluted radial distribution function, or CRDF, is unfortunately more difficult to interpret than the RDF. It is therefore most desirable, when possible, to deconvolute the CRDF and find the components of the RDF.

The two chief purposes of the work of this thesis were to examine the CRDF's and microstructure of vapor-deposited Ge-Se thin films of two different compositions in order to 1) obtain information about the local atomic order in amorphous Ge-Se films, and 2) investigate any structural changes which occur in these films when they are heated with an electron beam. A direct recording scanning electron diffraction system which can reject inelastically scattered electrons was used to obtain the electron diffraction data. This data was computer processed to yield the CRDF's. Transmission electron microscopy was employed to examine the microstructure of these films.

In the following chapter the theory of electron scattering from amorphous binary thin films is presented and the origin and significance of the RDF and CRDF is examined. In Chapter III the experimental procedures and apparatus are described. The experimental results are presented in Chapter IV. An analysis of the CRDF's and a discussion of the experimental results comprise Chapters V and VI, respectively. The conclusions and suggestions for future work are presented in Chapter VII.

CHAPTER II

ELECTRON DIFFRACTION THEORY AND ORIGIN OF THE RDF

The theoretical foundation for the understanding of diffraction from disordered materials was laid by Debye,[7] Debye and Menke,[8] and Zernike and Prins in their analysis of diffraction by gases and liquids.[9] Detailed discussions of scattering from amorphous materials may be found in several modern sources, such as the texts by Guinier[10] and Warren.[11]

A Fourier transform of the interference function obtained from the diffraction pattern of an elemental amorphous material will yield a measure of the radial distribution function (RDF) of the material. The RDF provides a spectrum of characteristic bond lengths in the material in addition to an estimate of the number of atoms surrounding a randomly-selected reference atom.

It has been pointed out by Pings and Waser[12] and by Dove[13] that the diffraction intensity data from amorphous materials composed of more than one element may be analyzed using the same Fourier transform techniques employed in the single element case, without making simplifying assumptions regarding the scattering factors of the elements. The

discussion of the RDF analysis of amorphous binary thin films which follows in this chapter is an elaboration on Dove's presentation.

Consider a region of a thin film of material consisting of an array of N atoms located at positions $\underset{\sim}{r}_1$, $\underset{\sim}{r}_2$, ... $\underset{\sim}{r}_n$ with respect to an arbitrary origin, and having the respective atomic scattering factors f_1, f_2, ... f_n. If a beam of parallel monochromatic electrons is directed onto these N atoms, the electrons will be scattered by the varying electrostatic potential set up by the positively charged atomic nuclei and their negatively charged electron clouds. Let $\underset{\sim}{S}_o$ and $\underset{\sim}{S}$ be unit vectors directed along the incident beam and along the direction of observation respectively as shown in Fig. 1. The intensity of coherent radiation scattered in a direction parallel to $\underset{\sim}{S}$ is given by

$$I(s) = \sum_{j=1}^{N} f_j^2 + \sum_{\substack{p=1 \\ p\neq q}}^{N} \sum_{q=1}^{N} f_p f_q \exp(2\pi i \underset{\sim}{s}\cdot\underset{\sim}{r}_{pq}) \quad (2.1)$$

where $\underset{\sim}{s} = \frac{\underset{\sim}{S}-\underset{\sim}{S}_o}{\lambda}$ and $s = |\underset{\sim}{s}| = \frac{2\sin\theta}{\lambda}$

$\underset{\sim}{r}_{pq}$ = vector from atom p to atom q

λ = wavelength of incident and scattered radiation

2θ = angle of deflection of electron beam

When dealing with amorphous materials the assumption is often made that any given atomic separation $r_{pq} = |\underset{\sim}{r}_{pq}|$ occurs with equal probability in all directions. In this case, Eq. (2.1) may be averaged over all orientations to

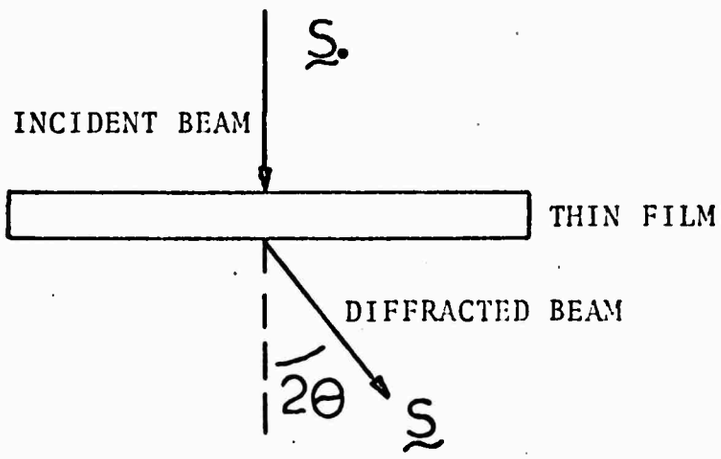

Figure 1. Definition of unit vectors $\underset{\sim}{S}_o$ and $\underset{\sim}{S}$ and scattering angle 2θ.

give the Debye Equation:

$$I(s) = \sum_{j=1}^{N} f_j^2 + \sum_{\substack{p=1 \\ p\neq q}}^{N} \sum_{q=1}^{N} f_p f_q \frac{\sin(2\pi s r_{pq})}{2\pi s r_{pq}} \qquad (2.2)$$

Consider the binary compound A_mB_n. Let $x_1 = m/(m+n)$ and $x_2 = n/(m+n)$ represent the atomic fractions of elements A and B, where subscript "1" designates A-type atoms and "2" designates B-type atoms. Let f_1 and f_2 be the electron scattering factors for these elements. We may now define the following terms:

ρ_o = density of atoms in A_mB_n

$\bar{\rho}_1$ = mean density of A-type atoms = $x_1\rho_o$

$\bar{\rho}_2$ = mean density of B-type atoms = $x_2\rho_o$

$4\pi r^2\rho_{12}(r)dr$ = number of B-type atoms in the spherical shell between r and r+dr surrounding a randomly-selected A-type atom [similar definitions follow for $\rho_{11}(r)$, $\rho_{22}(r)$ and $\rho_{21}(r)$].

$$\rho(r) = \sum_{i=1}^{2} \sum_{j=1}^{2} x_i\rho_{ij}(r)$$

$4\pi r^2\rho(r)$ = Radial Distribution Function (RDF).

Using the above definitions and considering only two-element materials, Eq. (2.2) may be rewritten as

$$I(s) = N \sum_{j=1}^{2} x_j f_j^2 + N \sum_{i=1}^{2} \sum_{j=1}^{2} x_i f_i f_j \int_o^\infty 4\pi r^2[\rho_{ij}(r) - \bar{\rho}_j + \bar{\rho}_j] \frac{\sin(2\pi s r)dr}{2\pi s r} \qquad (2.3)$$

The term $(+\bar{\rho}_j)$ included within the integral in Eq. (2.3) arises from the small angle scattering contribution to the diffracted intensity. Since this contribution is usually lost in the edge of the undeflected beam and is hence unobservable, the $(+\bar{\rho}_j)$ term will be omitted in all following expressions.

Equation (2.3) can be expanded to give

$$I(s) = N[x_1 f_1^2 + x_2 f_2^2] + Nx_1 f_1^2 \int_o^\infty 4\pi r^2 [\rho_{11}(r) - \bar{\rho}_1] \frac{\sin(2\pi sr)}{2\pi sr} dr$$

$$+ Nx_1 f_1 f_2 \int_o^\infty 4\pi r^2 [\rho_{12}(r) - \bar{\rho}_2] \frac{\sin(2\pi sr)}{2\pi sr} dr$$

$$+ Nx_2 f_2 f_1 \int_o^\infty 4\pi r^2 [\rho_{21}(r) - \bar{\rho}_1] \frac{\sin(2\pi sr)}{2\pi sr} dr$$

$$+ Nx_2 f_2^2 \int_o^\infty 4\pi r^2 [\rho_{22}(r) - \bar{\rho}_2] \frac{\sin(2\pi sr)}{2\pi sr} dr \qquad (2.4)$$

Let f^2 be a normalization function, typically chosen to be

$$f^2 = (x_1 f_1 + x_2 f_2)^2 \quad . \qquad (2.5)$$

By defining $i(s) = [I(s) - N(x_1 f_1^2 + x_2 f_2^2)]/Nf^2$ and recalling that $\bar{\rho}_i = x_i \rho_o$, Eq. (2.4) may be rearranged to give

$$si(s) = \frac{f_1^2}{f^2} \int_{-\infty}^{\infty} r[x_1\rho_{11}(r)-x_1^2\rho_o] \sin(2\pi sr)dr$$

$$+ \frac{f_1 f_2}{f^2} \int_{-\infty}^{\infty} r[x_1\rho_{12}(r)-x_1x_2\rho_o] \sin(2\pi sr)dr$$

$$+ \frac{f_1 f_2}{f^2} \int_{-\infty}^{\infty} r[x_2\rho_{21}(r)-x_2x_1\rho_o] \sin(2\pi sr)dr$$

$$+ \frac{f_2^2}{f^2} \int_{-\infty}^{\infty} r[x_2\rho_{22}(r)-x_2^2\rho_o] \sin(2\pi sr)dr \qquad (2.6)$$

In practice, the experimentally-obtained intensity $I(s)$ must be divided by a normalization constant C_n. Since $I(s)$ approaches f^2 at large values of s, a plot of $I(s)/f^2$ vs s should execute a damped oscillation about a constant value equal to C_n. Such plots, however, are sometimes found to oscillate about a line with a positive slope. This undesirable effect is usually attributed[14] to the sample being of sufficient thickness to allow multiple scattering.

Using a double summation, Eq. (2.6) may be rewritten as

$$si(s) = \sum_{i=1}^{2} \sum_{j=1}^{2} si_{ij}(s)$$

$$= \int_{-\infty}^{\infty} \sum_{i=1}^{2} \sum_{j=1}^{2} \frac{f_i f_j}{f^2} r[x_i\rho_{ij}(r)-x_ix_j\rho_o] \sin(2\pi sr)dr \qquad (2.7)$$

where

$$si_{ij}(s) = \int_{-\infty}^{\infty} \frac{f_i f_j}{f^2} r[x_i\rho_{ij}(r)-x_ix_j\rho_o] \sin(2\pi sr)dr \qquad (2.8)$$

From now on, whenever the double summation symbol $\Sigma\Sigma$ is written it will be assumed that the limits of the sums are the same as those employed in Eq. (2.7).

The Fourier transform of si(s) can be written as

$$\int_{-\infty}^{\infty} \Sigma\Sigma \; si_{ij}(s) \exp(2\pi rs)ds \tag{2.9}$$

In order to evaluate expression (2.9), one may apply the Fourier Convolution Theorem to each of the terms of the double sum within the integral. The Convolution Theorem may be stated as follows: If $X_1(s)$ is the Fourier transform of $Y_1(r)$ and $X_2(s)$ is the transform of $Y_2(r)$, then

$$\int_{-\infty}^{\infty} X_1(s)X_2(s) \exp(2\pi sr)ds = \int_{-\infty}^{\infty} Y_1(t)Y_2(r-t)dt \tag{2.10}$$

Let's consider the term within the sum in which i = 1 and j = 2. In this case, we may let

$$X_1(s) = \frac{f_1 f_2}{f^2}$$

$$X_2(s) = \int_{-\infty}^{\infty} r[x_1\rho_{12}(r)-x_1x_2\rho_o][\cos(2\pi sr-i \sin(2\pi sr)]dr$$

$$Y_1(r) = \int_{-\infty}^{\infty} \frac{f_1 f_2}{f^2} [\cos(2\pi sr)+i \sin(2\pi sr)]ds$$

$$Y_2(r) = r[x_1\rho_{12}(r)-x_1x_2\rho_o] \tag{2.11}$$

Since $Y_2(r)$ is an odd function,

$$\int_{-\infty}^{\infty} Y_2(r) \cos(2\pi sr)dr = 0.$$

Since $X_1(s)$ is an even function,

$$\int_{-\infty}^{\infty} X_1(s) \sin(2\pi sr)ds = 0.$$

It follows that

$$X_2(s) = -i \int_{-\infty}^{\infty} r[x_1\rho_{12}(r)-x_1x_2\rho_o] \sin(2\pi sr)dr \qquad (2.12)$$

and

$$Y_1(r) = \int_{-\infty}^{\infty} \frac{f_1 f_2}{f^2} \cos(2\pi sr)ds \qquad (2.13)$$

Applying the Convolution Theorem, we obtain

$$\int_{-\infty}^{\infty} \frac{f_1 f_2}{f^2} \{-i \int_{-\infty}^{\infty} r[x_1\rho_{12}(r)-x_1x_2\rho_o]\sin(2\pi sr)dr\} \exp(2\pi sr)ds$$

$$= \int_{-\infty}^{\infty} \{\int_{-\infty}^{\infty} \frac{f_1 f_2}{f^2} \cos(2\pi ts)ds\}[r-t][x_1\rho_{12}(r-t)-x_1x_2\rho_o]dt \qquad (2.14)$$

It can be seen that the left-hand side of Eq. (2.14) is the product of (-i) times the Fourier transform of $si_{12}(s)$. This expression may be simplified by noting that since $X_1(s)X_2(s)$ is an odd function,

$$\int_{-\infty}^{\infty} X_1(s)X_2(s) \exp(2\pi sr)ds = i \int_{-\infty}^{\infty} X_1(s)X_2(s) \sin(2\pi sr)ds$$

The left-hand side of Eq. (2.11) may therefore be written as

$$\int_{-\infty}^{\infty} \frac{f_1 f_2}{f^2} \{\int_{-\infty}^{\infty} r[x_1\rho_{12}(r)-x_1x_2\rho_o] \sin(2\pi sr)dr\} \sin(2\pi sr)ds \tag{2.15}$$

In a similar manner expressions using si_{11}, si_{22}, and si_{21} may be obtained. These four expressions may then be added together to yield the following equation:

$$\int_{-\infty}^{\infty} si(s) \sin(2\pi sr)ds = 2 \int_{o}^{\infty} si(s) \sin(2\pi sr)ds$$

$$= 2 \Sigma\Sigma \int_{o}^{\infty} [r-t][x_i\rho_{ij}(r-t)-x_ix_j\rho_o]Q_{ij}(t)dt \tag{2.16}$$

where $$Q_{ij}(t) = \int_{-\infty}^{\infty} \frac{f_i f_j}{f^2} \cos(2\pi ts)ds \tag{2.17}$$

It should now be noted that in practice the upper limit of infinity shown for the integral in Eq. (2.16) cannot be realized due to the unfavorable signal to noise ratio which accompanies the diminuation of scattering intensity with increasing values of s. The integral must therefore be computed from zero to some value s_{max}. In order to simplify the calculation, one may retain the upper limit of infinity by evaluating the integral of si(s) multiplied by a step function g(s) defined as follows:

$$g(s) = \begin{cases} 1 \text{ for } -s_{max}<s<s_{max} \\ 0 \text{ otherwise} \end{cases} \tag{2.18}$$

Therefore,

$$2\int_0^{s_{max}} si(s)\,\sin(2\pi rs)ds = 2\int_0^{\infty} si(s)g(s)\,\sin(2\pi rs)ds \tag{2.19}$$

One of the effects of terminating the integral in Eq. (2.19) at s_{max} is the generation of peaks in a plot of the terminated integral vs r which are absent in a plot of the unterminated integral. These termination peaks may be reduced by multiplying si(s) by a termination function of the form $\exp(-\alpha s^2)$. The termination effect can be still further reduced by the application of a method due to Kaplow.[15]

If we let $h(s) = g(s)\exp(-\alpha s^2)$, then multiplication of si(s) by a termination function yields the following corrected form of Eq. (2.19):

$$2\int_0^{s_{max}} si(s)\,\exp(-\alpha s^2)\,\sin(2\pi rs)ds = 2\int_0^{\infty} si(s)h(s)\,\sin(2\pi rs)ds \tag{2.20}$$

Equation (2.16) may be rewritten in the following corrected form:

$$2\int_0^{s_{max}} si(s)\exp(-\alpha s^2)\sin(2\pi rs)ds = \Sigma\Sigma \int_{-\infty}^{\infty} [r-t]\, x_i\rho_{ij}(r-t)dt - \Sigma\Sigma \int_{-\infty}^{\infty} [r-t]\, x_i x_j \rho_o H_{ij}(t)dt \tag{2.21}$$

where $H_{ij}(t) = \int_{-\infty}^{\infty} \frac{f_i f_j}{f^2} h(s) \cos(2\pi ts)ds$ (2.22)

The integral $\int_{-\infty}^{\infty} [r-t]x_i x_j \rho_o H_{ij}(t)dt$ within Eq. (2.21) may be rewritten as follows:

$$x_i x_j \rho_o [r \int_{-\infty}^{\infty} H_{ij}(t)dt - \int_{-\infty}^{\infty} tH_{ij}(t)dt] \quad (2.23)$$

Since $tH_{ij}(t)$ is an odd function, the second integral in expression (2.23) is equal to zero. The first integral is equal to the area under a plot of $H_{ij}(t)$ vs t. Since the area under a curve is equal to the value of its cosine transform at the origin, the total area under $H_{ij}(t)$ is given by $f_i(o)f_j(o)/f^2(o)$. It follows that

$$\int_{-\infty}^{\infty} [r-t]x_i x_j \rho_o H_{ij}(t)dt = r\rho_o x_i x_j \frac{f_i(o)f_j(o)}{f^2(o)} \quad (2.24)$$

Summing Eq. (2.24) over i and j yields

$$r\rho_o \Sigma\Sigma' x_i x_j \frac{f_i(o)f_j(o)}{f^2(o)} = r\rho_o \frac{[x_1 f_1(o)+x_2 f_2(o)]^2}{f^2(o)} \quad (2.25)$$

Using the results of Eqs. (2.24) and (2.25), Eq. (2.21) may be rewritten as

$$2 \int_o^{s_{max}} si(s)\exp(-\alpha s^2)\sin(2\pi rs)ds$$

$$= \Sigma\Sigma \int_{-\infty}^{\infty} [r-t]x_i \rho_{ij}(r-t)dt - r\rho_o \frac{[x_1 f_1(o)+x_2 f_2(o)]^2}{f^2(o)} \quad (2.26)$$

If we let the convolution product of any two functions f(r) and F(r) be represented as f(r)*F(r), Eq. (2.26) may be expressed as

$$2\int_o^{s_{max}} si(s)\exp(-\alpha s^2)\sin(2\pi rs)ds$$

$$= \Sigma\Sigma\,[rx_i\rho_{ij}(r)*H_{ij}(r)] - r\rho_o\,\frac{[x_1f_1(o)+x_2f_2(o)]^2}{f^2(o)} \qquad (2.27)$$

Let $\rho'(r)$ and ρ_o' be defined as follows:

$$\rho'(r) = r^{-1}\,\Sigma\Sigma\,[rx_i\rho_{ij}(r)*H_{ij}(r)] \qquad (2.28)$$

$$\rho_o' = \rho_o\,\frac{[x_1f_1(o)+x_2f_2(o)]^2}{f^2(o)} \qquad (2.29)$$

Equation (2.27) may now be rewritten as

$$2\int_o^{s_{max}} si(s)\exp(-\alpha s^2)\sin(2\pi rs)ds = r[\rho'(r)-\rho_o'] \qquad (2.30)$$

A plot of $\rho'(r)$ vs r yields a series of peaks. The positions of the maxima of these peaks (excluding those peaks due to the termination effect) correspond to the interatomic spacings in the material being analyzed. Unfortunately, the positions of the $\rho'(r)$ vs r peaks are often slightly shifted due to the termination effect. The positions of the peaks in a plot of $r[\rho'(r)-\rho_o']$ vs r are essentially unaffected by the termination effect and are often used in preference to the $\rho'(r)$ plot to determine the interatomic spacings.

Multiplying both sides of Eq. (2.30) by $4\pi r$ yields

$$8\pi r \int_0^{s_{max}} si(s)\exp(-\alpha s^2)\sin(2\pi rs)ds = 4\pi r^2[\rho'(r)-\rho_o'] \quad (2.31)$$

Recalling our definition of the RDF,

$$RDF = 4\pi r^2 \Sigma\Sigma\, x_i\rho_{ij}(r),$$

it is evident that although all of the terms of the RDF are present in the expression $4\pi r^2\rho'(r)$, the $rx_i\rho_{ij}(r)$ terms are convoluted with the H_{ij} functions. We shall therefore refer to the expression $4\pi r^2\rho'(r)$ as the CRDF, or convoluted radial distribution function. Although the integral in Eq. (2.30) may be numerically evaluated for a series of values of s, one can only find the CRDF as a function of r; a deconvolution of each of the convolution products of the CRDF must be performed to obtain the RDF.

The expression for the CRDF can be greatly simplified in the case where s_{max} is allowed to become very large. If $H_{ij}(r)$ can be represented by a sharp peak centered at r = o and if $rx_i\rho_{ij}(r)$ is slowly varying, then $[rx_i\rho_{ij}(r)*H_{ij}(r)]$ covers only a small region near r = o and, for all values of t where $H_{ij}(t)$ is not zero, $(r-t)x_i\rho_{ij}(r-t)$ is approximately equal to its average value of $rx_i\rho_{ij}(r)$. Therefore, in this case,

$$[rx_i\rho_{ij}(r) * H_{ij}(r)] \approx rx_i\rho_{ij}(r) \int_{-\infty}^{\infty} H_{ij}(t)dt$$

$$\approx rx_i\rho_{ij}(r) \frac{f_i(o)f_j(o)}{f^2(o)} \qquad (2.32)$$

If these approximations are made, it follows that

$$4\pi r^2\rho'(r) \approx 4\rho r^2 \sum\sum x_i\rho_{ij}(r) \frac{f_i(o)f_j(o)}{f^2(o)} \qquad (2.33)$$

A plot of the CRDF vs r consists of a superposition of peaks which are due to the interferences between the various atom pairs. If expression (2.33) is employed in the analysis of the peaks comprising a CRDF plot, the area under a peak located between $r = r_o$ and $r = r_o'$ will be given by

$$\text{Area} \approx \int_{r_o}^{r_o'} 4\pi r^2 \sum\sum \left[x_i\rho_{ij}(r) \frac{f_i(o)f_j(o)}{f^2(o)}\right] dr \qquad (2.34)$$

Consider, for example, the case where the first peak in a CRDF plot is due only to the interaction between A-type atoms. In this case Eq. (2.34) becomes

$$\text{Area} \approx \frac{f_A^2(o)x_A}{f^2(o)} \int_{r_o}^{r_o'} 4\pi r^2\rho_{AA}(r)dr \qquad (2.35)$$

Since $4\pi r^2\rho_{AA}(r)dr$ gives the number of A-type atoms in the spherical shell between r and r+dr surrounding a randomly-selected A-type atom, the integral in Eq. (2.35) gives the number of A-type atoms

located between concentric spheres of respective radii r_o and r_o' which have a randomly-selected A-type atom at their center. The area under the first CRDF peak in this case is therefore equal to the first coordination number of the A-type atoms multiplied by $\{x_A f_A^2(o)/f^2(o)\}$.

If the integral in Eq. (2.31) could be evaluated out to infinity, one would obtain CRDF peaks whose breadth was due only to the statistical distribution of bond lengths within the material and to the thermal vibrations of the atoms. Termination of the integral at the finite value s_{max} results in a broadening of the CRDF peaks. The use of the termination factor $\exp(-\alpha s^2)$ introduces further peak broadening. In addition to these broadening factors, the value chosen for the film density ρ_o will also influence the size of each CRDF peak. Since the area under a CRDF peak is quite sensitive to these factors, the coordination numbers determined from a CRDF plot are, in general, less reliable than the nearest neighbor distances determined from a plot of $4\pi r[\rho'(r)-\rho_o']$ vs r.

CHAPTER III

EXPERIMENTAL PROCEDURES AND APPARATUS

Preparation of Bulk Samples and Thin Films

Bulk samples of Ge-Se compounds of several different compositions were obtained from R. E. Loehman. The samples had been prepared by weighing the powdered elements (having purity 99.99% or better) into vycor tubes, sealing the tubes off under vacuum, and then heating the ampoules in a resistance furnace held between 890°C and 950°C for 18 to 24 hours. To ensure homogeneity, the samples were agitated while in the furnace. Immediately after an ampoule was removed from the furnace, it was quenched in cold water. Pieces of each sample were crushed into a coarse powder using a porcelain mortar and pestle. An agate mortar was used to grind the coarse powder of each sample into a finely-powdered form.

Thin films of Se and of two of the Ge-Se samples were deposited on freshly-cleaved mica substrates by flash evaporation of the respective powdered samples from a resistance-heated tantalum single-grain box source (Model SG-8 by R. D. Mathis Company). The film thicknesses were determined by a quartz crystal thickness monitor to be less than 350 Å. Flash evaporation is a technique often employed for the deposition of films whose constituents have different vapor

pressures. The technique is used in order to produce a vapor stream whose composition is uniform and identical to that of the powder being evaporated. A schematic diagram of the evaporation apparatus is shown in Fig. 2. All evaporations were performed within a vacuum system (Veeco Model VE-400) employing a mechanical pump, a four-inch diffusion pump, and a cold trap. The cold trap was filled with liquid nitrogen during each evaporation in order to avoid poisoning of the pump oils by the evaporating selenium. After the pressure within the bell jar was reduced to less than 5×10^{-5} Torr, sufficient current was sent through the box source to heat it to a temperature of 1500°C, as measured with an optical pyrometer. A shutter separating the box source from the mica substrates was then opened and the powdered material was sent slowly down an electromagnetically-vibrated chute into the heated source. During the period of time when the source was at its maximum temperature, the pressure within the bell jar was observed to increase to approximately 10^{-4} Torr. After a sufficient amount of powder was evaporated, the flow of material down the chute was stopped, the shutter was closed, and the current through the box source was reduced to zero. The contents of the bell jar were allowed to cool under vacuum for approximately 15 minutes, after which time the samples were removed from the system.

Each film was stripped off its mica substrate by gently immersing the substrate in de-ionized water. The films were

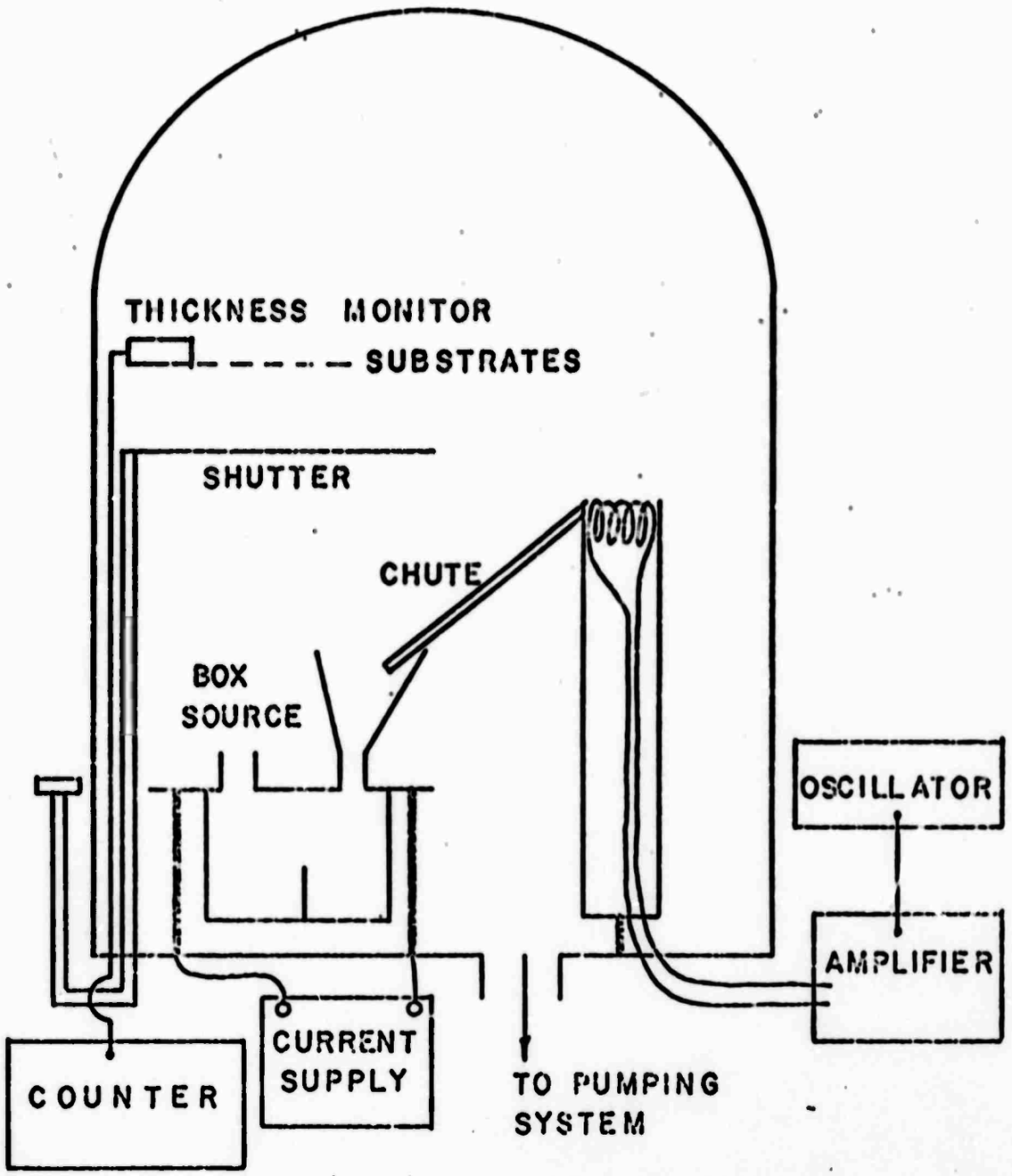

Figure 2. Schematic diagram of evaporation apparatus.

lifted off the water's surface on pieces of very fine copper mesh (1,500 &pi). After a set of films was dry, the films were placed in the specimen holder of the scanning electron diffraction (SED) system. Selected films were also examined in the Philips EM 200 electron microscope.

Using the same evaporation technique and powdered bulk samples as described above, films of approximately 1,500 Å thickness were deposited on glass microscope slides. A value of the weight percent x of germanium present in the films deposited from the two bulk Ge_xSe_{1-x} samples was determined by W. L. Wilson using x-ray fluorescence spectroscopy. The x values were 0.57 and 0.275, which implies that the empirical formulas for the thin films evaporated from the two bulk samples are $GeSe_{0.7}$ and $GeSe_{2.4}$, respectively.

Thin film preparation by flash evaporation of mechanical mixtures of the powdered elements was also attempted. The elemental germanium was found to react with the tantalum of the box source, however, so this technique was discarded.

Scanning Electron Diffraction System

The diffraction system used in this research was developed by Grigson and coworkers at the University of Cambridge[16] and by Dove and Denbigh at Bell Laboratories.[17] A schematic diagram of this system is shown in Fig. 3.

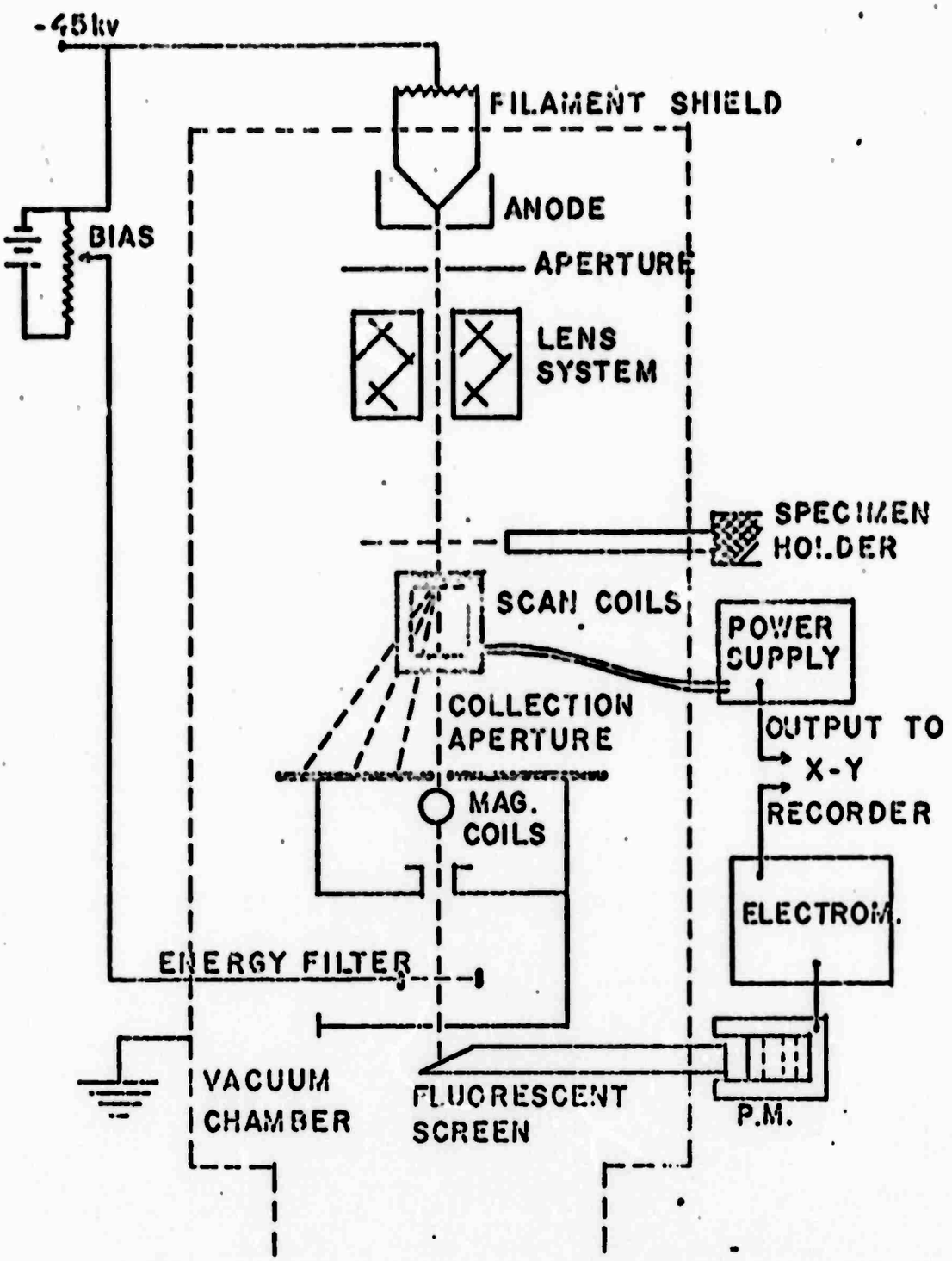

Figure 3. Schematic diagram of scanning electron diffraction system.

The scanning electron diffraction system employs a conventional electron gun whose filament is held at a constant potential of between -45 and -50 kV. A six-inch carbon oil diffusion pump allows the pressure within the system to be reduced to 10^{-6} Torr. The electron beam produced by the heated filament first passes through an aperture and a magnetic lens system before it strikes one of the thin films in the specimen holder. The specimen holder can hold up to five films at one time, allowing several specimens to be examined in succession without breaking the vacuum in the system. The electrons scattered by the film produce a diffraction pattern which, along with the direct beam, can be translated back and forth across a very small collection aperture by varying the current through a pair of coils located below the sample. A phosphor-coated surface located on the plane of the collection aperture allows the diffraction pattern to be observed. The diffraction pattern may be focussed by adjusting the current through the lens system located above the specimen.

After passing through the collection aperture, all of those electrons which have lost more than a few volts in energy (i.e., the inelastically scattered electrons) are rejected by an electrostatic filter. The filter is connected to the gun filament through a variable bias voltage. A pair of magnetized coils directly below the collection aperture is driven in synchronism with the scan coils so that after

the electrons pass through the aperture they are directed along a path close to the electron optic axis, regardless of the angle at which the electrons enter the aperture. This correction of the deviation angle of deflected rays entering the aperture is necessary for the satisfactory operation of the electrostatic filter. After the elastically scattered electrons pass through the filter, they hit a fluorescent screen, and the light generated by the screen is detected by a photomultiplier (PM) tube. The output current of the PM tube is measured by an electrometer and the dc output of the electrometer is displayed versus scan angle on an x-y recorder.

Processing of Diffraction Data

A number of films, especially many of the $GeSe_{0.7}$ films, were found to contain small crystallites as deposited. The diffraction patterns of these films consisted of a series of sharp Bragg peaks superimposed on an amorphous background. Even films which initially displayed diffuse diffraction patterns began to crystallize when irradiated in an electron beam of moderate intensity. In an effort to control such beam-heating effects, the beam intensity of the SED system was decreased considerably.

The diffuse diffraction patterns of selected films of $GeSe_{0.7}$ and $GeSe_{2.4}$ were recorded. These films were then

heated using the electron beam. The changes in the diffracted intensity profiles were recorded after various degrees of beam heating. The diffraction pattern from a crystallized flash-evaporated selenium film floated off a mica substrate was also obtained.

I/f^2 was calculated as a function of s for a series of $GeSe_{0.7}$ and $GeSe_{2.4}$ films. The integral in Eq. (2.30) was numerically evaluated from s = 0 to s_{max} = 2.08 for these films, yielding a series of values of $r[\rho'(r)-\rho'_o]$ as a function of r for each film. The integral was evaluated both with and without the exponential termination function $\exp(-0.36\ s^2)$. The CRDF was evaluated as a function of r for each film by multiplying each of the calculated values of $r[\rho'(r)-\rho'_o]$ by $4\pi r$ and then adding $4\pi r\rho'_o$ to the quantity obtained.

The electron scattering factors given by Vainstein[18] (calculated using the Thomas-Fermi method) were used for Ge and Se. The normalization function f^2 was chosen to equal $(x_{Ge}f_{Ge}^{\ 2} + x_{Se}f_{Se}^{\ 2})$.

The density values used for $GeSe_{0.7}$ and $GeSe_{2.4}$ were 5.00 g/cc and 4.33 g/cc, respectively. The density value chosen for $GeSe_{2.4}$ was taken to be equal to the measured density of the bulk glass from which these films were prepared. The density chosen for $GeSe_{0.7}$ is 9% less than the density reported by Kannewurf[19] for crystalline GeSe.

CHAPTER IV

EXPERIMENTAL RESULTS

Introduction

The diffraction patterns of amorphous films of $GeSe_{0.7}$ and $GeSe_{2.4}$ underwent significant changes as the films were heated with the electron beam. The most noticeable changes which occurred with increased heating were an increase in sharpness of the diffuse diffraction intensity peaks and a change in the relative intensity of the peaks.

Two different diffuse diffraction patterns were obtained for $GeSe_{0.7}$. The pattern labeled "first stage" represents the most diffuse pattern obtained. The pattern labeled "second stage" represents the pattern obtained when a film initially in the first stage was heated with the electron beam. Three diffuse patterns are presented for $GeSe_{2.4}$. The first stage represents a $GeSe_{2.4}$ film in its as-deposited state. The second and third stages represent the state of a $GeSe_{2.4}$ film after progressive beam heating.

For each stage of $GeSe_{0.7}$ and $GeSe_{2.4}$ a plot is presented within this chapter for diffracted intensity I vs s, I/f^2 vs s, the CRDF (calculated without an exponential termination function) vs r, the CRDF (with an exponential function) vs r, and $4\pi r[\rho'(r)-\rho_o']$ vs r, calculated

without an exponential function. A list of these plots with their corresponding figure numbers is given in Table I.

Results Obtained for $GeSe_{0.7}$

A plot of I vs s for the most diffuse diffraction pattern obtained for $GeSe_{0.7}$ is shown in Fig. 4. A very weak intensity peak exists at $s \simeq 0.16$. The strongest intensity peak has its maximum at $s = 0.31$. A third and fourth peak are located at $s = 0.52$ and $s = 0.82$, respectively, as listed in Table II. Figure 5 gives an I vs s plot for a $GeSe_{0.7}$ film which was heated with the electron beam. A small intensity hump is present at $s \simeq 0.20$. The next three intensity maxima occur at the same s values at which the maxima occur for the first stage. The peaks of the second stage are much sharper than those of the first stage, however, and the peak at $s = 0.52$ exceeds the peak at $s = 0.31$ in intensity.

Further heating of a $GeSe_{0.7}$ film resulted in the appearance of sharp diffraction peaks superimposed on an amorphous background, indicating the presence of crystallites in the film. The comparison shown in Fig. 6a and c of the diffraction pattern of a partially-crystallized $GeSe_{0.7}$ film with the pattern of a crystalline selenium film indicates that it was selenium which first crystallized out when the $GeSe_{0.7}$ film was heated.

Table I

Directory of Plots for Ge-Se Films

Plot / Sample	$GeSe_{0.7}$ (First Stage)	$GeSe_{0.7}$ (Second Stage)	$GeSe_{2.4}$ (First Stage)	$GeSe_{2.4}$ (Second Stage)	$GeSe_{2.4}$ (Third Stage)
I vs s	Fig. 4	Fig. 5	Fig. 15	Fig. 16	Fig. 17
I/f^2 vs s	" 7	" 8	" 18	" 19	" 20
CRDF vs r (without exp)	" 9	" 11	" 21	" 23	" 25
CRDF vs r (with exp)	" 10	" 12	" 22	" 24	" 26
$4\pi r[\rho'(r)-\rho'_o]$ vs r (without exp)	" 13	" 14	" 27	" 28	" 29

I vs s for crystallized Se, $GeSe_{0.7}$ and $GeSe_{2.4}$ - Fig. 6.

Table II

Location of Intensity Peaks
for Ge-Se Films

Sample	Location of Prominent Intensity Maxima ($Å^{-1}$)
$GeSe_{0.7}$	
First Stage	s = (0.16), 0.31, 0.52, 0.80
Second Stage	s = (0.20), 0.31, 0.52, 0.80
$GeSe_{2.4}$	
First Stage	s = 0.18, 0.32, 0.55, 0.84
Second Stage	s = 0.18, 0.32, 0.52, 0.82
Third Stage	s = 0.22, 0.31, 0.52, 0.82

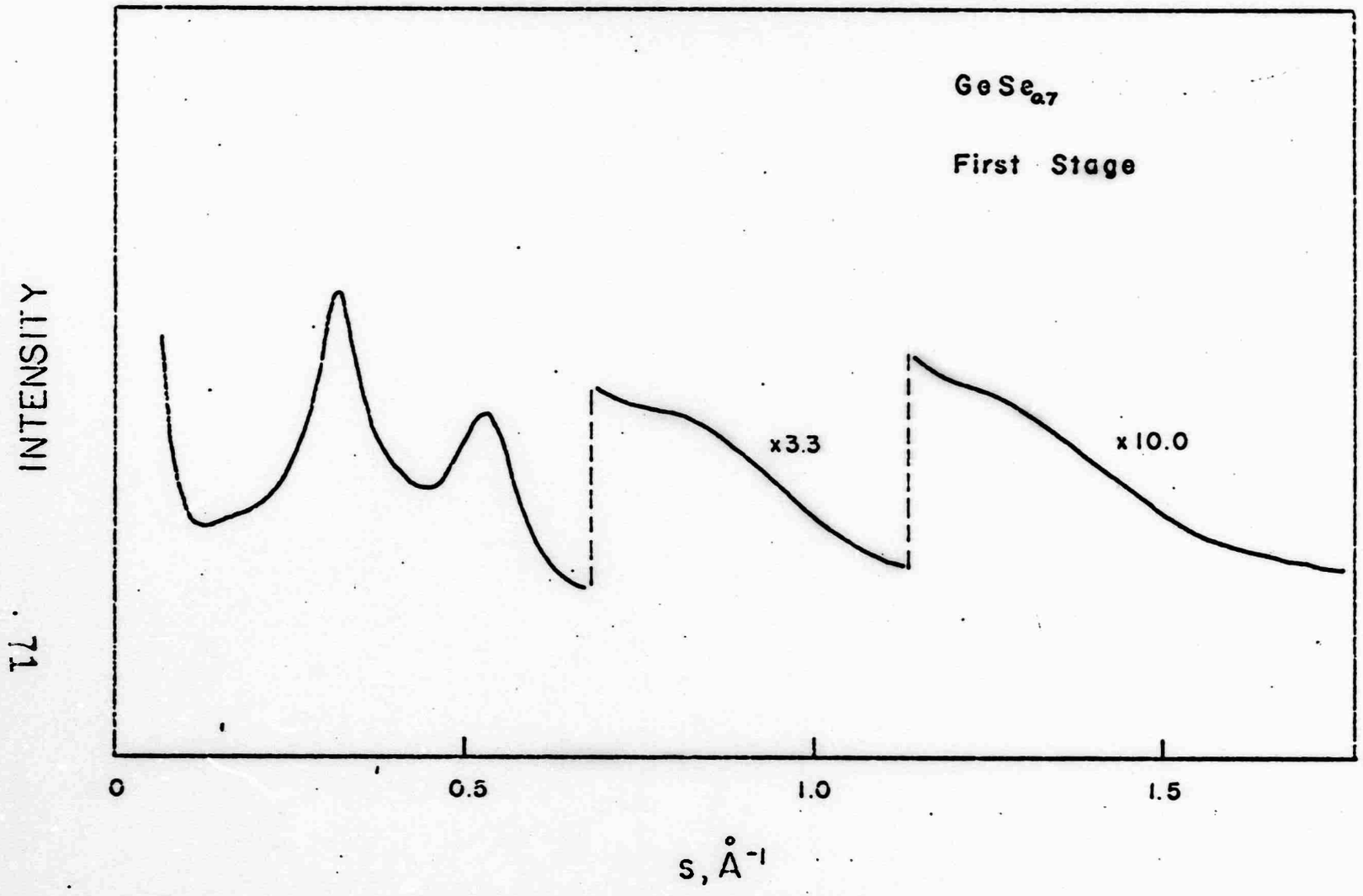

Figure 4. Diffracted intensity from an amorphous $GeSe_{0.7}$ film in the first stage.

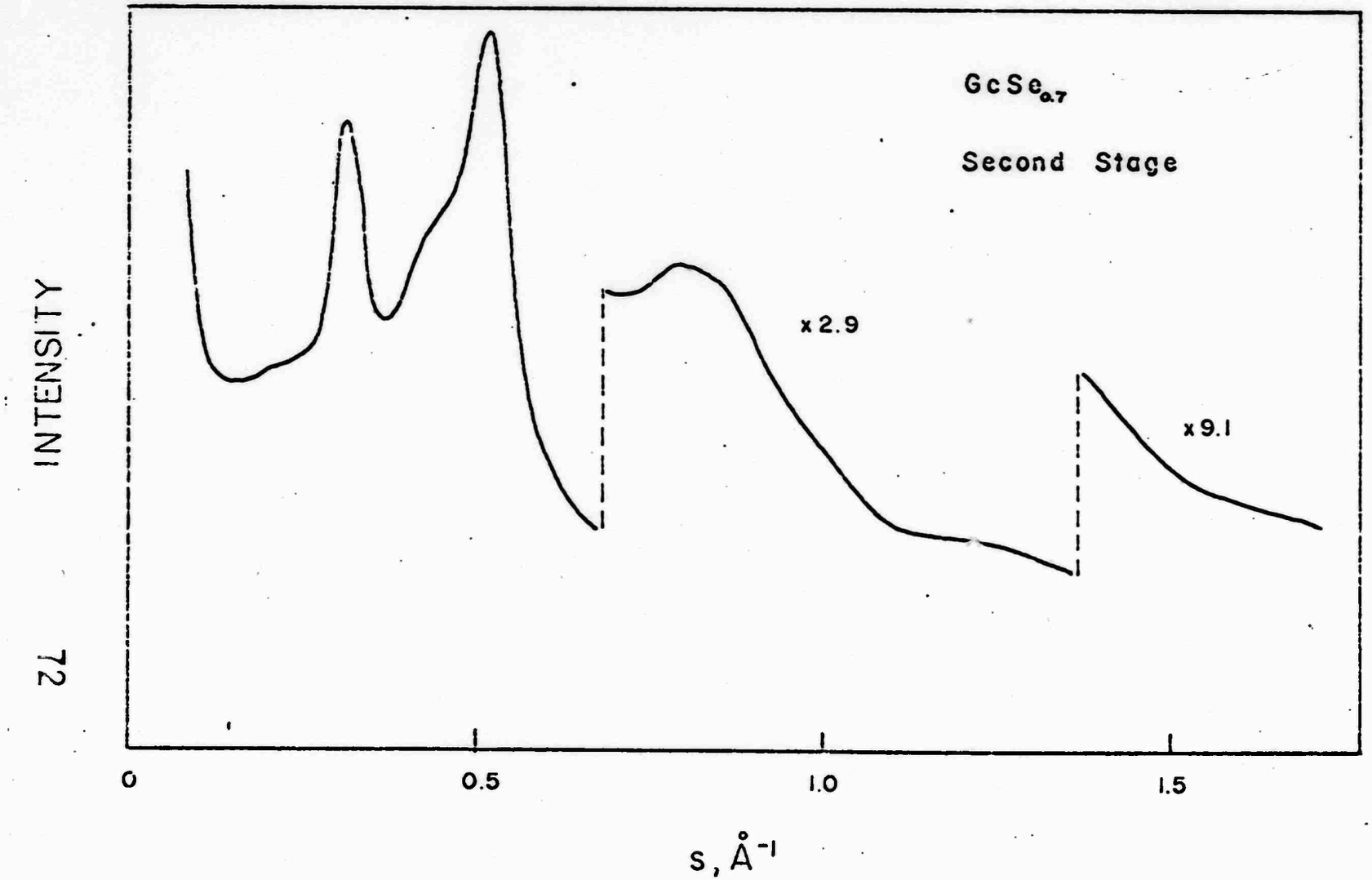

Figure 5. Diffracted intensity from an amorphous $GeSe_{0.7}$ film in the second stage.

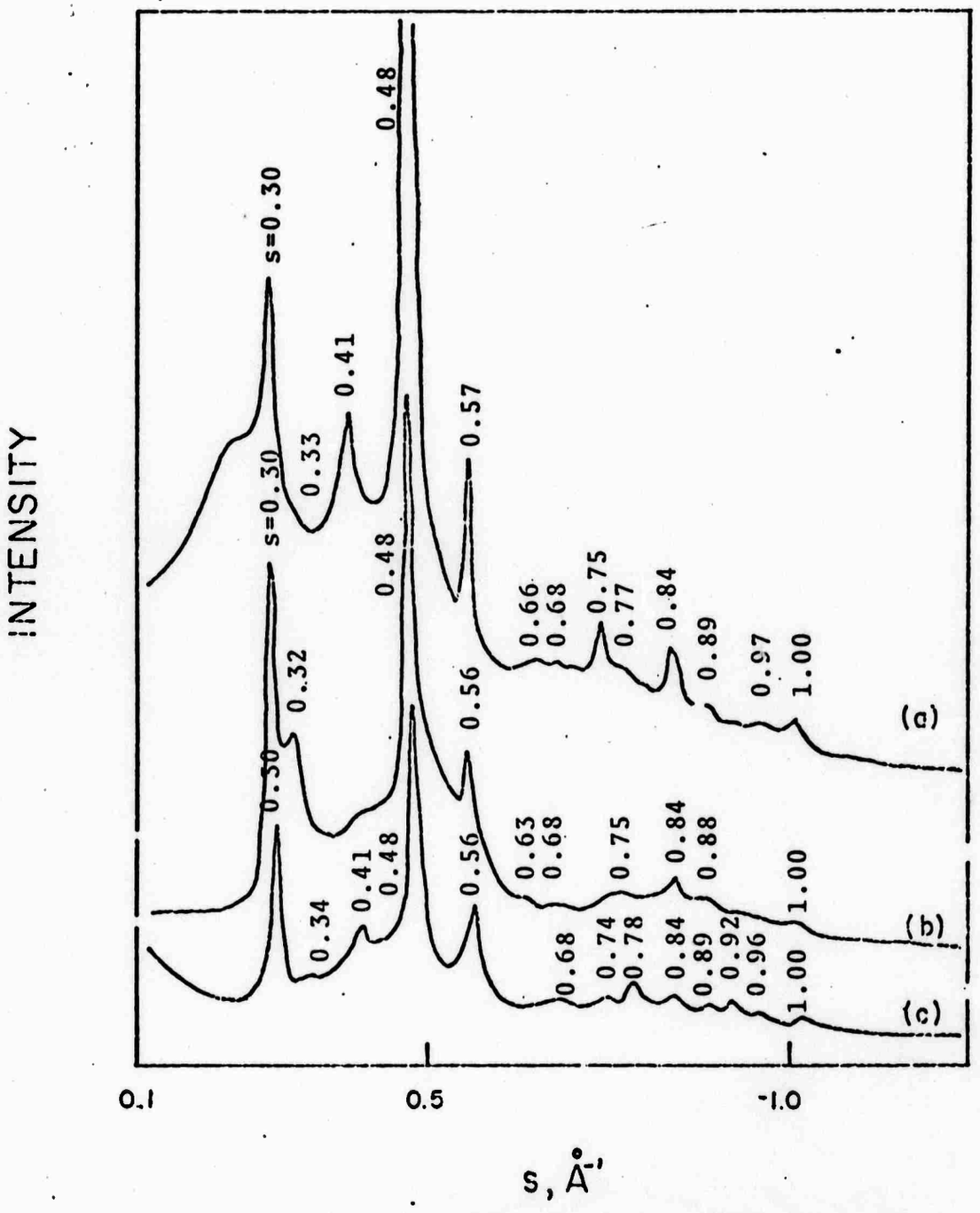

Figure 6. Diffracted intensity from a crystallized film of (a) $GeSe_{0.7}$, (b) $GeSe_{2.4}$, and (c) Se.

A plot of I/f^2 vs s is presented in Figs. 7 and 8 for the two stages of $GeSe_{0.7}$. The plot for the film in the second stage oscillates about a constant value. The plot for the film in the first stage, however, oscillates about a line with a positive slope. As mentioned in Chapter II, this failure of the I/f^2 vs s plot to oscillate about a constant value is most probably due to the film being of sufficient thickness to allow some multiple scattering.

A plot of the CRDF vs r, calculated both with (Fig. 10) and without (Fig. 9) the exponential termination function, is presented for the first stage of $GeSe_{0.7}$. The corresponding plots for the second stage are given in Figs. 11 and 12. It should be noted that all four CRDF plots for $GeSe_{0.7}$ have some peaks in the range r = 0 to r = 2.00 Å. The appearance of these peaks is due largely to the termination effect discussed in Chapter II. These peaks are reduced, but not eliminated, when an exponential termination function is used (Figs. 10 and 12) in evaluating the CRDF. The termination function also aids in reducing or eliminating termination peaks which occur at values of r greater than 2.00 Å. For example, the peak at r = 3.00 Å in Fig. 9 is absent in Fig. 10. Application of the termination function does cause some broadening in the CRDF peaks, as can be seen by comparing Figs. 9 and 10.

Figures 13 and 14 present a plot of $4\pi r[\rho'(r)-\rho_o']$ vs r, calculated using the termination function, for the first

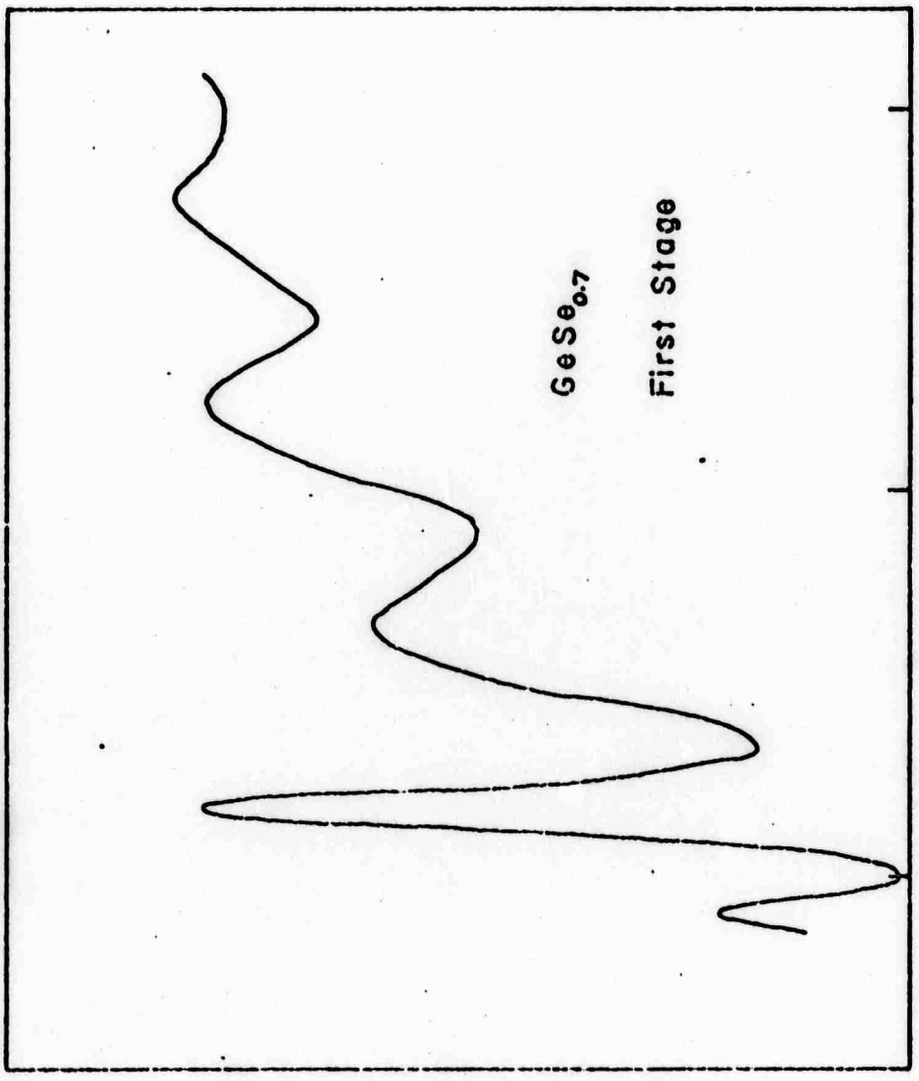

Figure 7. $I(s)/f^2(s)$ vs s for the $GeSe_{0.7}$ film of Figure 4.

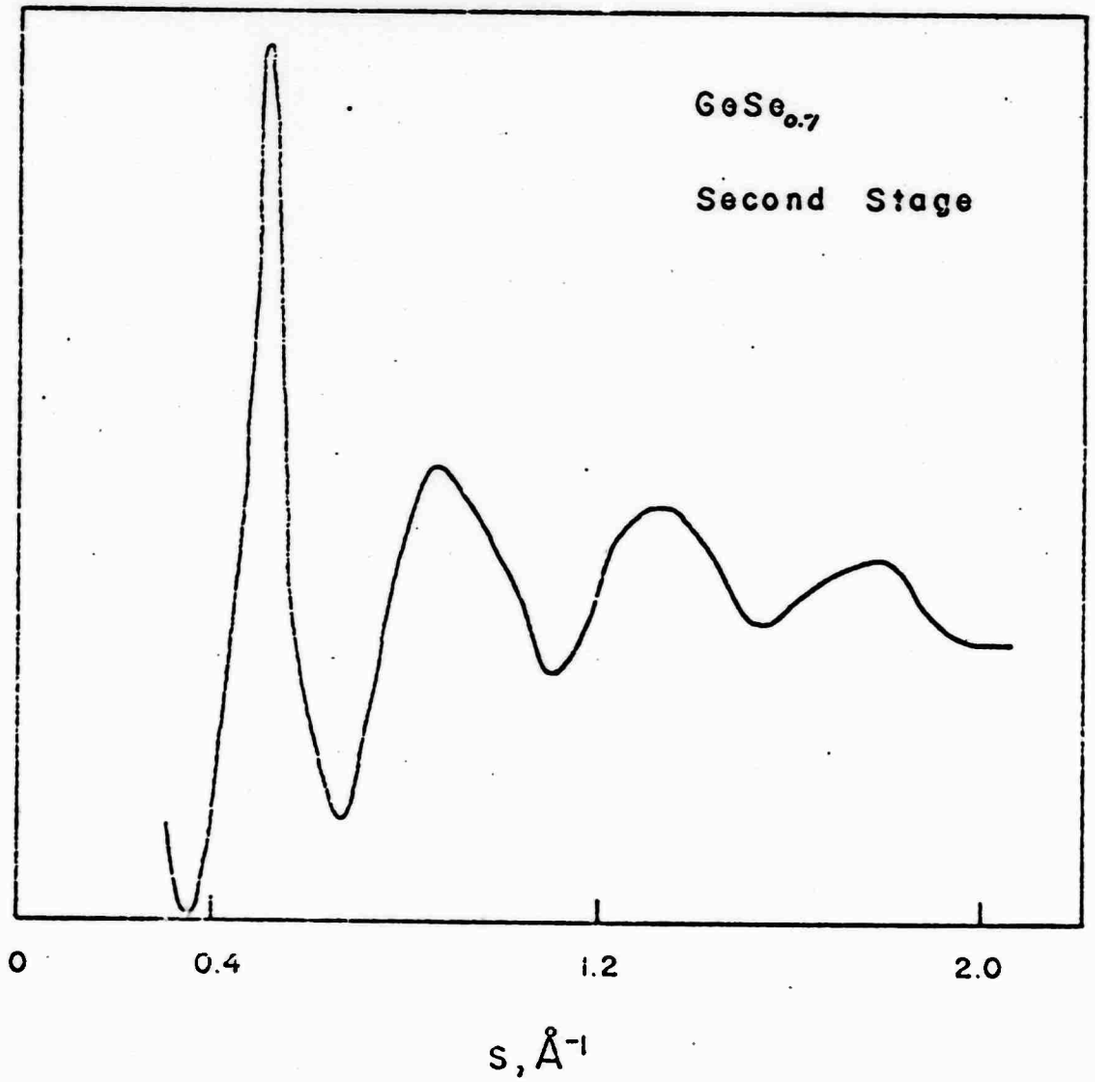

Figure 8. $I(s)/f^2(s)$ vs s for the $GeSe_{0.7}$ film of Figure 5.

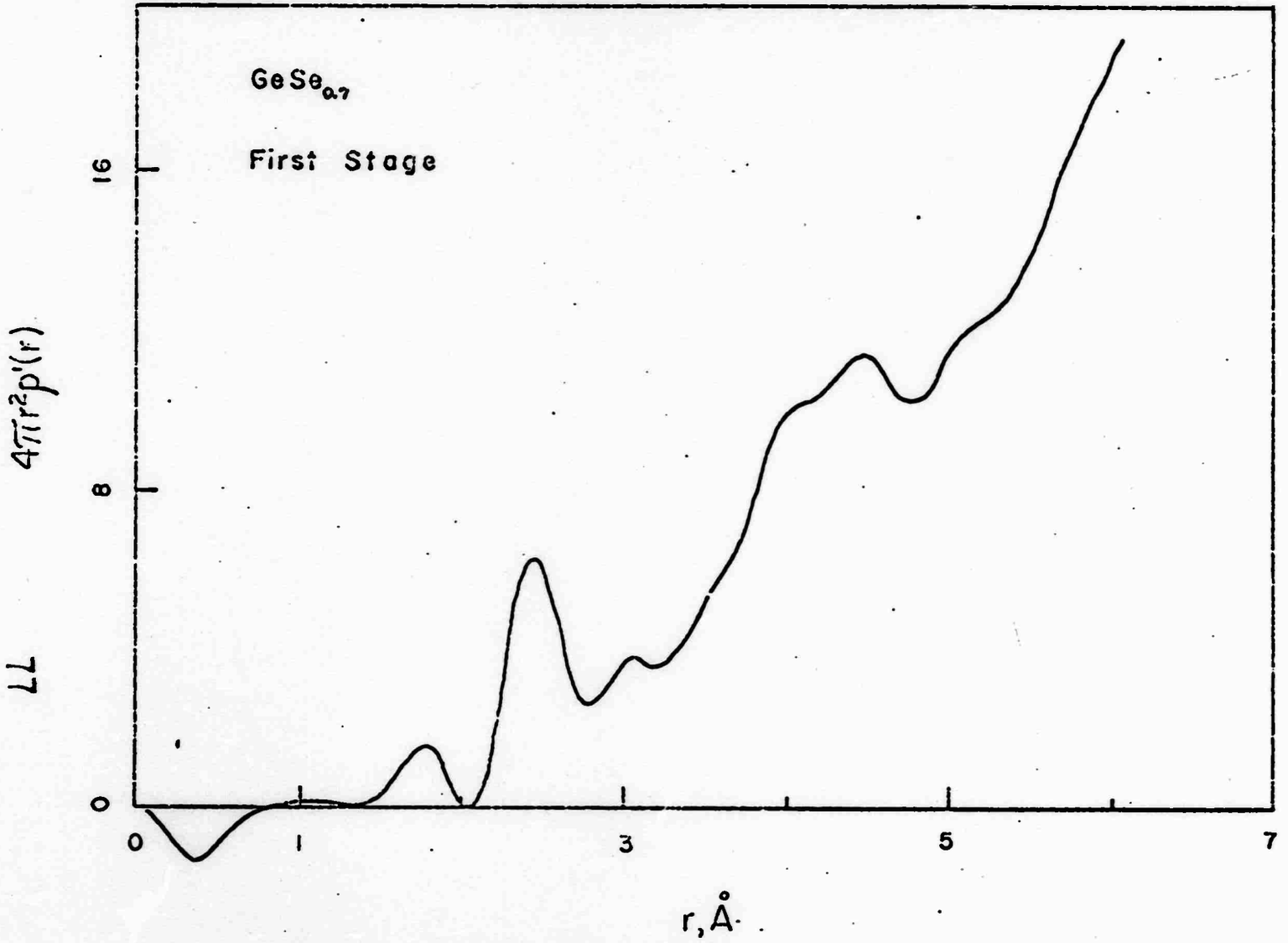

Figure 9. CRDF, calculated without an exponential termination function, for the $GeSe_{0.7}$ film of Figure 4.

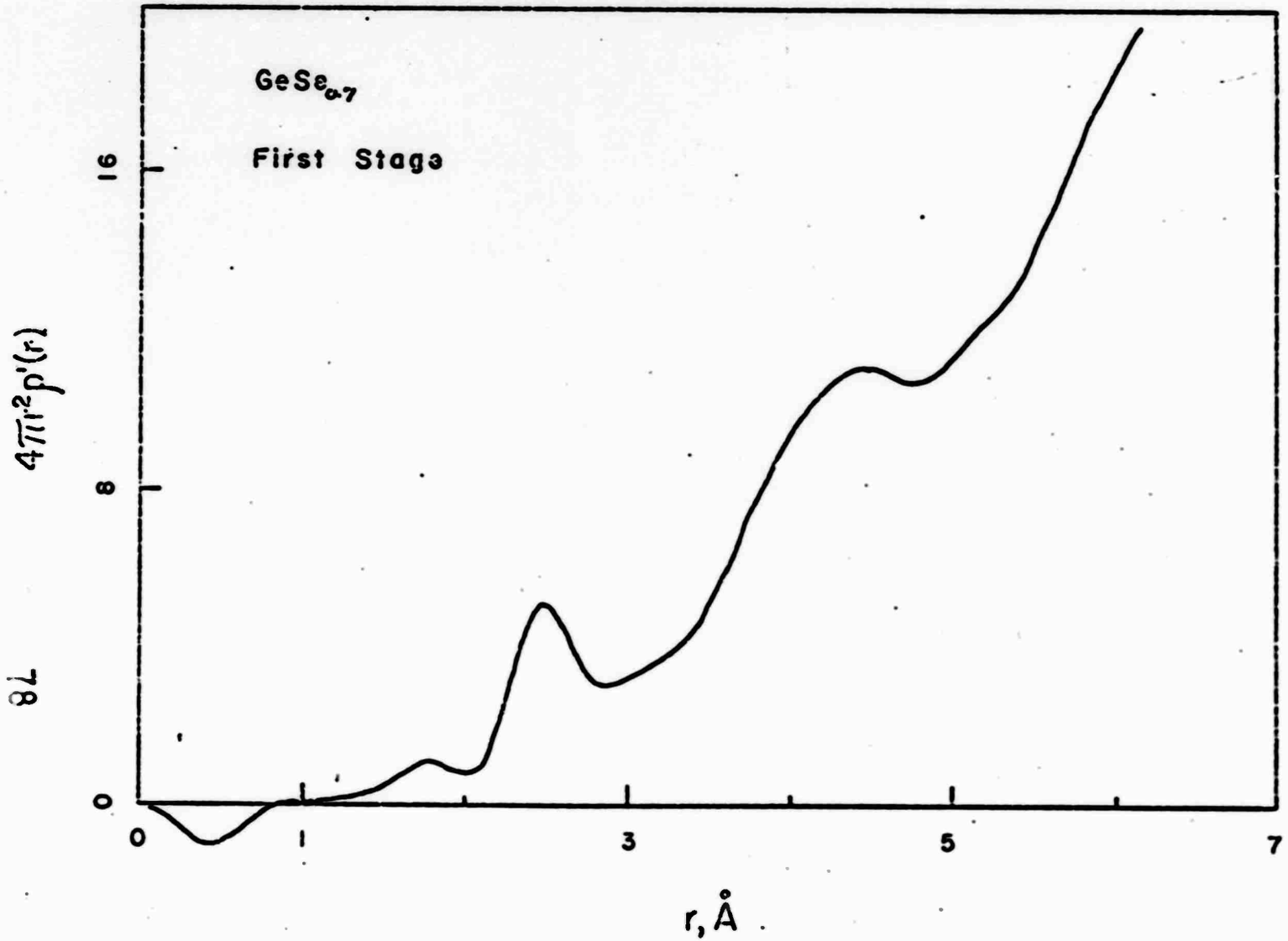

Figure 10. CRDF, calculated with an exponential termination function, for the $GeSe_{0.7}$ film of Figure 4.

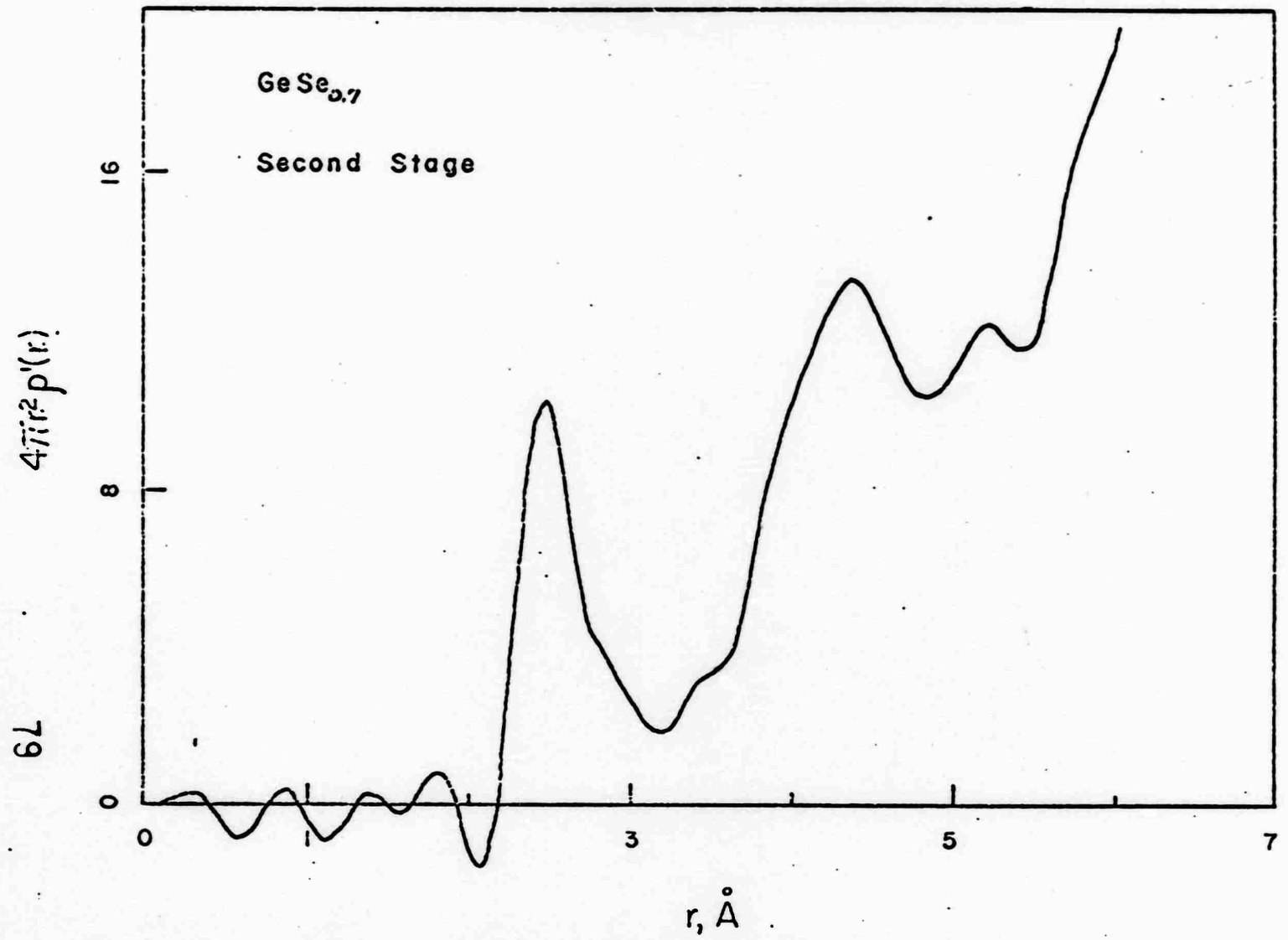

Figure 11. CRDF, calculated without an exponential termination function, for the $GeSe_{0.7}$ film of Figure 5.

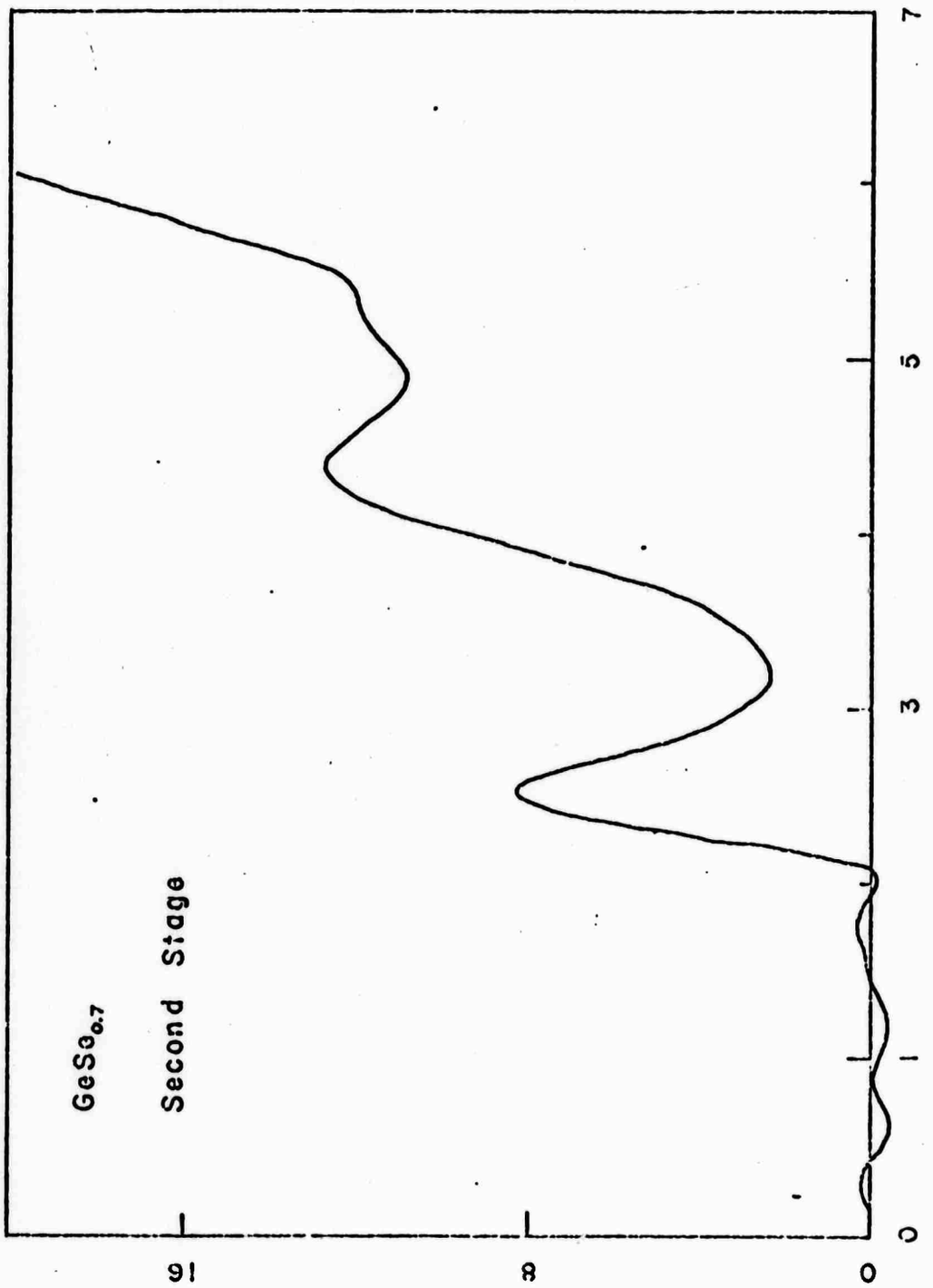

Figure 12. CRDF, calculated with an exponential termination function, for the $GeSe_{0.7}$ film of Figure 5.

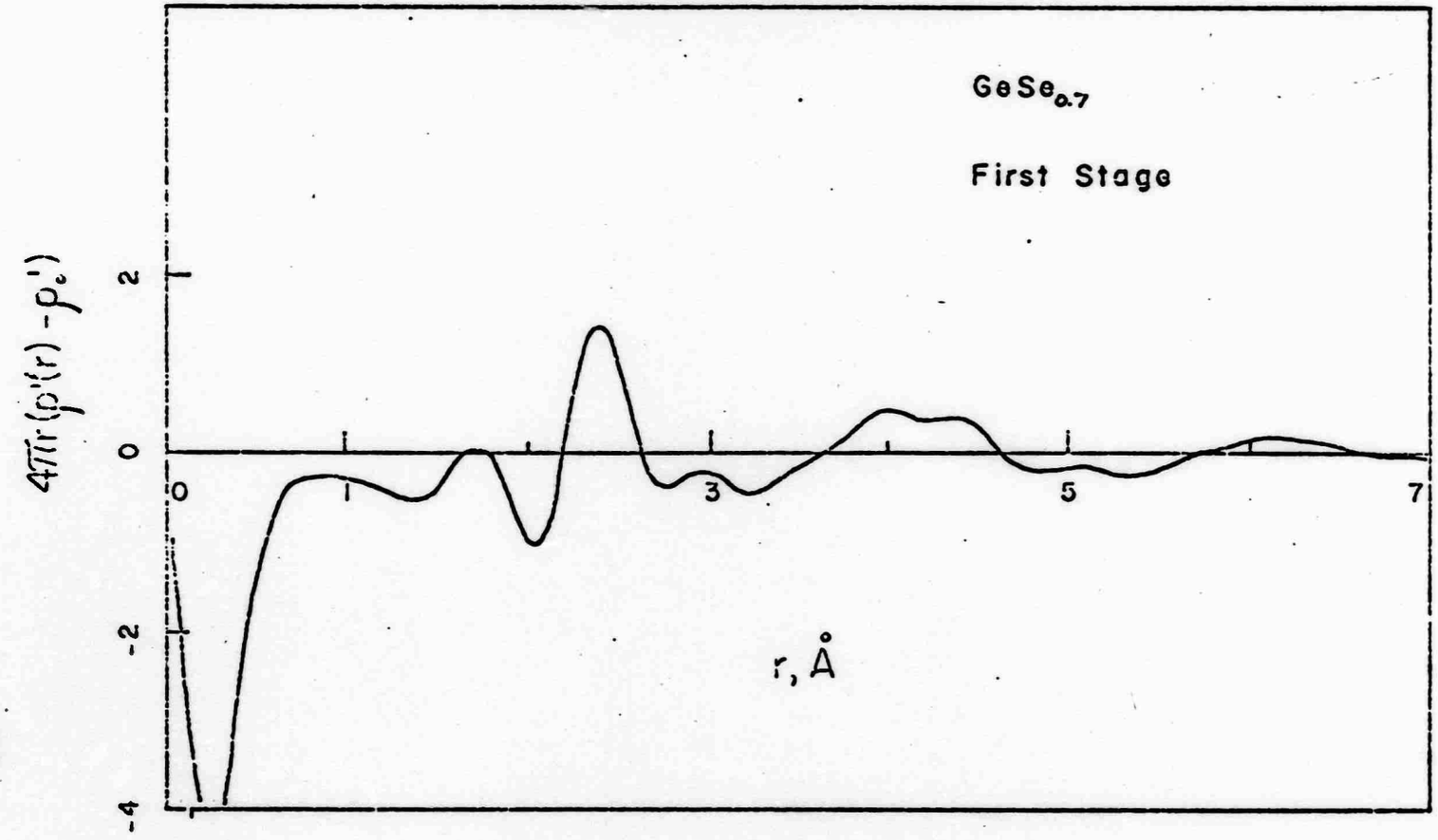

Figure 13. $4\pi r[\rho'(r)-\rho_o']$ vs r, calculated without an exponential termination function, for the $GeSe_{0.7}$ film of Figure 4.

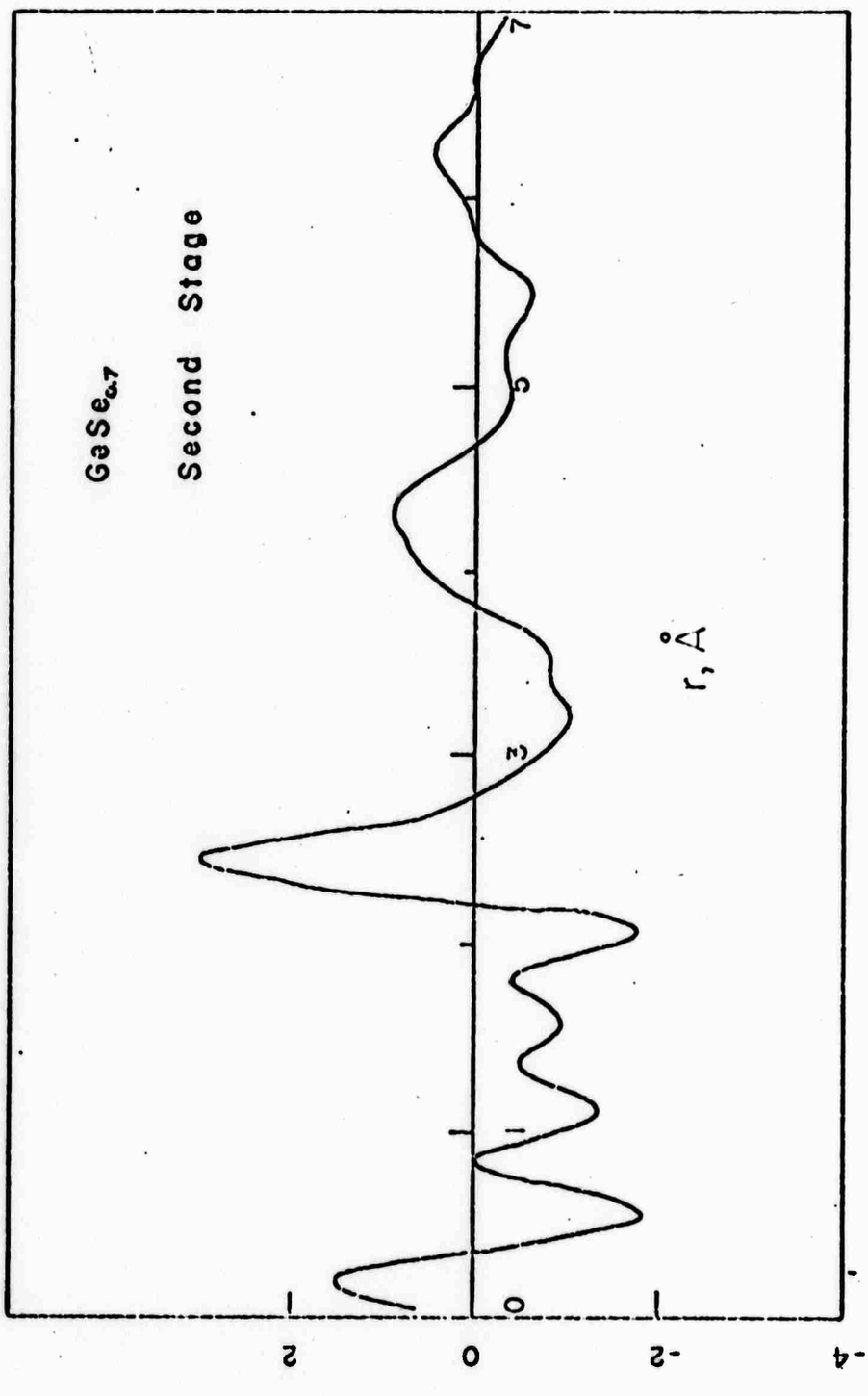

Figure 14. $4\pi r[\rho'(r)-\rho_0']$ vs r, calculated without an exponential termination function, for the $GeSe_{0.7}$ film of Figure 5.

and second stages of $GeSe_{0.7}$. The positions of the maxima of the peaks found in these plots (neglecting those peaks due to the termination effect) correspond to the interatomic spacings in the films they represent. The prominent interatomic spacings determined for the two stages of $GeSe_{0.7}$ are listed in Table II.

Results Obtained for $GeSe_{2.4}$

I vs s is plotted for the three stages of $GeSe_{2.4}$ in Figs. 15, 16 and 17. The positions of the prominent intensity maxima are given in Table III. The positions of the first four maxima do not change significantly as the film is heated. The relative intensity of the peaks does change, however. The peak at s = 0.18 undergoes a drastic decrease in intensity as the $GeSe_{2.4}$ film is heated from the first stage to the second stage. This peak is even smaller in the third stage. The peak at s = 0.55 undergoes a rise in intensity as the film progresses from the first to the third stage. In the third stage the peak at s = 0.55 exceeds the second peak in intensity. The peaks of the third stage are also much sharper than the peaks of the first two stages. Figure 6b shows the diffraction pattern of a $GeSe_{2.4}$-film which has been partially crystallized by the electron beam. Comparison of this pattern with the diffraction pattern shown

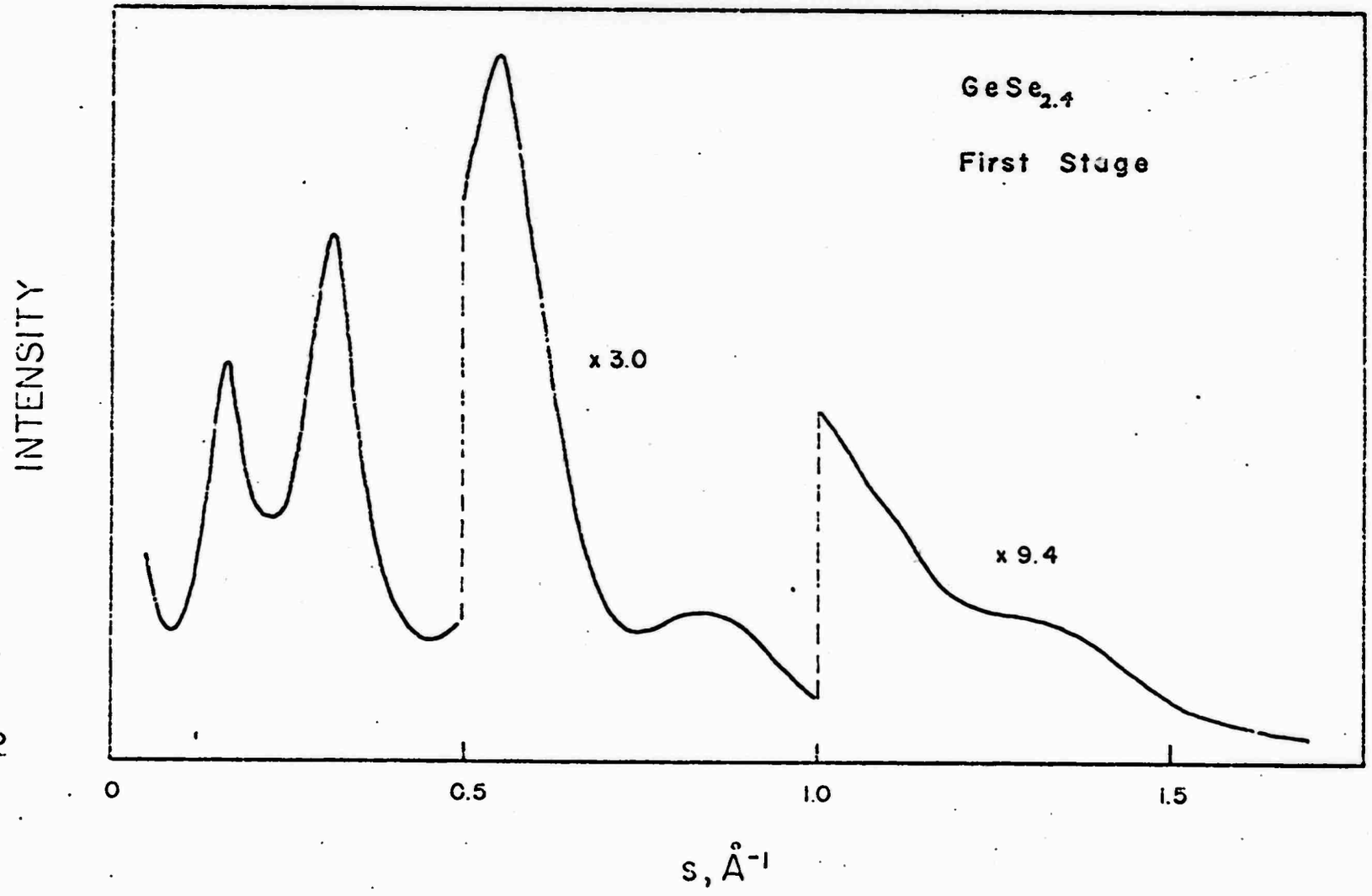

Figure 15. Diffracted intensity from an amorphous $GeSe_{2.4}$ film in the first stage.

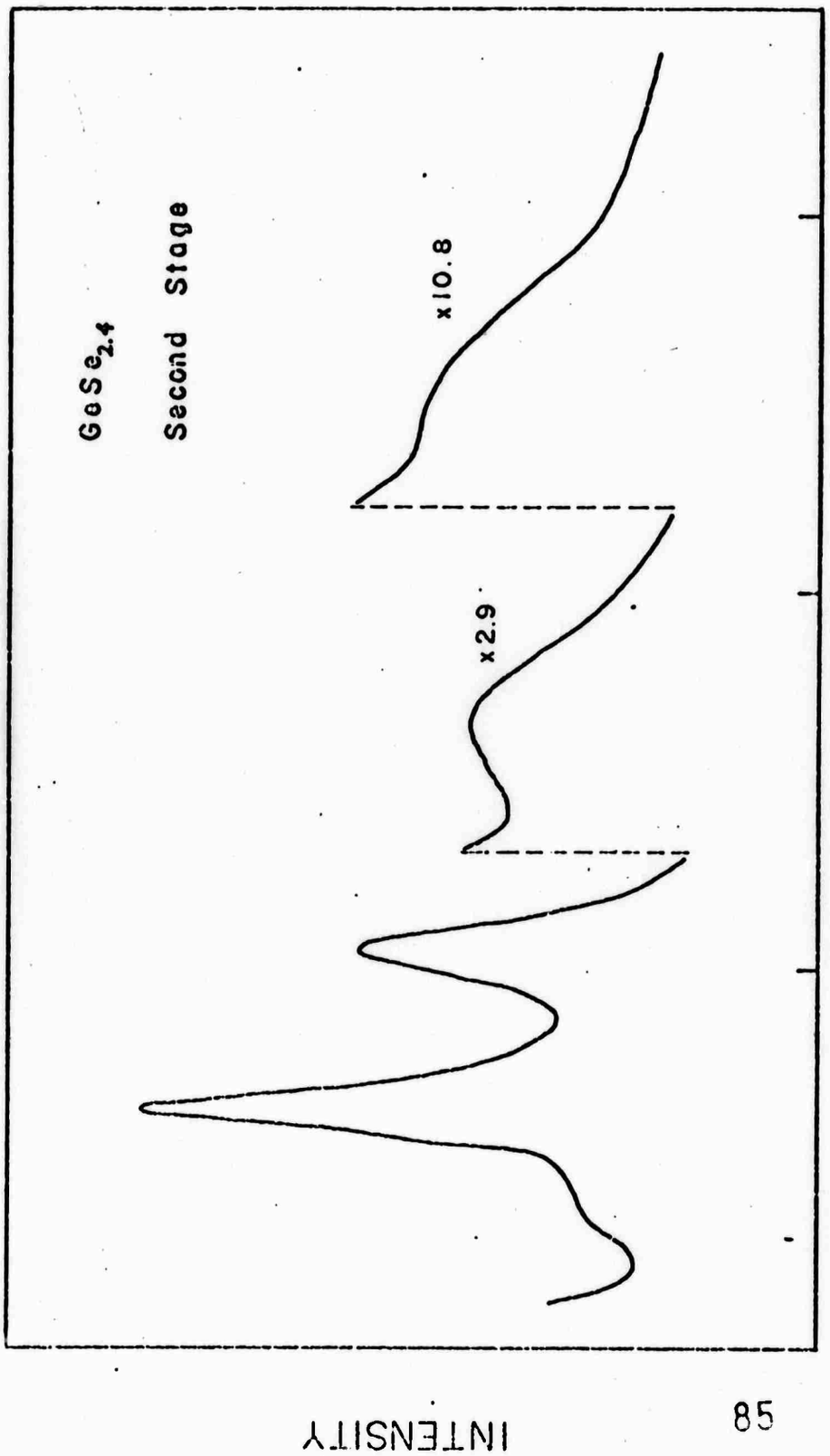

Figure 16. Diffracted intensity from an amorphous $GeSe_{2.4}$ film in the second stage.

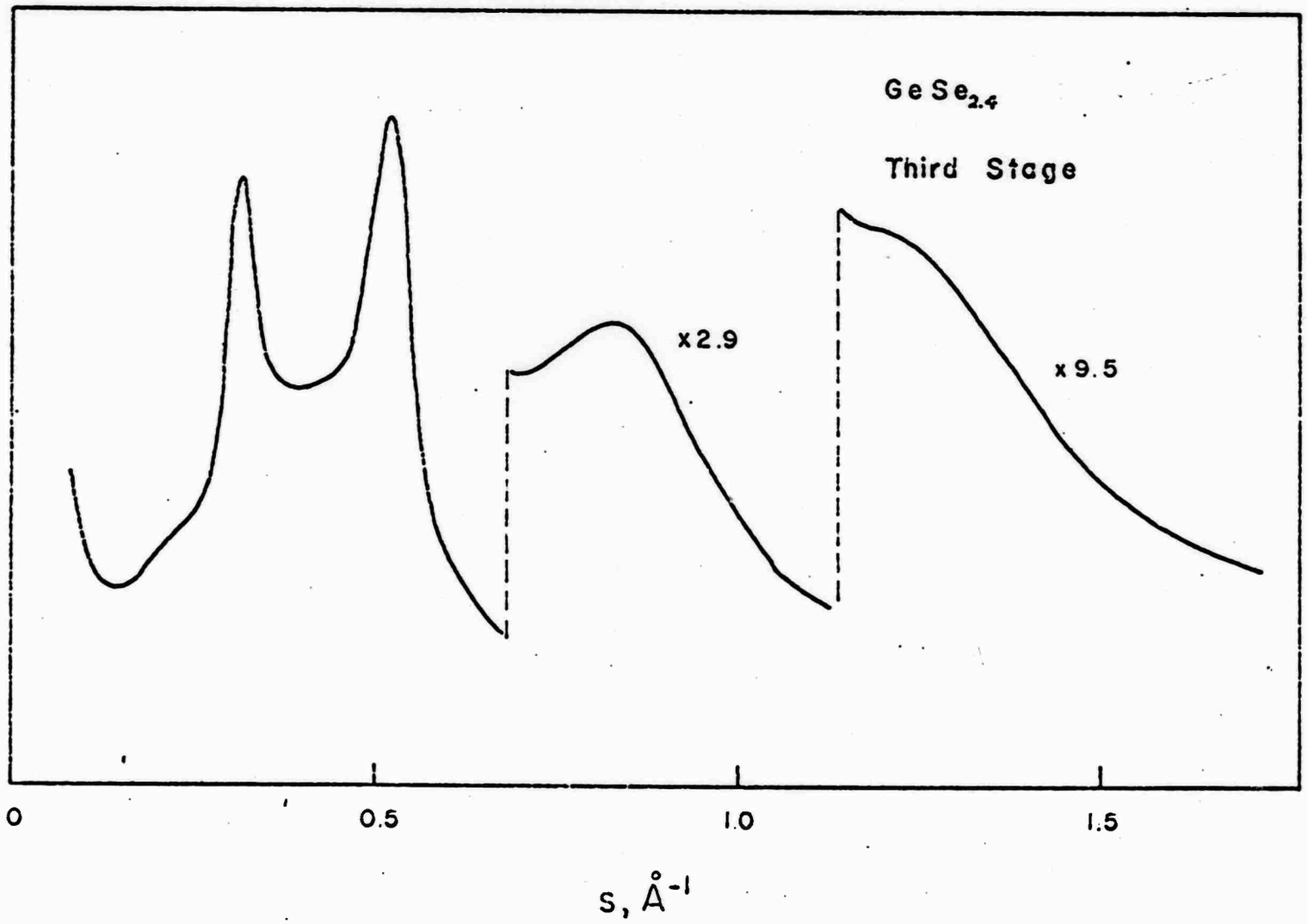

Figure 17. Diffracted intensity from an amorphous $GeSe_{2.4}$ film in the third stage.

Table III

Prominent Interatomic Spacings
for Ge-Se Films

Sample	Prominent Interatomic Spacings (Å)
$GeSe_{0.7}$	
First Stage	r = 2.40, 4.40, 5.07, 6.15
Second Stage	r = 2.47, 4.32, 5.17, 6.25
$GeSe_{2.4}$	
First Stage	r = 2.37, 3.87, 5.27, 5.80
Second Stage	r = 2.45, 4.02, 5.00, 6.05
Third Stage	r = 2.47, 4.15, 4.97, 6.35

in Fig. 6c of a crystalline Se film indicates that it is selenium which first crystallizes out when a $GeSe_{2.4}$ film is heated.

A plot of I/f^2 vs s is presented in Figs. 18-20 for the films representing the three stages of $GeSe_{2.4}$. The I/f^2 curves for the first and second stages (Figs. 18 and 19) oscillate about a constant value of I/f^2. The plot for the third stage (Fig. 20), however, exhibits somewhat of an upward slope.

A plot of the CRDF vs r, calculated both with and without the exponential termination correction, is presented in Figs. 21-26 for each of the three stages of $GeSe_{2.4}$ examined. The information which can be obtained from these plots will be discussed in Chapters V and VI.

A plot of $4\pi r[\rho'(r)-\rho_o']$ vs r, calculated using the termination function, is presented in Figs. 27-29 for the three stages of $GeSe_{2.4}$. The prominent interatomic spacings determined from these plots are listed in Table III.

Figure 30a shows an electron micrograph of an amorphous film of $GeSe_{2.4}$. The electron diffraction pattern of this film, which is shown in Fig. 30b, exhibits the diffuse diffraction halos characteristic of amorphous films. The two most intense halos occur at $s \approx 0.30$ and $s \approx 0.50$. These two halos appear to be about equal in intensity, indicating the film exists in a state somewhere between the second and third stages of $GeSe_{2.4}$. It is noted that the micrograph

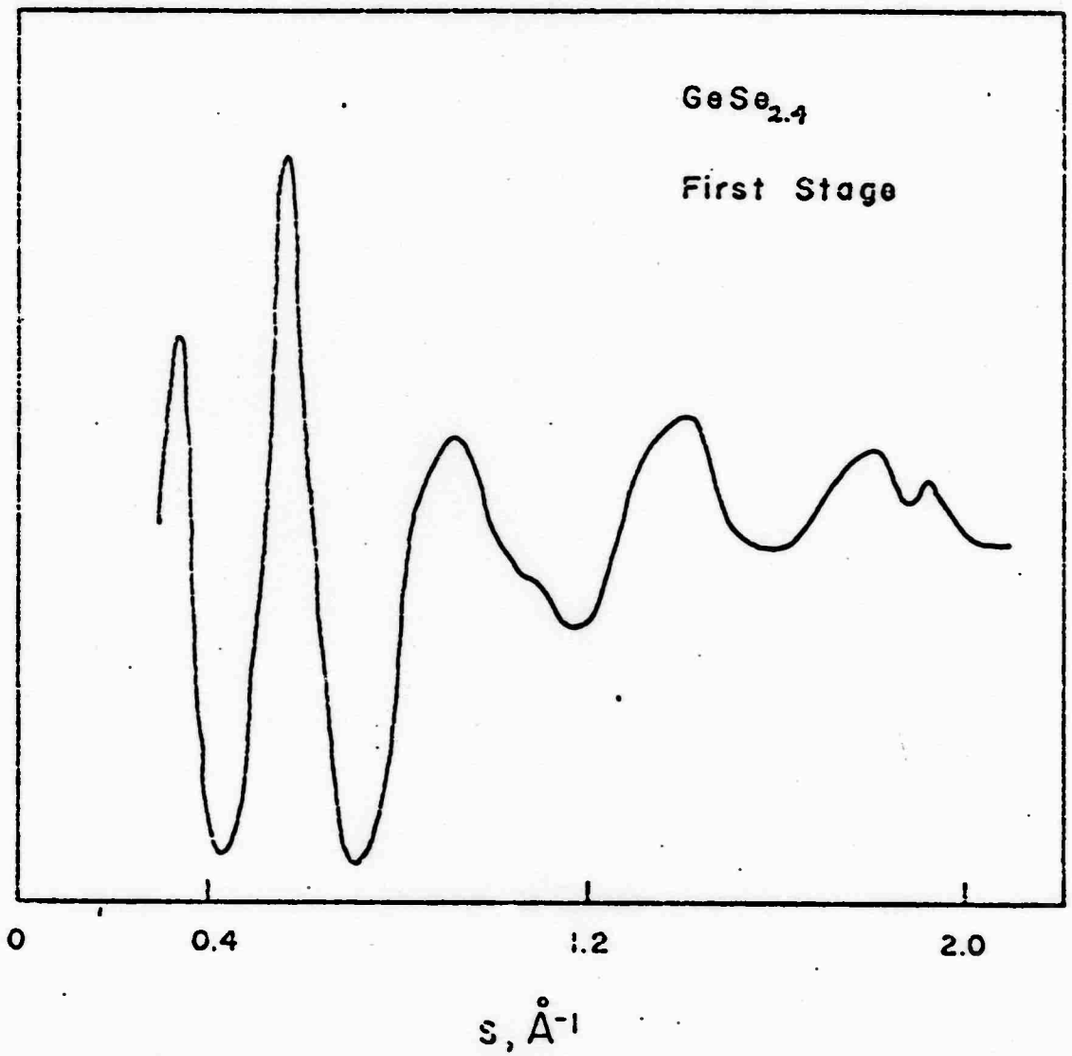

Figure 18. $I(s)/f^2(s)$ vs s for the $GeSe_{2.4}$ film of Figure 15.

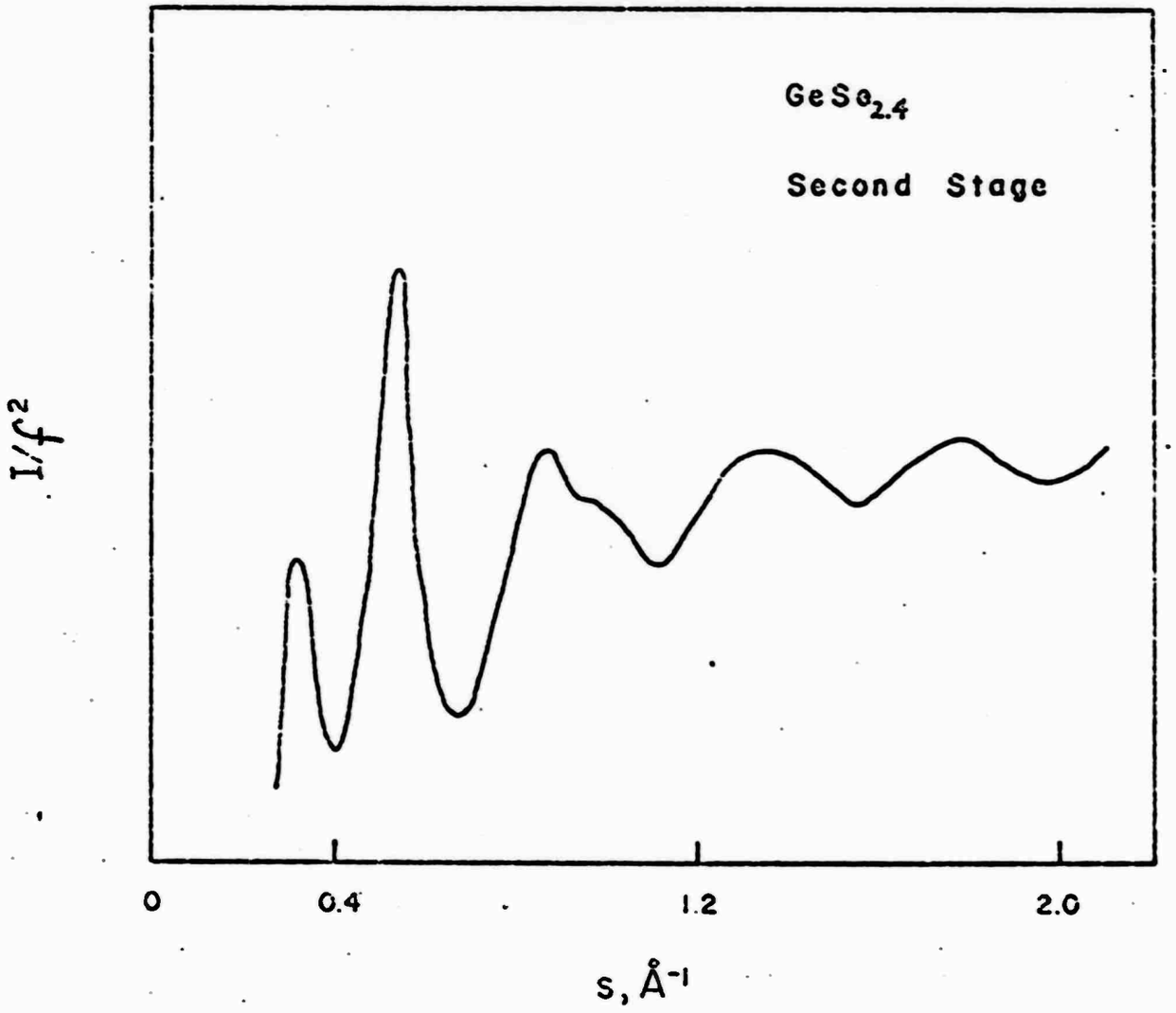

Figure 19. $I(s)/f^2(s)$ vs s for the $GeSe_{2.4}$ film of Figure 16.

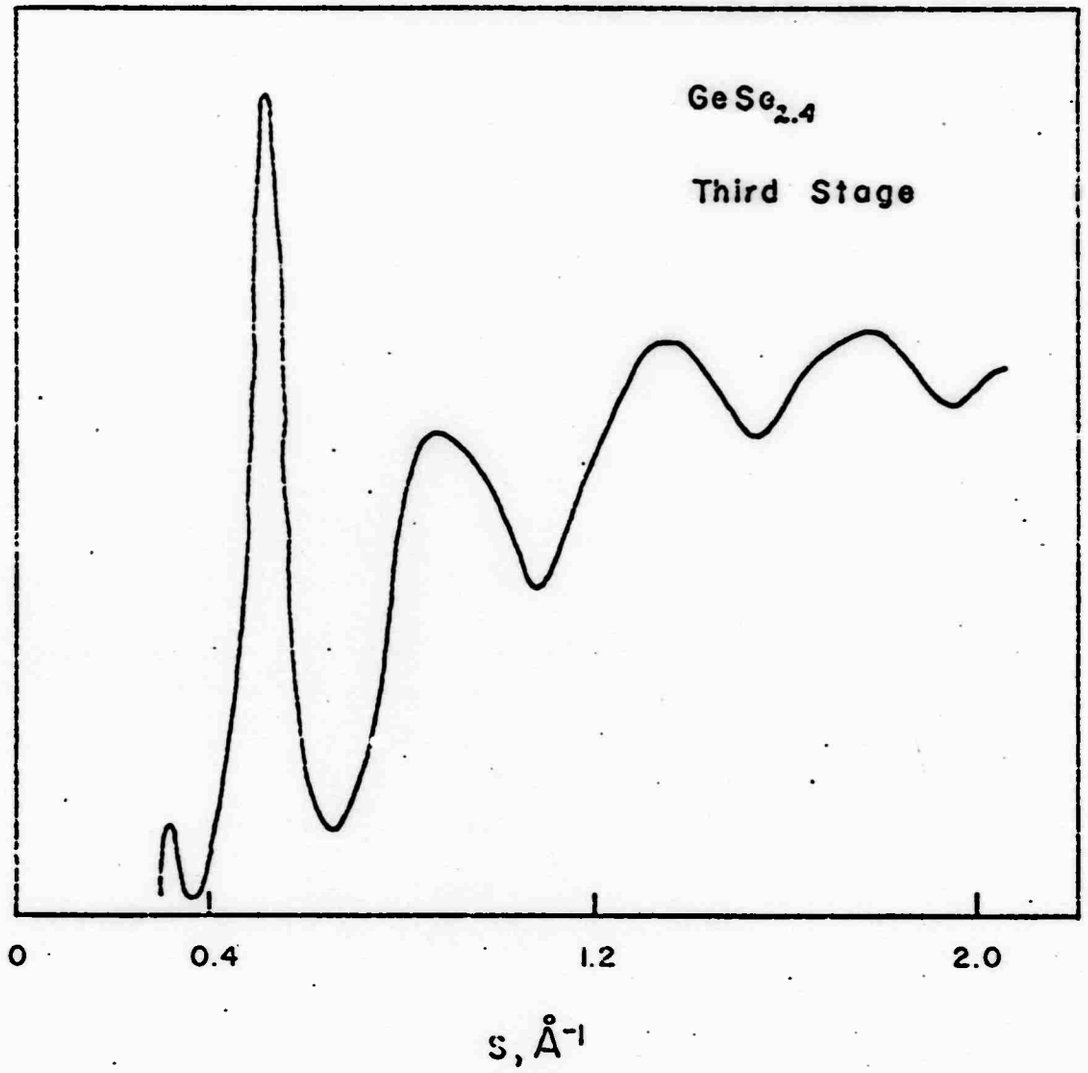

Figure 20. $I(s)/f^2(s)$ vs s for the $GeSe_{2.4}$ film of Figure 17.

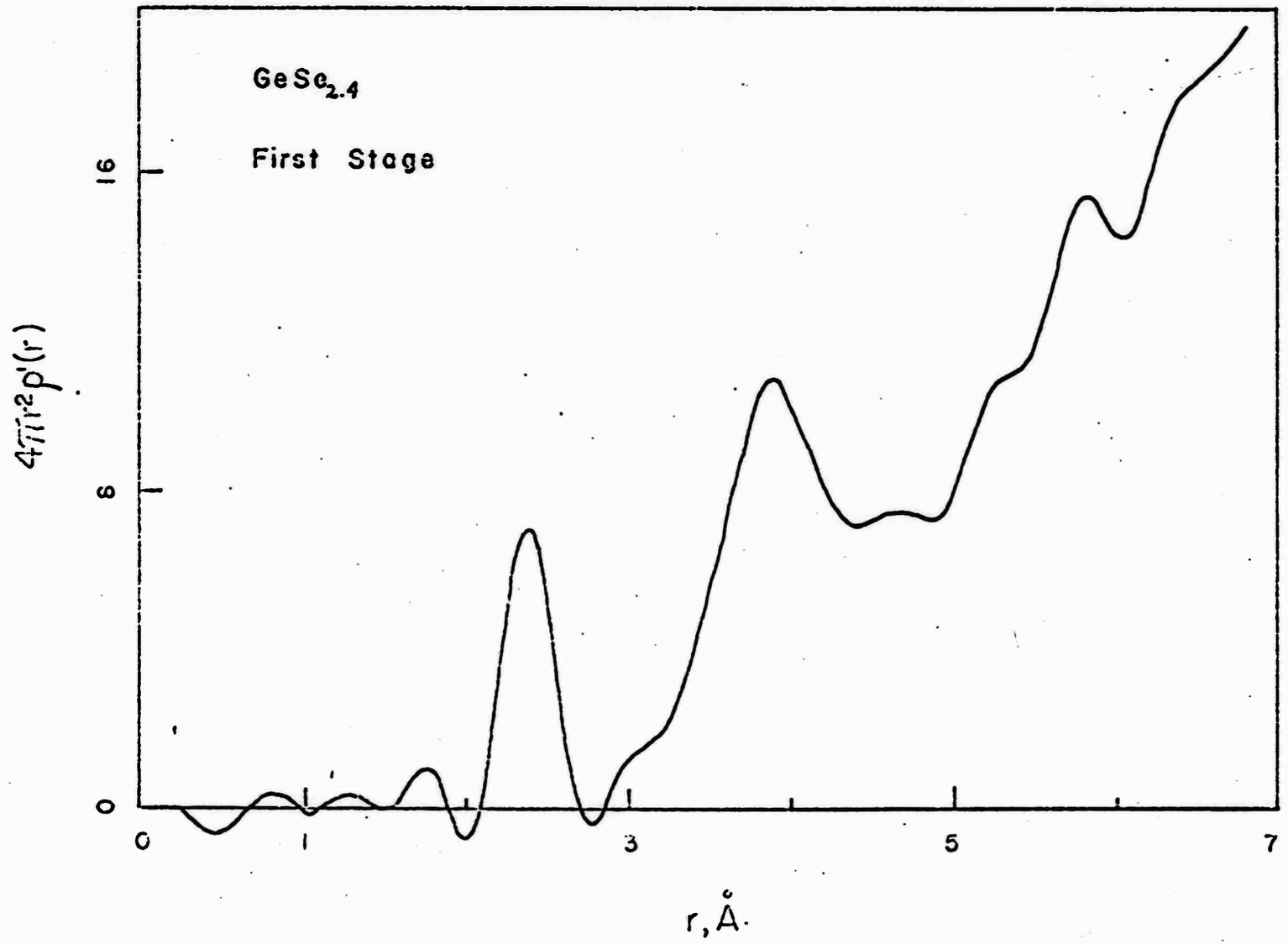

Figure 21. CRDF, calculated without an exponential termination function, for the $GeSe_{2.4}$ film of Figure 15.

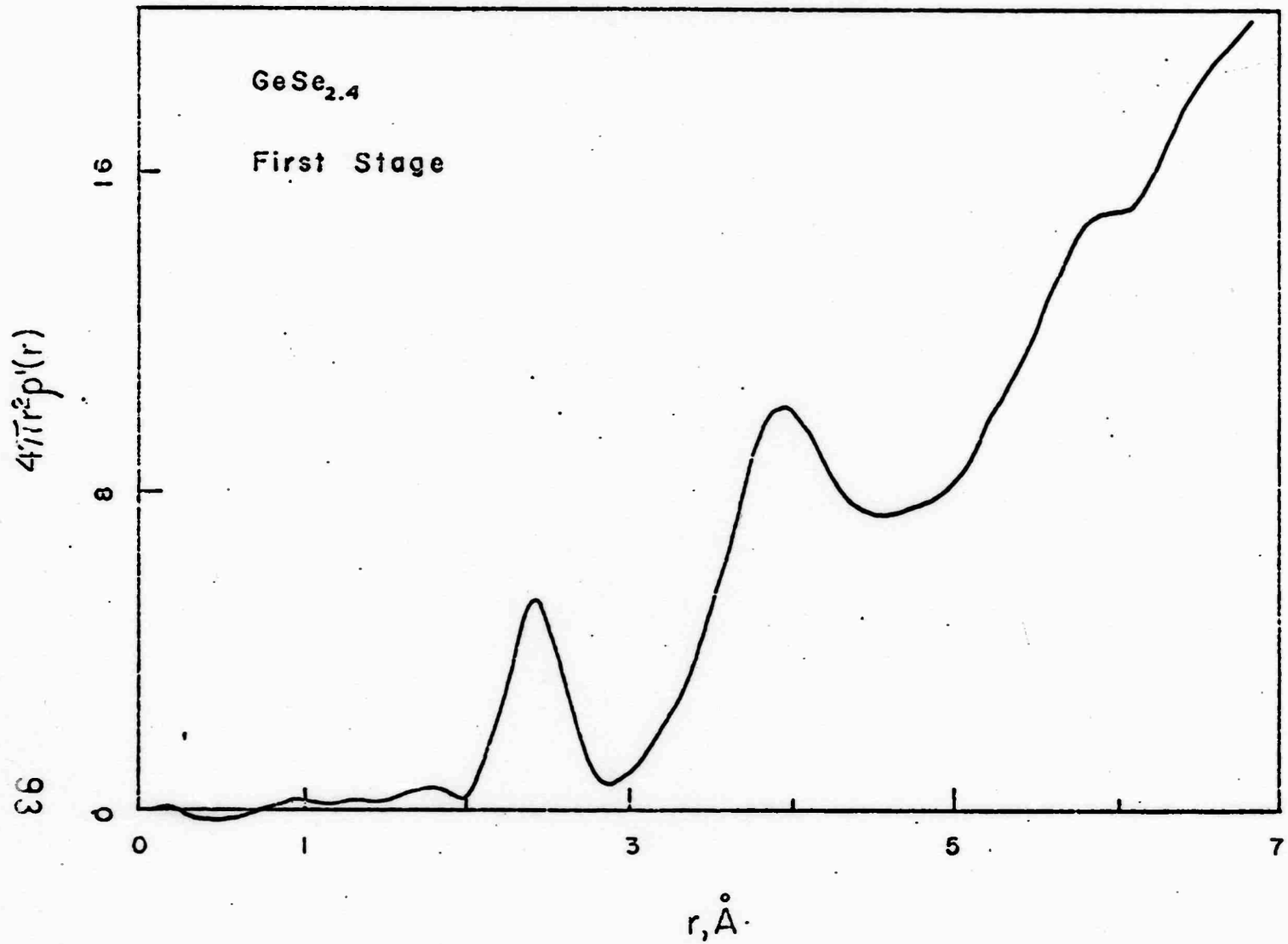

Figure 22. CRDF, calculated with an exponential termination function, for the $GeSe_{2.4}$ film of Figure 15.

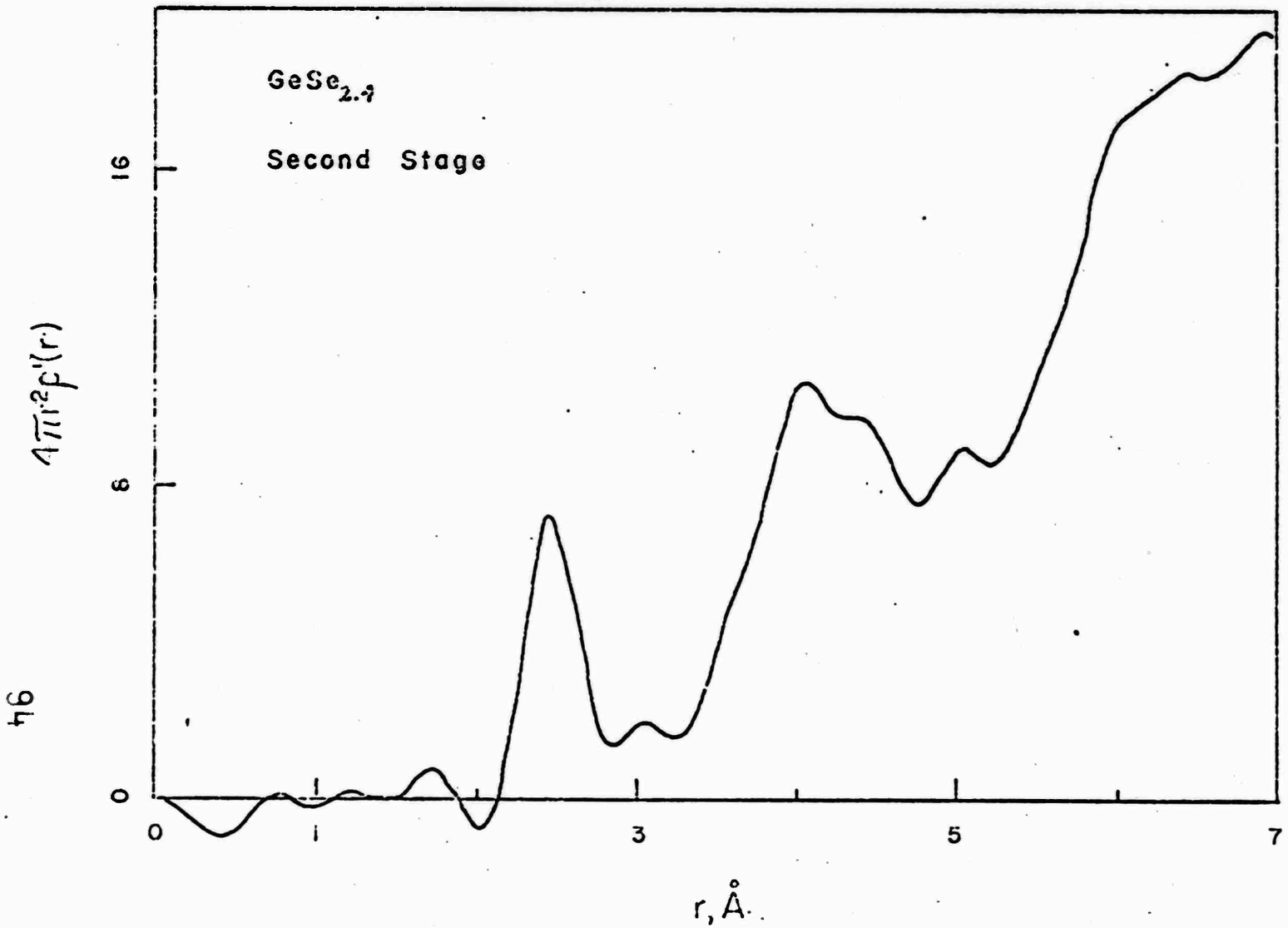

Figure 23. CRDF, calculated without an exponential termination function, for the $GeSe_{2.4}$ film of Figure 16.

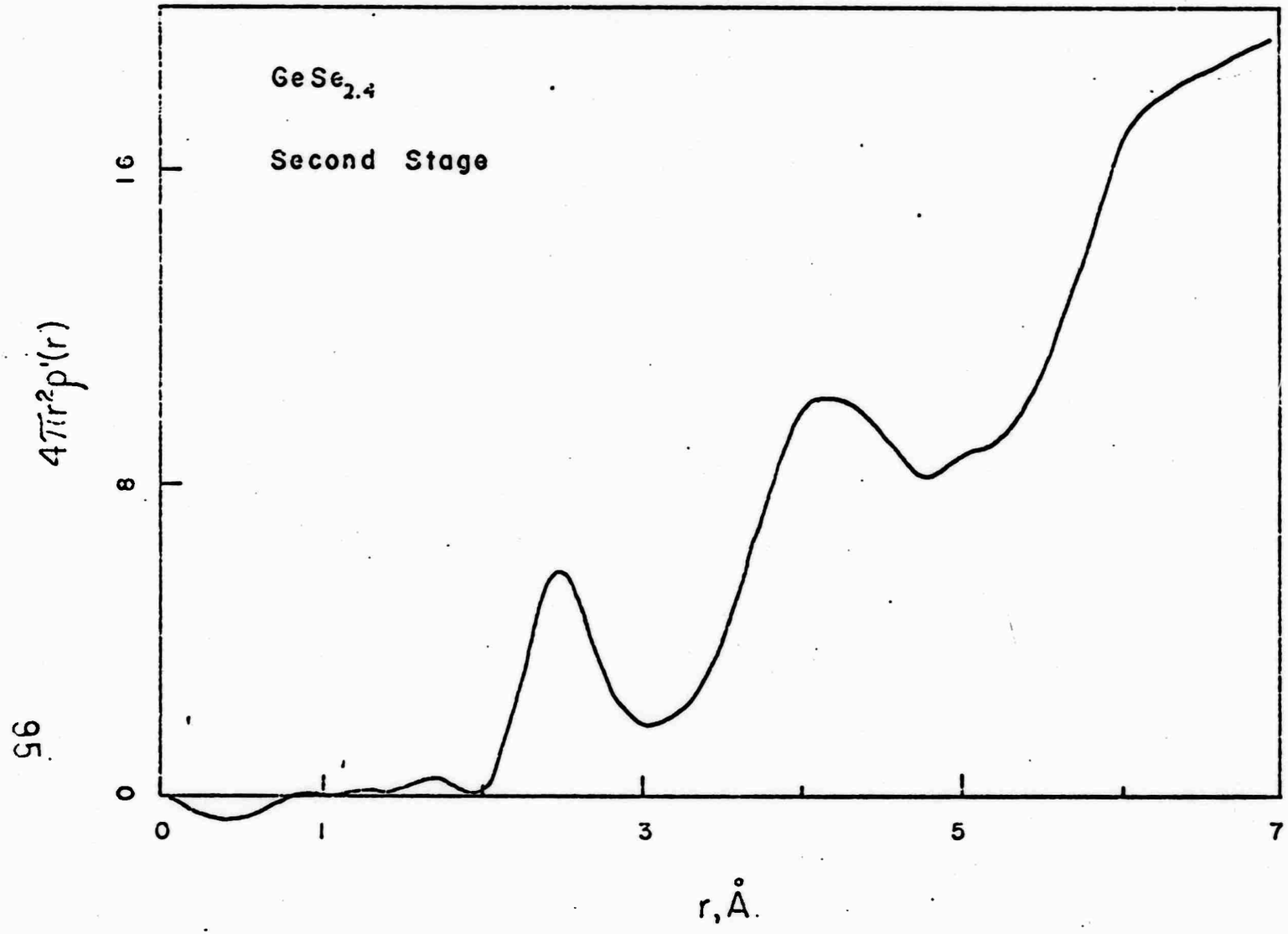

Figure 24. CRDF, calculated with an exponential termination function, for the $GeSe_{2.4}$ film of Figure 16.

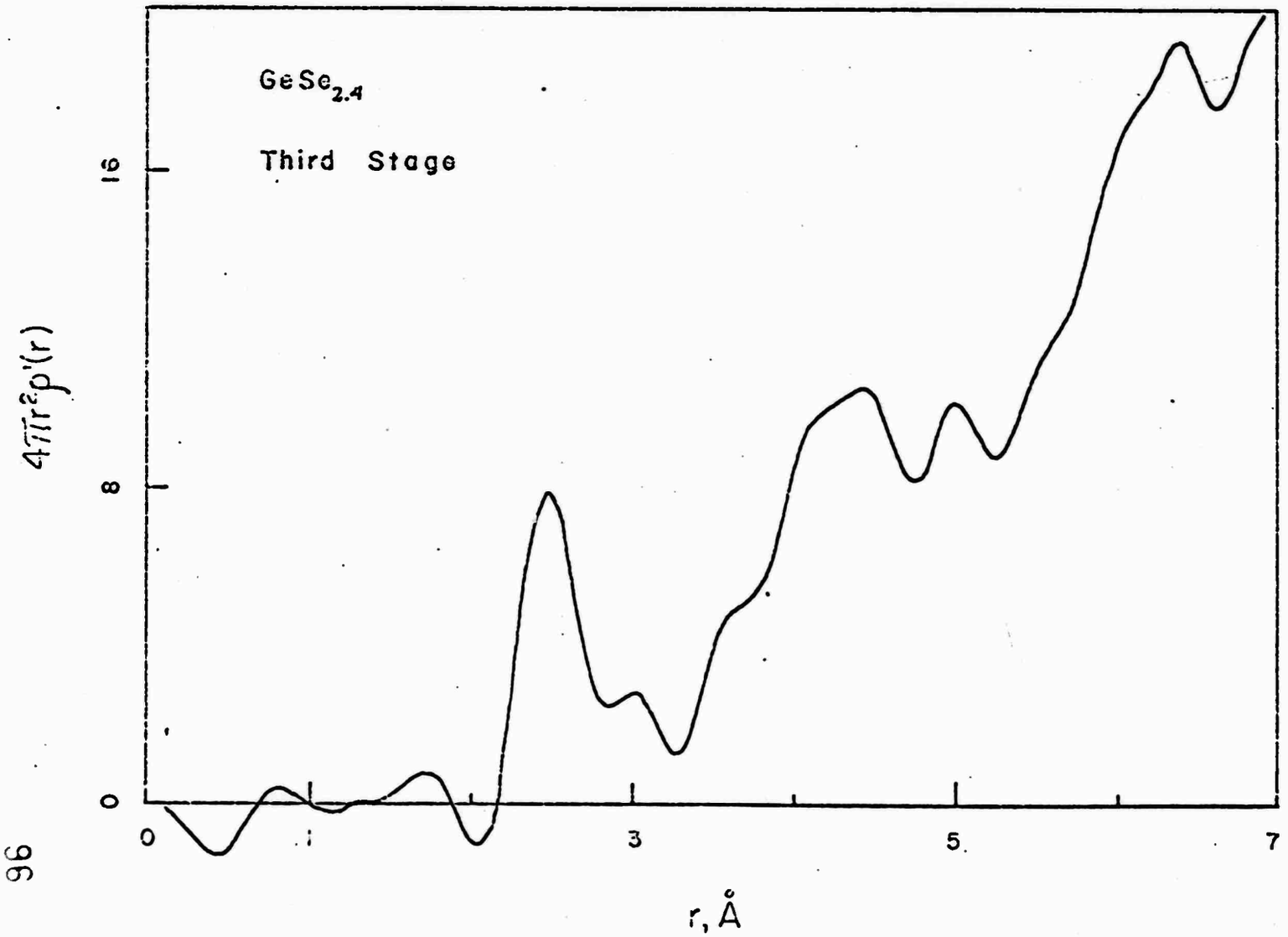

Figure 25. CRDF, calculated without an exponential termination function, for the $GeSe_{2.4}$ film of Figure 17.

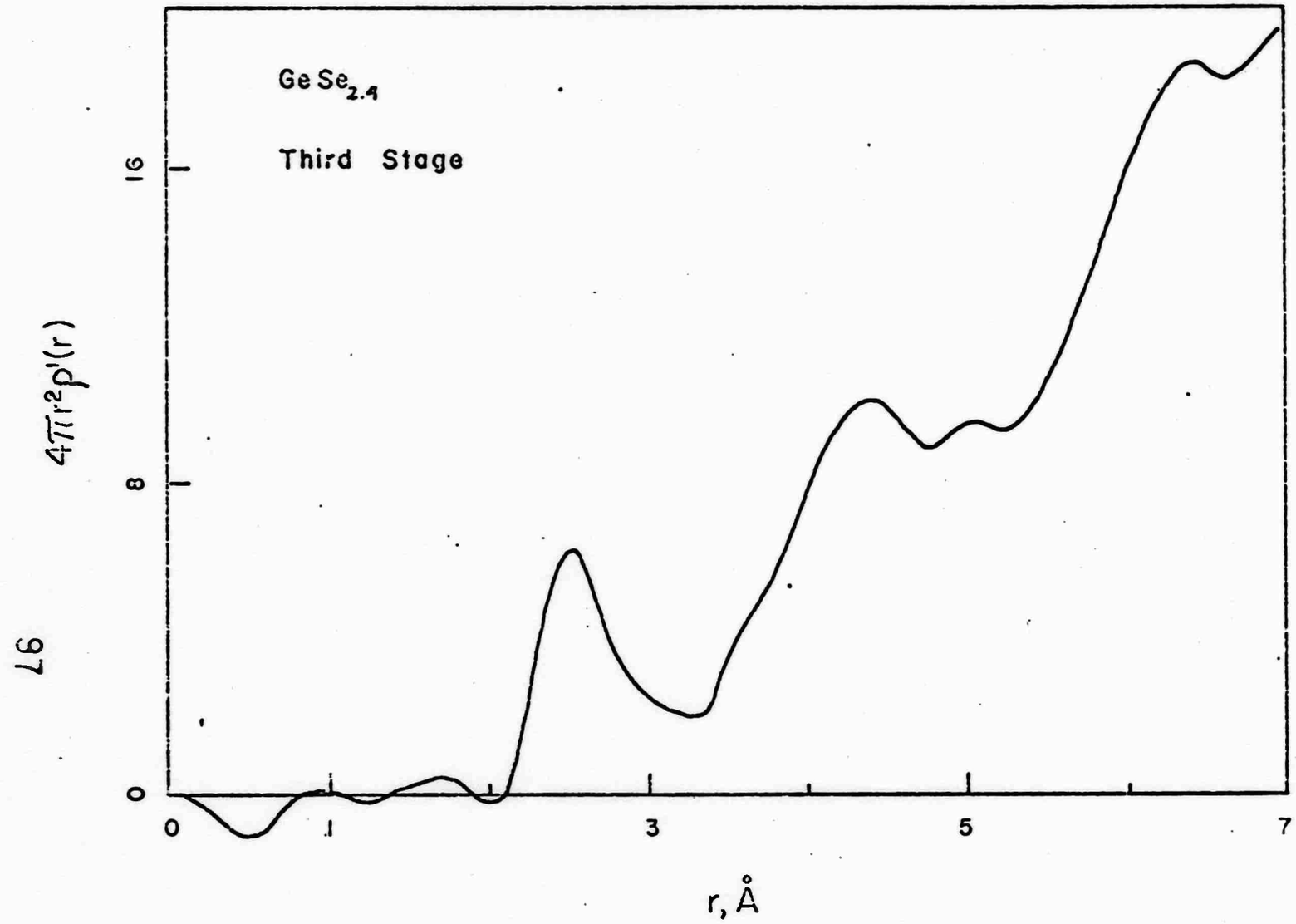

Figure 26. CRDF, calculated with an exponential termination function, for the $GeSe_{2.4}$ film of Figure 17.

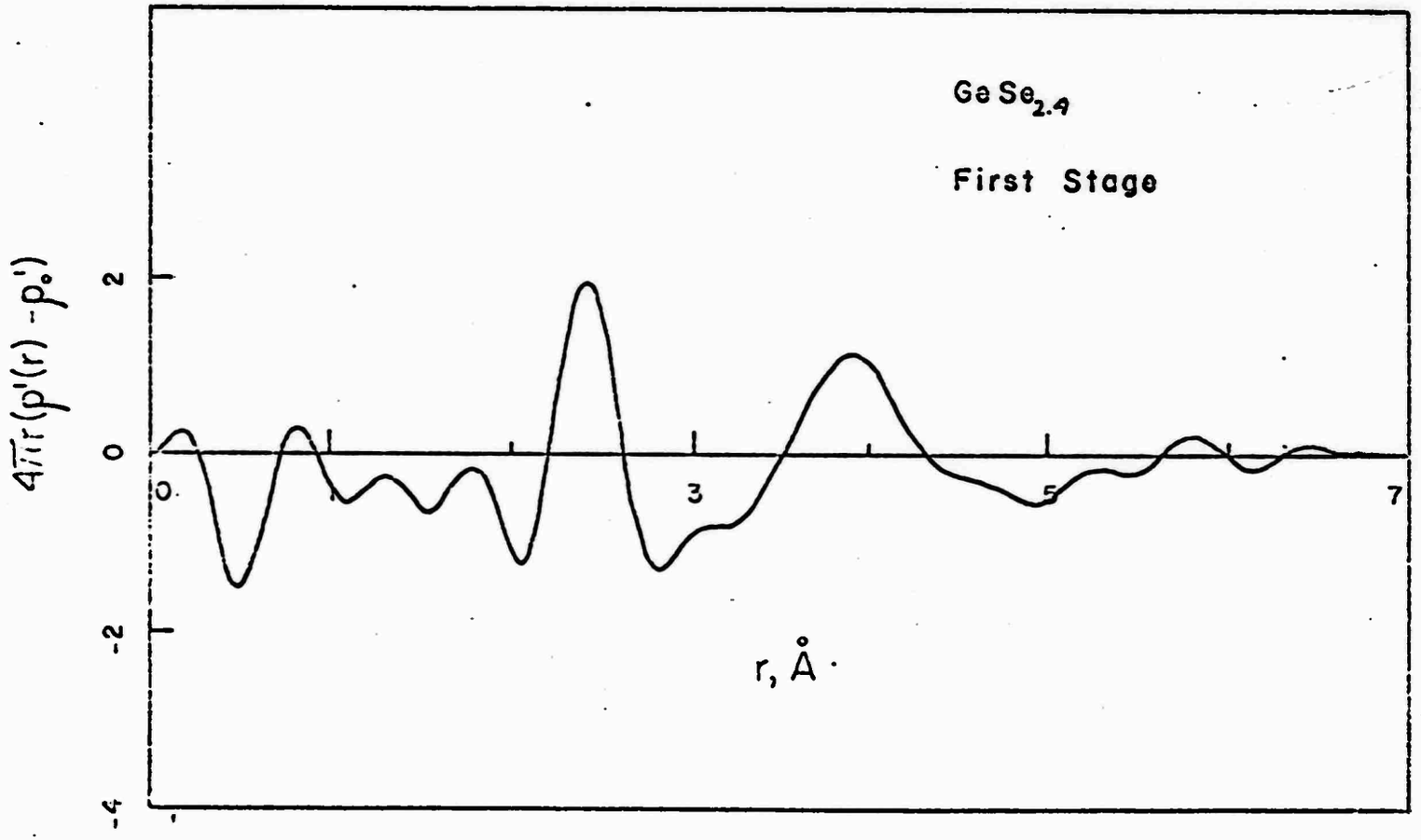

Figure 27. $4\pi r[\rho'(r)-\rho_0']$ vs r, calculated without an exponential termination function, for the $GeSe_{2.4}$ film of Figure 15.

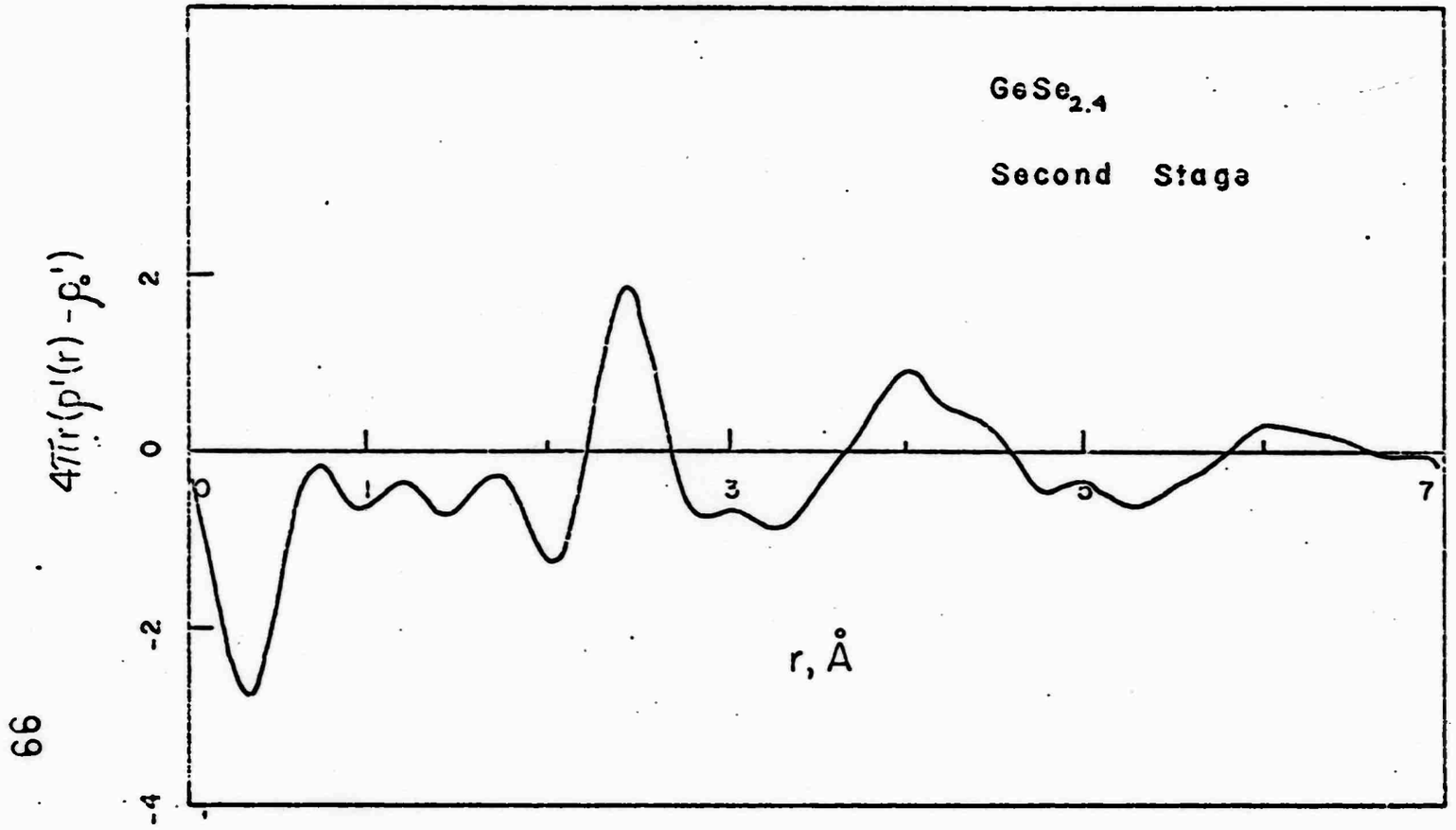

Figure 28. $4\pi r[\rho'(r)-\rho_0']$ vs r, calculated without an exponential termination function, for the $GeSe_{2.4}$ film of Figure 16.

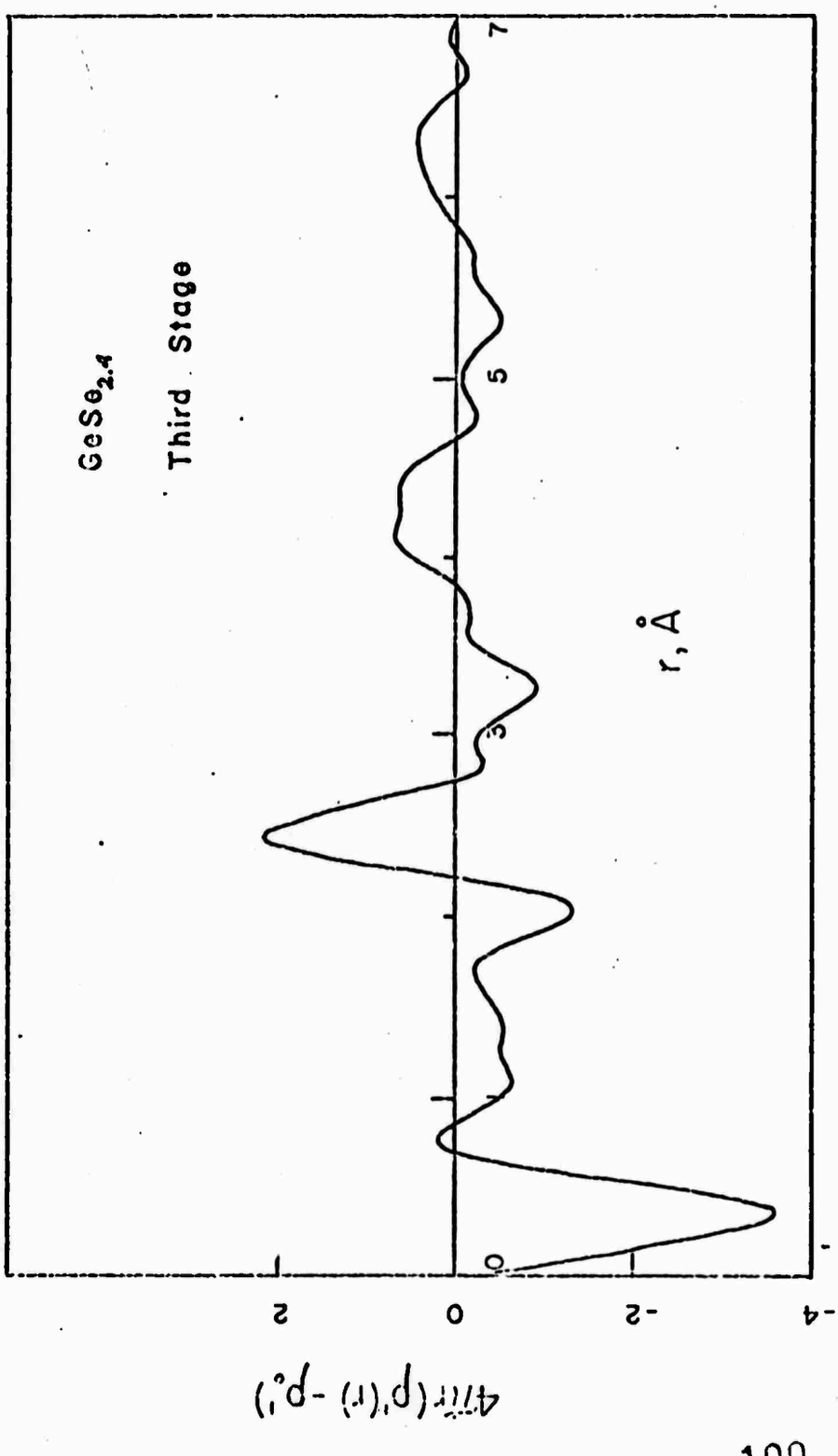

Figure 29. $4\pi r[\rho'(r)-\rho_0']$ vs r, calculated without an exponential termination function, for the $GeSe_{2.4}$ film of Figure 17.

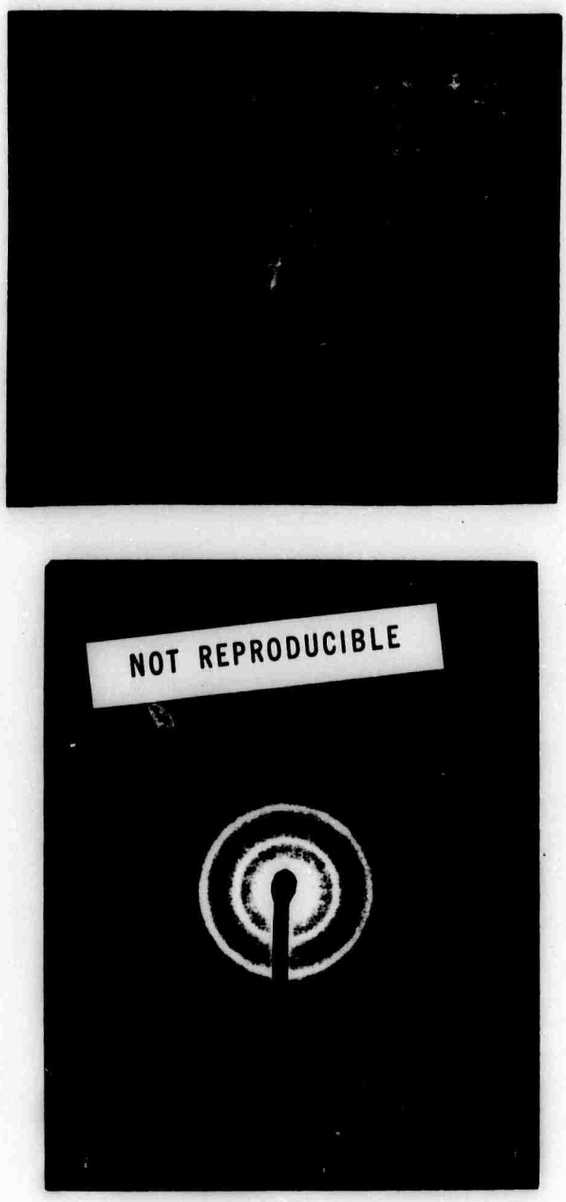

Fig. 30. (a) Electron micrograph of an amorphous $GeSe_{2.4}$ film.
(b) The diffuse electron diffraction pattern of (a).

does show some contrast on a scale of order 100 Å. This contrast cannot be attributed to the presence of crystallites in the film, however, since crystallites of such size would produce sharp rings in the diffraction pattern. The origin of this contrast has not been determined, although it seems to be characteristic of all amorphous films examined to date. The microstructure of amorphous $GeSe_{2.4}$, in fact, appears very similar to that observed for amorphous germanium and carbon films.[20]

The crystallites formed in a $GeSe_{2.4}$ film which was heated with the electron beam can be seen in Fig. 31a. These crystallites, which average approximately 200 Å in diameter, may be identified as being crystallites of selenium from the diffraction pattern of Fig. 31b.

Because of the difficulties encountered in keeping the $Ge_{0.7}$ films in a non-crystalline state, an electron micrograph of amorphous $GeSe_{0.7}$ was not obtained.

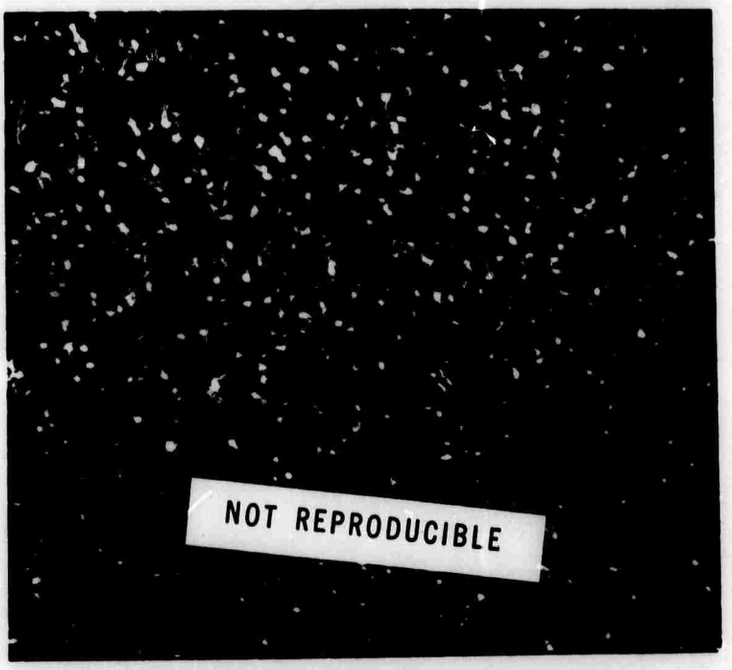

(a)

0.5μ

(b)

Fig. 31. (a) Dark-field electron micrograph of a $GeSe_{2.4}$ film which was heated with the electron beam.
(b) The electron diffraction pattern of (a).

CHAPTER V

ANALYSIS OF CONVOLUTED RDF CURVES

Each CRDF plot presented in Chapter IV consists of a superposition of peaks, with each peak centered at a particular value of r. Equation (2.34) states that the approximate area A under a CRDF peak located between r_o and r_o' is given by

$$A \simeq 4\pi \int_{r_o}^{r_o'} r^2 \, \Sigma\Sigma \, [x_i \rho_{ij}(r) \frac{f_i(o) f_j(o)}{f^2(o)}] dr \qquad (5.1)$$

Since $f_{Se}(o) = 7.6$, $f_{Ge}(o) = 7.3$,[18] and $f^2(o) = x_{Ge} f_{Ge}^2(o) + x_{Se} f_{Se}^2(o)$, the term $f_i(o) f_j(o)/f^2(o)$ in Eq. (5.1) is approximately unity for all combinations of i and j. Therefore, in the case of Ge-Se films, Eq. (5.1) may be rewritten as

$$A \simeq 4\pi \int_{r_o}^{r_o'} r^2 [x_{Ge} \rho_{Ge\text{-}Se}(r) + x_{Ge} \rho_{Ge\text{-}Ge}(r) + x_{Se} \rho_{Se\text{-}Ge}(r) + x_{Se} \rho_{Se\text{-}Se}(r)] dr \qquad (5.2)$$

Equation (5.2) implies that the area under a CRDF peak representing a Ge-Se film gives the average coordination number of the atomic species contributing to the peak.

Figures 32 and 33 show the first CRDF peak (calculated using the exponential termination function) for $GeSe_{0.7}$ and $GeSe_{2.4}$. The area under the first CRDF peak (centered at r = 2.37 Å) for the first stage of $GeSe_{2.4}$ was measured to be 2.30. Examination of the broad shape of the first CRDF peak in the case of the latter two stages of $GeSe_{2.4}$ and both stages of $GeSe_{0.7}$ indicates that in these cases the first CRDF peak consists of a superposition of subpeaks, each subpeak being centered at a different value of r. We would expect the first subpeak of each stage to be centered at that value of $r = r_1$ corresponding to the smallest prominent bond length determined for that stage.

Peak broadening due to the thermal vibrations of the atoms in a film gives rise to symmetric peaks in $4\pi r\rho'(r)$, but not in $4\pi r^2\rho'(r)$. In addition, the peaks in a plot of $4\pi r\rho'(r)$ vs. r are not rendered asymetric by the use of a termination function. Therefore, if a prominent bond length exists at a particular value $r = r_a$, a plot of $4\pi r\rho'(r)$ vs. r in the vicinity of r_a will yield a symmetric peak centered at r_a. Multiplication of this peak by r yields a CRDF peak centered at r_a. Applying this procedure, the shape of the CRDF peak centered at r_1 for the Ge-Se films examined was determined using the following steps.

Step 1: That portion of the first CRDF peak located between r_1 and the first minimum in the CRDF before r_1 was divided by r, yielding a plot of $4\pi r\rho'(r)$ vs. r.

Step 2: The curve obtained in step 1 was reflected about r_1 to produce a peak symmetric about r_1.

Step 3: The symmetric peak obtained in step 2 was multiplied by r to yield a plot of the CRDF peak centered at r_1.

Figures 32 and 33b and c show how the first CRDF peak was decomposed into two subpeaks, centered at r_1 and r_2, respectively, for the two stages of $GeSe_{0.7}$ and the latter two stages of $GeSe_{2.4}$. The portion of each first subpeak below $r = r_1$ lies on the original CRDF plot; the second half is shown as a dashed curve. The area measured under each first subpeak is written within that peak. The subpeak centered at r_2 is that peak which must be added to the first subpeak in order to give the first CRDF peak. The area measured under the peak at r_2 for the first and second stages of $GeSe_{0.7}$ was 1.6 and 0.8, respectively. An area of 0.8 was measured under the peak at r_2 for both the second and third stages of $GeSe_{2.4}$. It should be noted that the size and shape of the peak centered at r_2 are very sensitive to the position and shape of the peak centered at r_1.

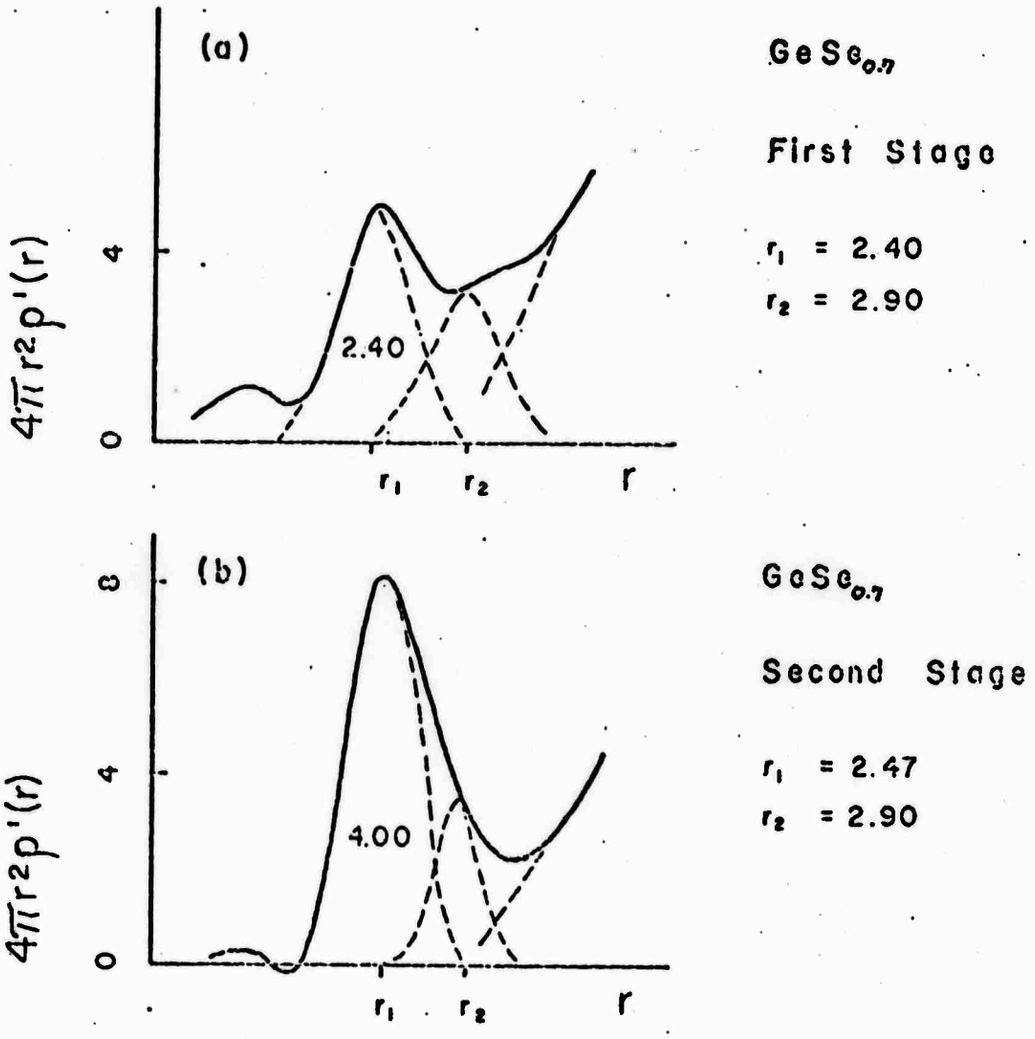

Figure 32. The first CRDF peak and its constituent sub-peaks for the $GeSe_{0.7}$ films of Figures (a) 4 and 9, and (b) 5 and 12.

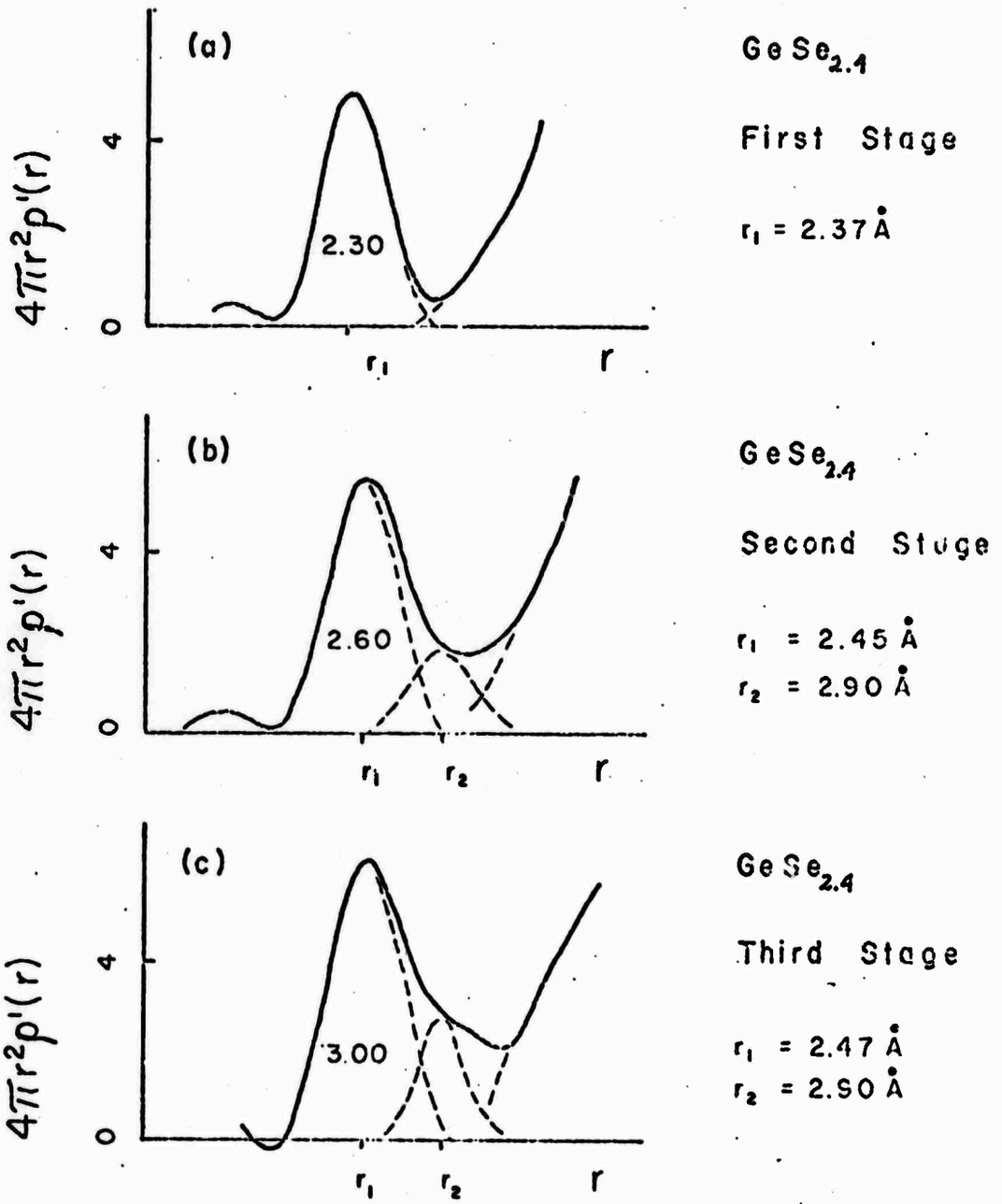

Figure 33. The first CRDF peak and its constituent sub-peaks for the $GeSe_{2.4}$ films of Figures (a) 15 and 22, (b) 16 and 24, and (b) 17 and 26.

CHAPTER VI

DISCUSSION OF EXPERIMENTAL RESULTS

Structure of Crystalline Ge-Se Materials

Most amorphous materials whose structures have been examined have been found to possess local order similar to that which occurs in their crystalline form. It is therefore of interest to examine the local order found in crystalline Ge-Se compounds and determine whether this order is preserved in the amorphous state.

There exist two known Ge-Se compounds, GeSe and $GeSe_2$. The crystal structure of GeSe has been found by Okazaki[21] to be of a highly distorted NaCl type, isomorphous with SnSe and SnS. The bond lengths of the six Ge-Se bonds which correspond to the six nearest-neighbor bonds in NaCl were determined to be the following: 2.54(1), 2.58 (2), 3.30(2) and 3.39(1). The figures in parentheses give the number of Ge-Se bonds of this type associated with each Ge atom. It is thought that GeSe undergoes a polymorphic transformation at 620°C.[22] The structure of this high temperature phase has not been reported in the literature, however.

The crystalline structure of $GeSe_2$ has been determined by Ch'un-hua[23] to be a highly deformed version of an eight-layered CdI_2 type. The Ge-Se bond distances present in

$GeSe_2$ have not been reported, however. Mande[24] concluded from an examination of the x-ray absorption spectra of $GeSe_2$ that the bonding in this material is strongly covalent. The covalent radii of Ge and Se are reported by Pauling to be 1.22 Å and 1.17 Å, respectively, whereas the respective crystal radii of Ge^{4+} and Se^{2-} are reported to be 0.53 Å and 1.98 Å, where the crystal radius of an ion is defined such that the sum of two crystal radii is equal to the actual equilibrium interionic distance in a crystal containing the ions.[25] One would therefore expect the average nearest neighbor distance in $GeSe_2$ to be somewhat larger than 2.39 Å, but less than 2.51 Å. The average coordination number of a Ge atom in a CdI_2 structure would be 6, and the average coordination number of a Se atom would be 3, so that the average coordination number within one layer of the structure would be 4.

Discussion of $GeSe_{2.4}$ CRDF's

Structure of As-deposited $GeSe_{2.4}$ Films

In the present work the first CRDF peak for the first stage of $GeSe_{2.4}$ occurs at r_1 = 2.34 Å. Since the covalent radii of Ge and Se are 1.22 Å and 1.17 Å, respectively, it seems reasonable to interpret this peak as being due to a superposition of Ge-Ge, Ge-Se, and Se-Se contributions.

If this interpretation is made, the area under the first CRDF peak should be equal to the average coordination number of covalently-bonded Ge and Se atoms in the material. If Ge and Se are taken to possess the same coordination number as in their covalently-bonded crystalline states, i.e., a coordination number of 4 for Ge and 2 for Se, then the area under the first peak should be given by

$$\text{Area} = 4x_{Ge} + 2x_{Se} = 2(1 + x_{Ge}) \qquad (6.1)$$

Since $x_{Ge} = 0.29$ for $GeSe_{2.4}$, Eq. (6.1) predicts an area of 2.58 for the area under the first peak, which is quite close to the measured area of 2.30.

It should be noted that the area predicted by Eq. (6.1) is independent of the way in which the Ge and Se atoms are mixed, provided the coordination of each atom is conserved. One cannot therefore determine solely from the area under this peak whether the Ge and Se atoms are mixed in a random fashion, or whether complete miscibility or complete immiscibility exists.

Effect of Heat Treatment on $GeSe_{2.4}$ CRDF's

Figure 33 shows that as a film of $GeSe_{2.4}$ is heated from the first to the second stage the position of the CRDF peak centered at r_1 shifts to a higher value of r, the area under this peak increases, and a peak emerges at 2.90 Å.

As the film is heated from the second to the third stage the area under the peak at r_1 continues to increase, but the size of the peak at 2.90 Å does not change significantly. These changes in the CRDF indicate a change in amorphous film structure with heating prior to crystallization. The information contained in the CRDF's does not by itself allow a unique determination of the structural changes occurring. A tentative model for the structural changes observed, however, is presented in the following section.

A Tentative Model

The changes in the CRDF observed when a $GeSe_{2.4}$ film is heated might be due to the separation of the as-deposited film into the following amorphous phases:

1) An amorphous phase of GeSe whose local order approximates a NaCl structure and whose nearest neighbor distance is equal to 2.95 Å, which is the average nearest neighbor distance present in crystalline GeSe. The formation of this phase would account for the growth of the peak at 2.90 Å.

2) An amorphous phase of $GeSe_2$ whose local order resembles a CdI_2 structure and whose bonding, like that of crystalline $GeSe_2$, is largely covalent. If the Ge-Se nearest neighbor distance in this phase is taken to be the same as the nearest neighbor distance in crystalline $GeSe_2$, i.e., between 2.40 Å and 2.50 Å, the formation of this phase would add a Ge-Se contribution to the first CRDF peak which would shift the position of this peak to a higher value of r. The Ge and Se atoms in a CdI_2 structure would have coordination numbers greater than those possessed by the four-coordinated Ge and two-coordinated Se atoms

in the unseparated mixture. The presence of these atoms of higher coordination number would therefore cause an increase in the area under the peak centered at r_1.

3) An amorphous phase of Se. It is clear that selenium must separate out during some stage of the heat treatment since it is selenium which first crystallizes as the temperature of the film is raised. Amorphous selenium has been found to have an average nearest neighbor distance of 2.34 Å and a first coordination number of two.[26,27] The presence of this phase would therefore contribute to the area under the peak centered at r_1.

If a $GeSe_{2.4}$ film which has already partially separated into GeSe, $GeSe_2$, and Se is heated to a sufficiently high temperature, the phase separation described above would continue, but the amorphous phase of GeSe would begin to separate into amorphous $GeSe_2$ and amorphous Ge. Amorphous germanium has been found to have a nearest neighbor distance of 2.43 Å and first coordination number of 4.[20] The amorphous germanium would therefore contribute to the area under the peak centered at r_1. The increase in the amount of $GeSe_2$ present would result in an increase in the number of covalently-bonded Ge and Se atoms with coordination numbers greater than 4 and 2, respectively, and would therefore cause an increase in the area under the peak centered at r_1. The area under the peak at r_2 would not be expected to increase significantly if most of the GeSe being formed was separating into $GeSe_2$ and Ge.

The occurrence of phase separation in amorphous chalcogenides is not uncommon. In his study of bulk non-

crystalline chalcogenides, R. Roy[28] found all of the materials he examined to consist of more than one amorphous phase. Even monoelement materials such as amorphous selenium and sulfur were found to have a polyphasic structure. It is interesting to note that, although the CRDF plots for $GeSe_{2.4}$ seem to indicate the occurrence of phase separation as a film is heated, no evidence of this separation was observable in the electron microscope. The contrast between different amorphous phases is expected to be small, however, since the electron densities of Ge and Se are quite close to each other, and might therefore be very difficult to observe.

Discussion of $GeSe_{0.7}$ CRDF's

Structure of $GeSe_{0.7}$ Films in First Stage

None of the prominent bond lengths determined for the two stages of $GeSe_{0.7}$ (Table III) compare with the six Ge-Se bond lengths presented earlier in this chapter for crystalline GeSe. This result implies that the local order in the amorphous $GeSe_{0.7}$ films examined in the present work differs from the local order present in crystalline GeSe.

Figure 32 shows that the first CRDF peak for the first stage of $GeSe_{0.7}$ can be decomposed into two subpeaks, one centered at r_1 = 2.40 Å and one at 2.90 Å, with respective areas of 2.40 and 1.60. As a $GeSe_{0.7}$ film is heated from

the first to the second stage, the position of the peak centered at r_1 moves to a higher value of r, the area under this peak increases, and the area under the peak at r_2 decreases.

If a $GeSe_{0.7}$ film in the first stage consists of simply a mixture of four-coordinated Ge atoms and two-coordinated Se atoms, the area under the peak centered at 2.40 Å should be approximately $2(1+x_{Ge}) = 3.18$. The fact that the measured area beneath this peak is considerably less than 3.18 indicates that a film in this stage does not consist solely of such a mixture. The presence of a peak at 2.90 Å leads one to suspect that this film has already been heated enough by the electron beam to cause some phase separation. Therefore, the CRDF plot given for the first stage of $GeSe_{0.7}$ may not be representative of the structure of a $GeSe_{0.7}$ film in the as-deposited state.

A Tentative Model

As in the case of $GeSe_{2.4}$, the CRDF's alone do not contain sufficient information to allow a unique characterization of the structural changes which occur as a $GeSe_{0.7}$ film is heated. The following tentative model, however, suggests what structural changes might be occurring.

Consider an as-deposited $GeSe_{0.7}$ film to consist of a mixture of four-coordinated germanium atoms and two-coordinated selenium atoms. When the film is heated, the mixture

begins to separate into an amorphous phase of GeSe (whose structure is the same as that structure given for GeSe in the previous section), plus amorphous germanium and amorphous selenium. The formation of GeSe would result in an increase in the number of Ge-Se bonds of bond length 2.90 Å and a decrease in the number of Ge-Se bonds which are largely covalent. This phase separation would therefore result in the formation of a peak at approximately 2.90 Å and a decrease in the area of the peak centered at 2.40 Å to some value less than 3.18. It is therefore possible that the CRDF labeled as representing $GeSe_{0.7}$ in its first stage actually represents the partially phase-separated structure described above.

When a film which has already partially phase separated is heated to a sufficiently high temperature, the amorphous phase of GeSe begins to separate into amorphous $GeSe_2$ and amorphous Ge. This second separation would result in the peak at r_1 shifting to a higher value of r, the area under this peak increasing, and the area under the peak at 2.90 Å either decreasing or remaining constant. The initiation of this second separation would account for the changes in the $GeSe_{0.7}$ CRDF as the film is heated from the first to the second stage.

Comparison of $GeSe_{0.7}$ CRDF's with Results Reported for GeSe

One would not expect the size and location of the first few CRDF peaks of amorphous GeSe films to differ significantly from the CRDF results of amorphous $GeSe_{0.7}$. The GeSe radial distribution plot reported by Mikolaichuk et al.,[29] however, has its first two peaks located at 2.6 Å and 4.0 Å, respectively, and gives a Ge coordination number of 5.8. The distinctive differences which exist between Mikolaichuk's results and the results given in the present work for $GeSe_{0.7}$ can perhaps be explained by the fact that the techniques used to prepare the GeSe films was quite different from the technique described in Chapter III for the preparation of the films of $GeSe_{0.7}$. The GeSe films were prepared by evaporation of the initial compound from a quartz crucible heated with a molybdenum spiral. The films were deposited on cellulose nitrate, glass, and single-crystalline substrates held at a temperature between 300°K and 500°K. Mikolaichuk reported observing a change in the relative intensity of the electron diffraction peaks of his films as the substrate temperature was varied. Unfortunately, he did not report what effect a change in substrate temperature had on his radial distribution results.

The Ge-Se Phase Diagram

A question which must be considered is whether one can interpret the structural changes which occur when a Ge-Se film is heated in terms of the known Ge-Se phase diagram (even though, strictly speaking, phase diagrams apply only to materials in thermodynamic equilibrium). Figure 34 shows the phase diagram determined by Ch'un-hua et al.[22] for the Ge-Se system. From the phase diagram one would expect a dissociation of $GeSe_{2.4}$ into $GeSe_2$ and Se as a film of $GeSe_{2.4}$ was heated. This would initially be an amorphous separation. As the film temperature was increased, crystalline Se would appear, followed by crystalline $GeSe_2$. If this is the correct separation mechanism, one must interpret the CRDF peak at 2.90 Å as being due to the amorphous $GeSe_2$.

From the phase diagram one would expect a heat treated $GeSe_{0.7}$ film to separate into amorphous GeSe and amorphous Ge, and hence one would not expect to see Se crystallites. This is obviously not consistent with what was found experimentally in the present work. In addition, the peak at 2.90 occurs in the CRDF's of both $GeSe_{0.7}$ and $GeSe_{2.4}$, and it is extremely unlikely that this peak is due to both $GeSe_2$ and GeSe.

It therefore appears that one cannot predict the structural changes which occur simply by examining the phase diagram, unless, of course, gross compositional variations

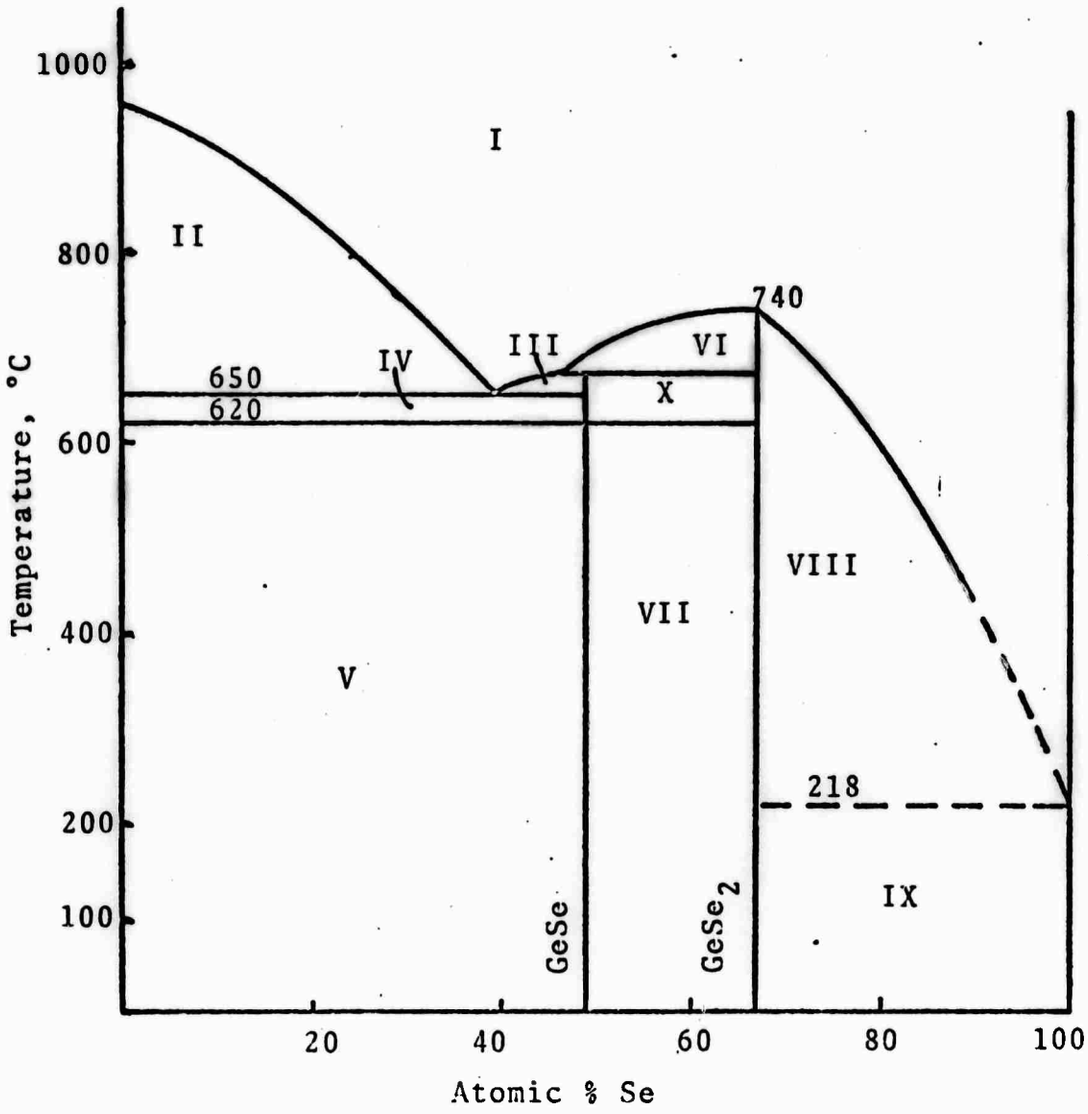

Fig. 34. The system Ge-Se (Ref. 22).

I - melt
II - melt + Ge
III - melt + GeSe
IV - Ge + GeSe(β)
V - Ge + GeSe(α)
VI - melt + $GeSe_2$
VII - GeSe(α) + $GeSe_2$
VIII - melt + $GeSe_2$
IX - $GeSe_2$ + Se
X - GeSe(β) + $GeSe_2$

exist within each as-deposited film. If each Ge-Se film in its as-deposited state consists of regions of $GeSe_2$, GeSe, Ge, and Se in some ratio, then these local regions could possibly follow the phase diagram, enabling one to account for the changes observed in the CRDF's simply from phase diagram considerations.

CHAPTER VII

CONCLUSION

Summary

The radial distribution studies indicate that vapor-deposited films of $GeSe_{0.7}$ and $GeSe_{2.4}$ possess some degree of short-range atomic order. The local order present in amorphous $GeSe_{0.7}$ films differs from the distorted NaCl structure of bulk crystalline GeSe. Therefore a band structure different from that of crystalline GeSe must be employed to explain the optical and electronic properties of amorphous Ge-Se films whose composition lies within at least a few atomic percent of $GeSe_{0.7}$.

The electron micrograph of an amorphous $GeSe_{2.4}$ film reveals some contrast on the order of 100 Å. The fact that this contrast is not due to the presence of crystallites is evidenced by the absence of sharp diffraction rings in the diffraction pattern of this film.

The radial distribution curves indicate a change in the structure of amorphous films of $GeSe_{0.7}$ and $GeSe_{2.4}$ as they are heated with an electron beam. A definitive determination of the nature of this change cannot be made solely from the CRDF results. A tentative model is suggested,

however, in which the as-deposited GeSe films are considered to consist of a mixture of four-coordinated Ge and two-coordinated Se atoms. Heating a film is considered to result in a dissociation of this mixture into amorphous phases of GeSe, $GeSe_2$, Ge, and Se. Heating to a sufficiently high temperature results in the crystallization of the Se.

Suggestions for Future Work

It is clear that before a complete characterization can be made of the structural changes which occur when a Ge-Se film is heated, additional experiments need to be carried out. A study of the infrared spectra of Ge-Se films which have undergone various amounts of heat treatment should aid in the determination of the structure of the amorphous phases present in these films. An investigation of the bond lengths present in the basic unit of structure of crystalline $GeSe_2$ also needs to be made.

The annealing time and temperature associated with each Ge-Se CRDF should be determined so that any particular amorphous stage of a film can be reproduced. The effect of substrate material and temperature on the composition and structure of the films in their as-deposited state also needs to be examined.

It would be of interest to compare the structure of Ge-Se films produced by sputtering and by simultaneous evaporation of elemental Ge and Se with films produced by flash evaporation. A comparison of the CRDF's obtained from x-ray diffraction analysis of bulk Ge-Se glasses with the CRDF's given in the present work would be of immediate interest.

BIBLIOGRAPHY

1. MacAvoy, T. C., "Liquid and Amorphous Materials: Structure and Properties," An Atomistic Approach to the Nature and Properties of Materials, J. A. Pask, Ed., John Wiley and Sons, New York, 1967.

2. Bowman, D. L. and J. C. Schottmiller, "Vitreous Bi-Se Layers as Near-Infrared Photodetectors," J. Appl. Phys., 39, 1659 (1968).

3. Ovshinsky, S. R., "Reversible Electrical Switching Phenomena in Disordered Structures," Phys. Rev. Letters, 21, 1450 (1968).

4. Tatarinova, L. I., "Study of Short-Range Order in Amorphous Semiconductors by the Electron Diffraction Method," Sov. Phys. Cryst., 4, 637 (1959).

5. Dove, D. B., M. B. Heritage, K. L. Chopra and S. K. Bahl, "Short-Range Order in Amorphous GeTe Films," Appl. Phys. Letters, 16, 140 (1970).

6. Adler, D., "Theory Gives Shape to Amorphous Materials," Electronics, 43, 61 (1970).

7. Debye, P., Ann. Physik, 46, 809 (1915).

8. Debye, P. and H. Menke, Ergeb. Techn. Roentgenkde., 2, 1 (1931).

9. Zernike, F. and J. A. Prins, Z. Physik, 41, 184 (1927).

10. Guinier, A., X-Ray Diffraction in Crystals, Imperfect Crystals, and Amorphous Bodies, W. H. Freeman and Co., San Francisco, 1963.

11. Warren, B. E., X-Ray Diffraction, Addison-Wesley, Reading, Massachusetts, 1969.

12. Pings, C. J. and J. Waser, "Analysis of Scattering Data for Mixtures of Amorphous Solids or Liquids," J. Chem. Phys., 48, 3016 (1968).

13. Dove, D. B., to be published in Physics of Electronic Ceramics, Marcel Dekker, New York.

14. Dove, D. B., M. B. Heritage, K. L. Chopra and S. K. Bahl, op. cit., p. 139.

15. Kaplow, R., S. L. Strong and B. L. Averbach, "Radial Density Functions for Liquid Mercury and Lead," Phys. Rev., 138, A1336 (1965).

16. Grigson, C. W. B., "On Scanning Electron Diffraction," J. Electronics and Control, 12, 209 (1962).

17. Dove, D. B. and P. N. Denbigh, "Modified Detection Arrangement for Scanning Electron Diffraction Instrument," Rev. Sci. Instr., 37, 1687 (1966).

18. Vainstein, B. K., Structure Analysis by Electron Diffraction, MacMillan Co., New York, 1964.

19. Kannewurf, C. R., A. Kelley and R. J. Cashman, "Comparison of Three Structure Determinations for Germanium
a Selenide, GeSe," Acta Cryst., 13, 450 (1960).

20. Chang, J., "Structure of Amorphous Germanium Films," Master's Thesis, University of Florida, 1970.

21. Okazaki, A., "The Crystal Structure of Germanium Selenide GeSe," J. Phys. Soc. Japan, 13, 1151 (1958).

22. Ch'un-hua, L., A. S. Pashinkin and A. V. Novoselova, "Investigation of the Germanium-Selenium System," Proc. Acad. Sci. USSR, Chem. Sect., 146, 892-3 (1962).

23. Ch'un-hua, L., A. S. Pashinkin and A. V. Novoselova, "Germanium Diselenide," Russ. J. Inorg. Chem. (English Transl.), 7, 1117 (1962).

24. Mande, C., R. N. Patil and A. S. Nigavekar, "Bond Character in Germanium Selenides by X-ray Spectroscopy," Nature, 211, 519 (1966).

25. Pauling, L., The Nature of the Chemical Bond, Cornell University Press, Ithaca, New York, 1960.

26. Lucovsky, G., "The Structure of Amorphous Selenium From Infrared Measurements," The Physics of Selenium and Tellurium, W. C. Cooper, Ed., Pergamon Press, New York, 1969.

27. Unger, P. and P. Cherin, "Coordination and Thermal Motion in Crystalline Selenium and Tellurium," The Physics of Selenium and Tellurium, W. C. Cooper, Ed., Pergamon Press, New York, 1969.

28. Roy, R. and V. Caslavska, "Di-Phasic Structure of Switching and Memory Device 'Glasses'," Solid State Communications, 7, 1467 (1969).

29. Mikolaicheck, A. G. and A. N. Kogut, "Preparation and Structure of Thin Films of Germanium Telluride and Selenide," Sov. Phys.-Crystallogr., 15, 296 (1970).